Biraj Singh Thapa

Effects of sediment erosion in guide vanes of Francis turbines

Thesis for the degree of Philosophiae Doctor

Trondheim, October 2016

Norwegian University of Science and Technology
Faculty of Engineering
Science and Technology
Department of Energy and Process Engineering

NTNU
Norwegian University of
Science and Technology

NTNU
Norwegian University of Science and Technology

Thesis for the degree of Philosophiae Doctor

Faculty of Engineering
Science and Technology
Department of Energy and Process Engineering

ISBN 978-82-326-1859-3 (printed version
ISBN 978-82-326-1859-0 (electronic version
ISSN 1503-8181

Doctoral theses at NTNU, 2016:260

Printed by Skipnes Kommunikasjon as

Unless you know yourself, what else can you know?

Preface

This study has been accomplished at the Waterpower Laboratory in the Department of Energy and Process Engineering at the Norwegian University of Science and Technology (NTNU) in Trondheim, Norway. The thesis is presented as a collection of papers written during the project period, August 2013 - July 2016. The work was funded by Norwegian Hydropower Center (NVKS), which aims to ensure and develop research and education in hydropower related technology. The work also aims to strengthen the cooperation between Kathmandu University (KU) and NTNU for further developing the research excellence in Nepal.

Abstract

Erosive wear of turbine components has been a major operational challenge for the run-off-river hydropower plants across the basins of Himalaya in Asia. The hard mineral particles, which are carried by rivers reach the turbines and erode the surface in contact. In Francis turbines, guide vanes, cover plates, hub at runner inlet and blades at runner outlet are the most affected areas due to the sediment erosion. Several attempts have been made in the past to minimize the losses due to the sediment erosion in the hydraulic turbines. However, the problem has not been solved satisfactorily.

A dry clearance gap between the guide vanes and the cover plates usually exists in the Francis turbines, from the design. The deflection of cover plates and the erosion of the components causes the clearance gap to increase by multiple times of its design value. Inherit pressure difference between guide vane surfaces forces a leakage flow from the increased clearance gap. A systematic study of the characteristics of the leakage flow, and its effects on the flow conditions inside the Francis turbine distributor has not been reported yet. Such studies are necessary for the design optimization of the turbine components and to plan the effective maintenance schedules for repairing the eroded turbine parts.

The main objective of this work is to study the effects of sediment erosion in hydro turbines, with the focus on the flow around the guide vanes of a low specific speed Francis turbine. Experimental investigations of the characteristics of leakage flow from the increased clearance gap between eroded guide vanes and cover plates, has been the focus of this study.

A one-guide vane cascade has been developed to represent the flow inside a low specific speed Francis turbine distributor. Cases with five different sizes of clearance gap are investigated for the guide vane shaped with a symmetric profile. Particle Image Velocimetry techniques are applied for the flow measurement. All experiments have been carried out at the Waterpower Laboratory of Norwegian University of Science and Technology. Flow velocity exceeding 35 m/s, at the runner inlet of Francis turbine, is reported for the first time from such experimental studies.

The results show that, that the clearance gap up to 0.5 mm does not have significant effects on the flow parameters and hence can be accepted as the maximum limit. The leakage flow, with clearance gap more than 1 mm, is found to change the velocity components at the runner inlet significantly. The case with the clearance gap of 2 mm is found to have the highest effects on the flow velocities and is considered as the critical size. The total cross-wise leakage flow, from the critical clearance gap, is measured to be more than 1% of the main flow. As the consequence of the leakage flow, the relative velocity at the runner inlet is found to increase locally up to three times from its design value. This local increase in

relative velocity is identified as the cause to have severe erosion at the runner hub in the sediment-laden projects. The leakage flow also changes the pressure distribution around guide vane, causing the torque on the guide vane shaft to increase up to 28%.

Further investigation of the propagation of the leakage flow into the turbine runner, and its effects on the runner's performance is necessary. Alternative designs of guide vane geometry, to minimize the differential pressure across is recommended as the future works.

Acknowledgments

I would like to express my sincere appreciation to my supervisor Professor Ole Gunnar Dahlhaug, for his continuous motivation and freedom to choose my own way during the study. I also thank Professor Torbjørn Nielsen and Professor Bhola Thapa for their support and advices as the co-supervisors. I am thankful to Professor Michel Cervantas for his grilling discussions. I pay my humble respect to all the technicians in laboratory for their hard work in setting up the test rig so perfectly. Special thanks goes to Trygve Opland, without whom the test rig would have never been the leakage free at such a high pressure. Bård Brandåstrø needs to be acknowledged for his follow-up of the procurement process and insuring everything happen on schedule.

I am grateful to have a helping and conducive atmosphere among the fellow PhD candidates in the laboratory. I am thankful to Bjørn Winther Solemslie, Carl Bergan and Peter Jochaim Gogstad for their support with MatLab. I thank the master's student for their contributions in this study, which is spread from the design of the test rig to the analysis of PIV data. Overlapping the study with Sailesh Chitrakar has insured the continuation of this work much further than where I have to stop. I thank him for the valuable discussions and ever-ready helping hands. I am grateful to Chirag Trivedi for his valuable suggestions and spending lunchtime with much humor. I also thank Rahul Goyal and Igor Iliev for the interesting discussions.

I am thankful to Vegard Brøtan and the Department of Production and Quality Engineering at NTNU for the 3D printing of the guide vane parts in the time of crisis. I also thank Einar Agnalt for his guidance in Creo and production of some parts for the test rig. Wenche Johansen deserves a huge respect for her humble support in the administrative issues, starting from the admission to the defense of this study. Her particular support during the submission process will remain in my heart forever.

I express my gratitude to my parents for their continuous encouragement and being together with me in Trondheim during the greatest need of time. Finally, I express my affection to my beloved wife who spent several evenings alone while I was busy to complete my works. A warm welcome to my son, who arrived to motivate me on the last month of my PhD period.

Structure of the thesis

This thesis comprises of the summary in Part I, and the papers in Part II.

Part I presents overview of the current work. Background, objectives of the current work and the test set-up are discussed in the introduction. Summary of the main research papers based on this work is included for a quick review. Key outcomes of the current work are discussed in the conclusion.

Part II comprises of the following five papers, as the main contributions to this thesis.

Paper-A	Sediment erosion in hydro turbines and its effect on the flow around guide vanes of Francis turbine This paper has been published in the Journal, *Renewable and Sustainable Energy Reviews, Vol 49 (2015), 1100-1113.* *(doi: 10.1016/j.rser.2015.04.178)*
Paper-B	Design and development of guide vane cascade for a low specific speed Francis turbine This paper has been published in the *Journal of Hydrodynamics, Ser. B., Vol 28 (2016), 676–689.* *(doi: 10.1016/S1001-6058(16)60648-0)*
Paper-C	Flow measurements in the distributor of Francis turbine: A PIV approach This paper has been submitted for publication in the Journal, *Renewable Energy*. The paper is currently under review.
Paper-D	Sediment erosion induced leakage flow from guide vane clearance gap in a Francis turbine This paper has been submitted for publication in the Journal, *Renewable Energy*. The paper is currently under review.
Paper-E	Effects of sediment erosion in guide vanes of Francis turbine This paper has been submitted for publication in the Journal, *Renewable Energy*. The paper is currently under review.

Part II also includes the following two additional papers produced from this study.

Paper-F Flow field measurement in guide vane cascade of a high head Francis turbine

This paper has been presented at the *6th International Conference on Water Resources and Hydropower Development in Asia* on March 2016 in Lao PDR. The paper is published in the conference proceedings.

Paper-G Velocity and pressure measurements in guide vane clearance gap of a low specific speed Francis turbine

This paper has been presented at the *28th IAHR symposium on Hydraulic Machinery and Systems* on July 2016 in France. The paper is published in the conference proceedings.

Contents

Part I

Summary

1. Introduction

This section introduces the outline of the thesis. The background for this study is presented and status of research relevant to this study is discussed. Objectives and scope for this study is listed. The test setup developed for this study is also introduced.

1.1. Background of study

Increase in demand of clean energy is promoting further explorations of renewable energy sources. Hydropower is one of the oldest and the most reliable sources of clean energy to supply electricity. Since the first installation of hydroelectric power plant in 1827, the technology has undergone several innovations and capacity enhancements. In practice, up to 96% turbine efficiency is possible, which makes hydropower one of the most efficient and economic energy resources [1]. At present hydropower sector produces more than 1211 GW electricity worldwide, which is about 20% of total electricity supply [2].

Two third of technically feasible hydropower resources are still undeveloped. More than 55% of global undeveloped hydropower potential lies in Asia alone [3]. Asian region also contributes to the highest growth in energy demand, accounting for 70% of the growth in global energy consumption since 2000 [4]. Hence, future of hydropower developments will be more localized in this region.

The total global sediment flux from rivers to the oceans has been estimated as 20E+12 kg per year, of which 6.3E+12 kg is contributed by Asian rivers, particularly those draining from the Himalaya–Tibetan Plateau region [5]. Thus, hydropower in Asian region suffers the problems of sediment handling. The consequences the sediments in flow include filling up of dams in the reservoir projects and damaging the mechanical components in the run-off-the-river projects [6]. Problems associated with the handling of sediments in hydro power projects is also reported from the Andes basins in South America, which holds about 12% of global untapped hydro power potential [3].

Francis type of turbines are widely used in hydroelectric projects, due to its flexibility and high efficiency. These are reaction machines, which utilizes both pressure energy and kinetic energy in water and convert them to mechanical energy inside rotating runner. Due to the topological formations, with both the high and the low altitude mountains in Himalaya and Andes areas, the Francis turbines are more suited for these regions. Studies have shown that up to 80% of hydro turbines required for future installations under Himalayan basins in Nepal will need Francis type of turbine [7].

The design philosophy for Francis turbines considers, the highest possible efficiency, the smallest possible dimensions, and avoiding cavitation, as the conventional design criterial

[8]. These design methods also creates conditions, where relative velocity between the turbine components and flowing water reaches very high. Such designs methods have yielded excellent performance in European and North American basins, where issues of sediment handling were virtually absent. However, in case of sediment-laden projects the conventional design methods meet an added operational challenge. The hard minerals present in rivers bypass the settling basins and reach the turbines. With the high flow velocities inside the turbine, the sediments carry sufficient momentum to damage the components by abrasive erosion [9]. Currently practiced methods to control sediment erosion in the turbine components includes, prevention of sedimentation in the catchment areas, tapping sediments at intakes, and applying preventative coatings on the turbine components exposed to high velocity water. Studies have shown that, despite of such control measures, hydro turbines have repeatedly failed to deliver the expected performance in case of sediment-laden flows [10-14]. Studies have also shown the need of optimization of assembly design to reduce the downtime in relation with the repair and maintenance of the eroded turbine parts [15].

One of the alternative solutions to prevent the erosion in Francis turbines is to reduce the relative velocity inside the runner by improving hydraulic design [16]. Ongoing research have shown the strong possibilities for design optimization of Francis runners for reducing the sediment erosion damage [17]. However, it was concluded that a systematic and long-term studies are needed to come to the point, when such optimized designs are ready for the commercial production. The present study aim to add a building block on this venture of the design optimization of Francis turbine for better performance in sediment-laden projects.

A strong cooperation exists between NTNU and KU for the common research and development activities in the field of sediment erosion of hydraulic turbines. The Norwegian government supported *RenewableNepal* program had started a project in 2010 that initiated the research to optimize the design of Francis turbine to handle the large sediment load. The research activities continues with the project supported by *EnergizeNepal* program. The long-term goal of the KU-NTNU cooperation is to develop and deliver technical support for the manufacturing of the optimized designs of Francis turbines in Nepal. A part of this study is combined with the ongoing activities under this KU-NTNU cooperation.

1.2. Status and current research

References to scientific studies on abrasion of hard minerals by sand particles can be found from 1873 [18]. A comprehensive work on erosion of surfaces by the solid particle has been published by Finnie on 1960 [19]. This work includes literature review of past research followed by theoretical and analytical analysis of the erosion with experimental

validations. An intensive study on abrasive wear in hydraulic machinery in general has been conducted by Truscott [20] and was published in 1972. It reviews findings from most of the peer and earlier researchers to identify the various types of wear and the factors affecting them.

Brekke [21] has made a very detailed investigation of sediment erosion in Hydraulic turbines. The cases of erosion in several hydropower plants were investigated and theoretical discussions were made. He has proposed the basic design criteria for hydro turbines operating in sediment-laden flows. Operation and maintenance strategies for the turbines operating in sediment-laden flows were also formulated.

A systematic study of sediment erosion in hydro turbines and components has been done in a PhD studies by Bhola Thapa [22]. An extensive literature review of the studies in this subject until 2004 has been documented. He has tested several types of turbine materials and coatings with the sediment particles from the different basins under Himalaya. He has also identified several areas for further research towards the development of optimized design of Francis turbines for sediment handling.

A series of PhD and Masters studies have been conducted after Bhola Thapa, each contributing to the next towards development of the optimized design. Neopane [23] has successfully implemented numerical models to estimate sediment erosion on Francis turbine components in his PhD study. Mette [24] has written her PhD thesis on methods and numerical studies of optimized hydraulic design of Francis turbines for sediment handling. Gjosater [25], Thapa [26] together has contributed to the development of design tools and parametric studies for the optimized designs with their Master thesis. Chitrakar [27] has done fluid structure interaction (FSI) analysis of the optimized designs and Rajkarnikar [28] has validated the optimized design of the runner blade with experimental investigations under different sediment loads. These studies have recognized that, reshaping the Francis runner blade geometry by lowering the reaction ratio and changing the blade loading distribution will reduce the relative velocity inside the runner. This will proportionately reduce the sediment erosion in the runner blades, particularly at the runner outlet. However, on the other hand, it was also observed that lowering the reaction ratio will also increase the absolute velocities around the guide vane and hence it further escalates the erosion in the guide vane instead. It was concluded that the additional studies by combining the design optimization problem for the runner and the guide vane together, with the objective of minimum erosion in both components are necessary.

The current study is aims to start the series of research activities to optimize the design of guide vanes in Francis turbines operating under large sediment loads. This work is focused to develop experimental methods to evaluate effects of guide vane erosion on the performance of Francis turbine. The knowledge and experience developed from this study

will eventually be used to identify the optimized designs of guide vane that match with the optimized designs of the runner. Data for the reference case measurements, which is without erosion in guide vane, has been thoroughly investigated and will be made public for validation of numerical models for similar studies, and for the comparison with the cases of the optimized designs.

A particular case of erosion in guide vane of Francis turbine, which causes to increase the clearance gap between guide vane walls and cover plates, has been the specific focus for this study. **Figure 1** shows a typical case of the erosion of guide vane operating under the Himalayan basins with its effects on increase of the clearance gap. The design clearance gap is reported to be 0.3 mm. **Figure 1a** shows the erosion at guide vane walls towards the trailing edge. The increase in clearance gap between guide vane walls and cover plates can be seen in **Figure 1b**. Measurements of such clearance gap has been done at the positions shown in **Figure 1c**. It can be observed (in **Figure 1d** & **Figure 1e**) that the clearance gap has increased considerably from its design value to 1.45 mm at the leading edge and 1.41 mm at the trailing edge respectively, within the operational time of 8500 hours. It further increases to 2.5 mm at the leading edge and 4.7 mm at the trailing edge respectively, within the operational time of 16500 hours. Thus, the rapid increase in the size of clearance gap due to erosion of guide vane in Francis turbine has been a major issue of sediment-laden projects.

Several past studies have outlined presence and adverse effects of guide vane erosion in Francis turbines operating in the sediment-laden flows [12, 29-31]. Some studies have been done to study leakage flow from the clearance gap [32, 33]. However, the experimental investigations of the characteristics of the leakage flow from the clearance gap in a Francis turbine has not been found to be reported so far. This work is aimed to understand the possible causes of such high erosion rates in the guide vane clearance gap and identify their effects on the runner's performance.

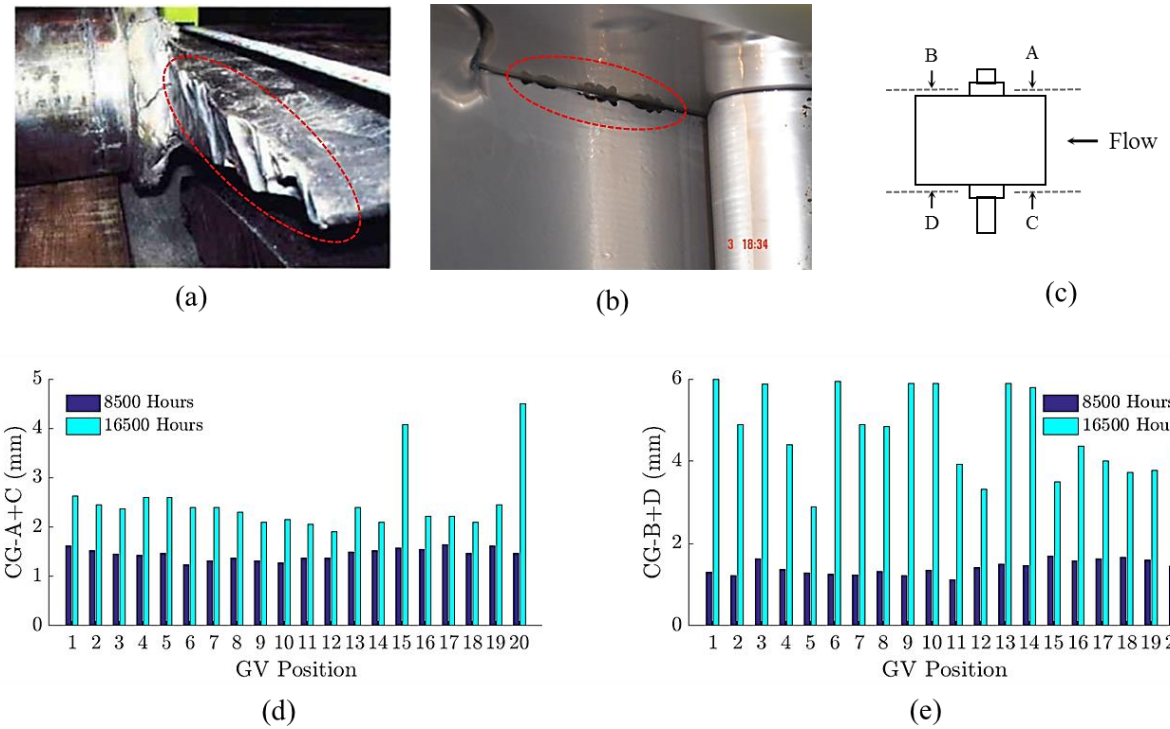

Figure 1. Sediment erosion in guide vane of Francis turbine in Himalaya [10]

(a) Erosion of guide vane end wall surface. **(b)** Formation of guide vane clearance gap. **(c)** Measurement location of guide vane clearance gap. **(d)** Guide vane clearance gap towards leading edge. **(e)** guide vane clearance gap towards trailing edge

1.3. Objectives of Study

The main objective of this work is to study the effects of sediment erosion in hydro turbines, with the focus on the flow around the guide vanes of a low specific speed Francis turbine.

Followings are the specific objectives of this work:

- Investigate the characteristics of leakage flow between the guide vanes and the cover plates in a low specific speed Francis turbine.
- Investigate effects of the leakage flow on velocity distribution in the distributor of a low specific speed Francis turbine.

1.4. The test setup

An experimental setup with one guide vane cascade representing the flow inside the distributor of a reference prototype Francis turbine has been developed for this study. Jhimruk Hydroelectric Center, in Nepal, which has been recorded as one of the most affected case of sediment erosion in Francis turbine [22], is chosen as the reference turbine. Flow in-between three adjacent guide vane, out of total 24 guide vane in the prototype turbine, is reproduced inside the cascade. The two outer guide vane forms part of cascade's walls and middle guide vane directs flow into the channel. The angular position covered by the periodic walls of the cascade is 30 degrees from the turbine center, which is $1/12^{th}$ size of the turbine in the angular direction. Simplifications are introduced for ease of manufacturing and for the optical excess to Particle Image Velocimetry (PIV) instrumentation. A computational fluid dynamics (CFD) based optimization of cascade's geometry has been done to compensate the limitations of the simplifications. The main criteria to satisfy the optimization goal is to have the similar velocity triangles, at the runner inlet position in the cascade, as that observed in case of an ideal turbine design. Details of the design procedures, the optimization methods and the validation of flow inside the cascade is discussed in Paper-B.

Figure 2 shows a schematic layout of the test setup developed for this study. The setup is mounted in a closed loop system consisting of pump, flow meter, and a pressure tank. The flowmeter is calibrated with volumetric methods as per IEC guidelines [34] and total uncertainty was found to be below $\pm$ 0.15%. Pressure and velocity measurements are done for the reference case without clearance gap, and for the cases with clearance gaps of 0.5 mm, 1.5 mm, 2 mm and 3 mm respectively.

Fourteen piezo- resistive pressure taps are inserted in the test section cover plate to measure pressure around the guide vane surface. All pressure sensors are pre-calibrated against a dead weight calibrator. Measurement uncertainly was maintained to be below 0.05% at all the measuring points. An average of 2000 samples, for each pressure point, measured at 5 HZ, is considered for the pressure analysis. PIV methods are devised for the velocity measurements for all the cases. Total 1103 grid points are equally spaced under the measurement area of 0.026 m^2 inside the flow channel. A pulsed light sheet with a thickness of 2 mm is generated, and a series of paired images are acquired at 150 μs and 4 Hz. Unique velocity vectors are obtained for each grid point, which are separated by 4.7 mm in physical space. It has been estimated that minimum 100 images pairs are needed for the statistical convergence of the time averaged velocity field. The uncertainty of the statistically conversed velocity measurements is estimated to be below 2.5%.

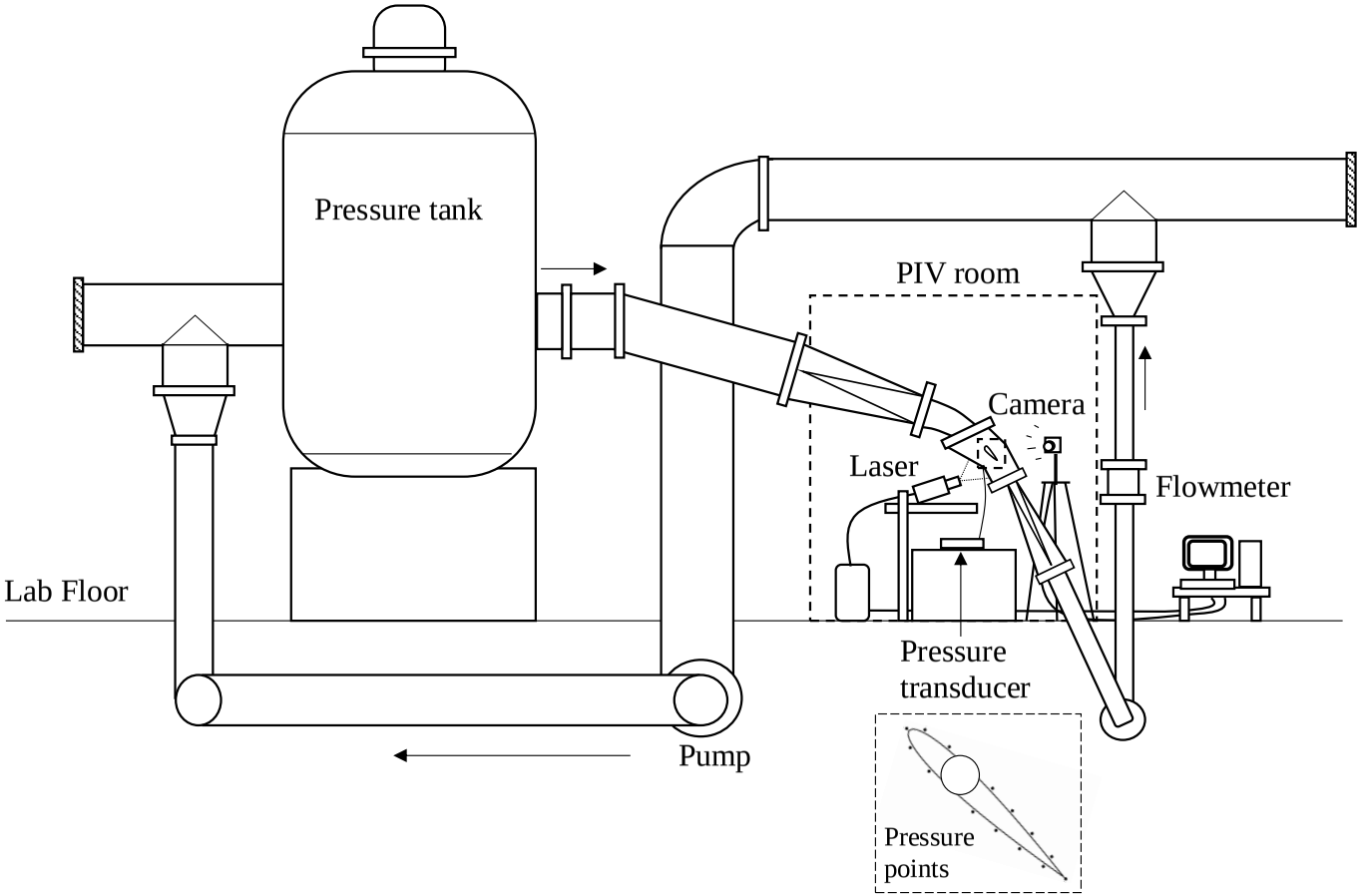

Figure 2. Schematic Layout of the test setup developed for this study

2. Summary of main publications

This section gives a summary of the content in the submitted papers. The papers are found in Part II in this thesis.

2.1. Summary of Paper-A

Sediment erosion in hydro turbines and its effect on the flow around guide vanes of Francis turbine

Biraj Singh Thapa, Ole Gunnar Dahlhaug and Bhola Thapa

Journal, Renewable and Sustainable Energy Reviews, Vol 49 (2015), 1100-1113. (doi:10.1016/j.rser.2015.04.178)

The paper reviews the major scientific studies conducted in the field of sediment erosion of hydro turbines. The need of further research to minimize effects of sediment erosion in Francis turbines components have been identified.

Studies of sediment in hydro turbines

Several run-off-river power plants across Asian and South American basins have reported severe cases of material erosion from turbine components due to high sediment load in the flow. Presence of hard minerals as quartz in sediment removes the base material of turbine gradually. Effects as progressive loss in turbine efficiency, increase of noise level, pressure oscillations and vibrations in components are the common consequences of the sediment erosion damage. Most of the conventional turbines manufactures have developed their turbine designs for the projects with lesser problems of sediments. Consequently, a proper solution to this age long problem in the other parts of world has not been found so far.

Studies to understand and minimize problems due to solid particle collisions have started back in 19th century. Most of the researches in past were focused to the applications for cutting industries and slurry transport phenomenon. Research on sediment erosion of hydro turbine components accelerated only on late 20th centuries and most of the publications on this area are found from the last decade. Thus, there is still need of further investigation in this subject to generate knowledge for better technology.

Several independent researches done at different times have established the factors effecting sediment erosion rate as, the factors associated with operating conditions, the factors associated with properties of the eroding particles and factors associated with the base material. More some advanced studies have shown that each of these factors have

different effects on intensity of damage depending upon specific applications and flow behavior. Thus, a general model of erosion cannot be established.

Currently practiced methods to control sediment erosion in the turbine components includes, prevention of sedimentation in the catchment areas, tapping sediments at intakes, and applying preventative coatings on the turbine components exposed to high velocity water. Studies have shown that, despite of such control measures, hydro turbines have repeatedly failed to deliver the expected performance in case of sediment-laden flows.

Future study should consider the design optimization of the turbine components as an additional field of investigation to the currently practiced methods to control sediment erosion in Francis turbine components. The design optimization goal should be directed to reduce the flow instabilities and minimize relative velocities inside the turbine, without compromise in the efficiency and life cycle cost.

2.2. Summary of Paper-B

Design and development of guide vane cascade for a low specific speed Francis turbine

Biraj Singh Thapa, Chirag Trivedi and Ole Gunnar Dahlhaug

Journal of Hydrodynamics, Ser. B., Vol 28 (2016), 676–689.
(doi: 10.1016/S1001-6058(16)60648-0)

The paper presents the methodology to design and optimize the guide vane cascade for the experimental investigations of flow conditions inside the distributor of a Francis turbine.

Guide vane cascade for a low specific speed Francis turbine

A symmetric section of reference turbine forms the flow cascade. A guide vane cascade of a low speed number Francis turbine is developed for the experimental investigations. The test setup is able to produce similar velocity distributions, at the runner inlet, as that of a reference prototype turbine. A new approach, for the hydraulic design and optimization of the cascade test setup layout, is proposed and investigated in details. Standard analytical methods are used to design the reference turbine. Stay vanes are not included as part of cascade, as they are mainly for strengthening spiral casing and do not play significant role for hydraulic design. Circular portion of spiral casing is replaced with flat plates, with the same height as that of the span of guide vane. Thus, section from inlet to outlet of cascade is embedded between two flat plates. This makes the design relatively simple and easy for manufacturing. However, such simplification would affect the flow conditions and hence the optimization of geometry of the cascade's periodic walls is necessary. CFD based optimization methods are used to define the final layout of the test setup. The optimum design is used to develop the test setup and experimental validation is conducted. The optimized design of cascade with the one guide vane is found to produce the similar flow conditions as that at the runner inlet of a low speed number Francis turbine.

2.3. Summary of Paper-C

Flow measurements in the distributor of Francis turbine: A PIV approach

Biraj Singh Thapa, Ole Gunnar Dahlhaug and Bhola Thapa

Journal, Renewable Energy, Submitted (2016).

The paper discusses results of the reference case measurements, which is without the guide vane clearance gap. Procedures for PIV measurements and data processing techniques are elaborated and generalized for the cases of similar measurements.

PIV measurements techniques and reference measurements

A 2D PIV measurement technique has been used to capture the velocity field inside the distributor of Francis turbine. A tailor made 'in-situ' calibration method has been developed for this study. Unique velocity vectors with spatial resolution of 4.7 mm and temporal resolution of 4 HZ has been computed for a flow area of 0.026 m^2. It has been estimated that minimum 100 pairs of images are needed for the statistical convergence of the velocity field. The uncertainty of the conversed velocity measurements is estimated to be ± 2.5%. The PIV measurements are done inside the flow cascade from the guide vane wall up to the guide vane mid-span in the 25 different parallel planes along the guide vane chord. Despite of absence of runner, the cascade flow is able to produce most of the flow phenomenon as in a turbine, expect the rotor-stator-interaction. The strong influence of periodic walls of cascade on the velocity distribution is observed. It is identified that flow inside the cascade between periodic positions of 50% to 80%, which represents one third of the total flow area in the meridional direction, give the most uniform velocity components. The velocity triangles, within these periodic positions, at runner inlet for the cascade, are comparable to that for the reference prototype turbine.

2.4. Summary of Paper-D

Sediment erosion induced leakage flow from guide vane clearance gap in a Francis turbine

Biraj Singh Thapa, Ole Gunnar Dahlhaug and Bhola Thapa

Journal, Renewable Energy, Submitted (2016).

The paper presents the results of pressure and velocity measurements inside the cascade with different sizes of clearance gaps between the guide vane and the wall. Characteristics of the leakage flow from the clearance gap and its effects on the main flow inside the turbine distributor has been discussed.

Characteristics of leakage flow from guide vane clearance gap

The guide vane in Francis turbines are positioned such that any two points on each side, along the same chord length, are located at different radii from turbine center. Thus, despite of uniform airfoil structure guide vane will have a pressure difference between each side along the chord. The higher pressure difference towards the trailing edge of guide vane causes higher secondary flows with vortex at the corner of the suction surface. This causes an increase in clearance gap due to higher erosion towards the guide vane trailing edge. The increase in the guide vane clearance gap induces strong cross-wise leakage flow, which produces the vortex filament for the critical size of clearance gap. The leakage flow is estimated to be close to 1% of total flow in the cascade, for the critical size clearance gap. Such a high flow rate through a narrow gap falls into turbulent regime. The results suggest that the leakage flow is drawn into the clearance gap from pressure side, uniformly in-between the leading edge and the trailing edge. The leakage flow exits out of the clearance gap from the trailing edge of suction side, between 70-90% of chord length. The leakage flow also clauses to change in the pressure distribution around the guide vane surfaces. Such change in pressure distribution increases the torque on guide vane shaft significantly and can affect the control system to regulate the guide vane openings.

2.5. Summary of Paper-E

Effects of sediment erosion in guide vane of Francis turbine

Biraj Singh Thapa, Ole Gunnar Dahlhaug and Bhola Thapa

Journal, Renewable Energy, Submitted (2016).

The paper aims to study the velocity distributions at the runner inlet of Francis turbine with different sizes guide vane clearance gaps. Efforts are made to quantify the effects on the flow parameters representing the velocity triangle at the runner inlet. Formation of vortex filament due to leakage flow and its trajectory into the runner is also investigated.

Guide vane clearance gap and the runner inlet flow conditions

The leakage flow from the guide vane clearance gap mixes with the main flow and effects all the velocity components that contributes to design and performance of the runner. The leakage flow, with clearance gap more than 1 mm, is found to change the velocity components and blade loading, in both the circumferential direction and in the span wise direction, at the runner inlet. The case with clearance gap 2 mm is found to have the highest effects on the flow velocities and is considered as the critical size. For the critical size of clearance gap, the relative velocity at the runner inlet is found to increase up to three times locally. This local increase in relative velocity is identified as the cause to have very high erosion at the runner hub, in sediment-laden projects. Formation of corner vortex between guide vane and walls, in absence of clearance gap has been observed from this study. A leakage vortex, with the higher strength than that of the corner vortex, occurs with the case of flow with the clearance gap. Both the corner vortex and the leakage vortex originates from the suction side of guide vane at about 75% of chord, close to the wall. The leakage vortex is drawn towards the mid-span as flow progresses down stream of guide vane. The leakage vortex is observed to pass into the runner with the flow.

3. List of other relevant publications

- Biraj Singh Thapa, Ole Gunnar Dahlhaug and Bhola Thapa, "Velocity and pressure measurements in guide vane clearance gap of a low specific speed Francis turbine", in *Proc. of 28th IAHR symposium on Hydraulic Machinery and Systems*, 4-8 July 2016, France.
- Sailesh Chitrakar, Biraj Singh Thapa, Hari Prasad Neopane, Ole Gunnar Dahlhaug, and Bhola Thapa, "Numerical investigation of the flow phenomena around a low specific speed Francis turbine's guide vane cascade", in *Proc. of 28th IAHR symposium on Hydraulic Machinery and Systems*, 4-8 July 2016, France.
- Biraj Singh Thapa, Ole Gunnar Dahlhaug and Bhola Thapa, "Flow field measurement in guide vane cascade of a high head Francis turbine", in *Proc. of 6th Int. Conf. On Water Resources and Hydropower Development in Asia*, 1-3 March 2016, Lao PDR.
- Balendra Chhetry, Bhola Thapa, Biraj Singh Thapa, "Assembly design to ease turbine maintenance in sediment-laden conditions", *The International Journal on Hydropower & Dams* (2014), Issues 2, 82–88.
- Subash Panth, Manish Lamsal, Bhola Thapa, Biraj Singh Thapa, "Prediction of turbine needed for hydro power projects in Nepal", *Hydro Nepal: Journal of Water, Energy and Environment* (2014), Issue14, 23-26.

4. Conclusions

In the presented work, the experimental investigations of flow around guide vanes of low specific speed Francis turbine have been carried out. A simplified 'one guide vane cascade' test setup has been developed to create the flow conditions inside the distributor of a low specific speed Francis turbine. Velocity and pressure measurements are done with different sizes of clearance gap between guide vane walls and cover plate. NACA 0012 airfoil has been taken as a reference profile to shape test guide vane for this study. The measurements are done with the flow conditions of the turbine Reynold's number 1.15E+07. PIV methods are applied to capture the 2D velocity field inside the cascade. Flow velocity exceeding 35 m/s, at the runner inlet of Francis turbine, is reported for the first time from such experimental studies.

The results for the reference measurements, which is without the clearance gap, gives information about the velocity and the pressure distribution around the guide vane surface. It is found that the guide vane shaped with symmetric NACA profile induces high velocities and adverse pressure gradients towards the trailing edge. These flow conditions causes to from a corner vortex from the suction side of the guide vanes. In case of sediment-laden projects, the corner vortex add turbulence to the sediments, which accelerates the erosion rates at the guide vanes and the cover plates. Such erosion causes the clearance gap between the guide vanes and the cover plates to increase by multiple times from its design value. The results show that the highest pressure difference between the adjacent guide vane surfaces is equivalent to 20% of net hydraulic head acting on the turbine. The location of the highest pressure difference is found to be at 75% of guide vane chord from the leading edge. The high differential pressure between the guide vane surfaces is sufficient to force a cross-wise leakage flow through increased the clearance gap due to erosion of guide vanes and cover plates.

The measurements with different sizes of the clearance gap give an overview of the flow field inside the distributor of Francis turbine with eroded guide vanes. It is found that the clearance gap up to 0.5 mm can be accepted without significant effects of the leakage flow on the main flow inside the distributor. All the sizes of clearance gap larger than 1 mm induces cross-flow, like a jet, which mixes with the main flow and disturbs the runner inlet flow conditions. The position of the cross-flow matches with the position of the highest pressure gradient across the guide vane surfaces. The maximum velocity of the cross-flow through the clearance gap is measured to be 50% of mainstream velocity. It is identified that the high velocity cross-flow blocks the flow passage at the suction side of guide vane and hence changes the pressure distribution around the guide vane surfaces. Such changes in the pressure distribution increases the torque on guide vane shaft up to 28%. The increase

of torque on guide vane shaft can affect the performance of the control system to regulate the guide vane openings.

The case with clearance gap of 2 mm is found to have the highest effects on the flow velocities and is considered as the critical size for this study. Such critical size of clearance gap has to be avoided as far as possible. For the critical clearance gap, the total cross-wise leakage flow is measured to be more than 1% of the main flow. Such a high flow rate through the narrow gap falls into turbulent regime with the Reynold's number in order of 3E10+4. For the critical size of clearance gap, the relative velocity at the runner inlet is found to increase locally up to three times from its design value. This local increase in the relative velocity is identified as the cause of the severe erosion at the runner hub, as that has been repeatedly observed in the sediment-laden projects.

A vortex filament is found to be developed due to the mixing of the leakage flow with the main flow, and is observed to pass into the runner. The leakage vortex is drawn towards the mid-span as flow progresses down stream of guide vane. Further investigation of interaction of the leakage vortex with the runner's performance is necessary.

5. Future works

The test conditions for this study was limited to the guide vane opening angle corresponding to the best efficiency point of the reference prototype turbine. Study of the leakage flow and its effects on velocity distributions at the operating points away from the best efficiency point is equally necessary. The current study is conducted with a single design of guide vane geometry with NACA 0012 profile. Alternative designs of guide vane geometry, to minimize the leakage flow, is necessary.

The 'one guide vane cascade' test setup, as developed for this study, bears significant effects from the periodic walls on the flow velocities. Further studies should be made with a three-guide vane cascade setup, as outlined in Paper-B. It is also recommended that such setup should try to avoid the simplifications on spiral casing section as done for this study.

The vortex developed due to cross-wise leakage flow from the clearance gap need more investigations. It will be very interesting and important to know if such vortex is dissipated by the effects of runner's presence in the flow field, or does it manage to inter the runner and interact with the flow instabilities inside the runner and the draft tube. Numerical studies validated with the experimental results from this study can be implemented for such analysis.

The guide vane torque needs to be studied in more detail than that done in this work. The location of guide vane axis should be optimized for the minimum torque on the guide vane shaft, for the wide range of turbine operation.

The analysis of results for this study are made with the time averaged velocity vectors assuming the steady state flow conditions. Study of instantaneous velocity field with high temporal and spatial resolutions can give better understanding of the flow phenomenon. However, such study demands better PIV instrumentation than that used for this study.

A simplified case of guide vane erosion, with a uniform increase in clearance gap, has been considered for this study. Observations have shown that erosion of guide vane occurs in much complex manner. Tests with guide vane geometry close to the actual eroded pattern will give more realistic conclusions. 3D scanning and re-printing of the eroded guide vane can be done with the available technology for such studies.

6. Abbreviation

CFD	Computational Fluid Dynamics
FSI	Fluid Structure Interaction
KU	Kathmandu University
NACA	National Advisory Committee for Aeronautics
NTNU	Norwegian University of Science and Technology
NVKS	Norwegian Hydropower Center
PIV	Particle Image Velocimetry

7. Bibliography

[1] J. Twidell and T. Weir, *Renewable energy resources*: Routledge, 2015.

[2] "2016 Key trends in hydropower," International Hydropower Association, (https://www.hydropower.org/2016-key-trends-in-hydropower).

[3] O. Edenhofer, R. Pichs Madruga, Y. Sokona, P. United Nations Environment, O. World Meteorological, C. Intergovernmental Panel on Climate, *et al.*, *Renewable energy sources and climate change mitigation : special report of the Intergovernmental Panel on Climate Change*. New York: Cambridge University Press, 2012.

[4] Y. Matsuo, A. Yanagisawa, and Y. Yamashita, "A global energy outlook to 2035 with strategic considerations for Asia and Middle East energy supply and demand interdependencies," *Energy Strategy Reviews,* vol. 2, pp. 79-91, 2013.

[5] J. D. Milliman and R. H. Meade, "World-wide delivery of river sediments to the oceans," *Journal of Geology,* vol. 91, pp. 1-21, 1983.

[6] D. L. Higgitt and X. X. Lu, "Sediment delivery to the three gorges: 1. Catchment controls," *Geomorphology,* vol. 41, pp. 143-156, 2001.

[7] S. Panta, M. Lamsal, B. Thapa, and B. S. Thapa, "Prediction of Turbine Needed For Future Hydropower Projects in Nepal," *Hydro Nepal: Journal of Water, Energy and Environment,* vol. 14, pp. 23-26, 2014.

[8] H. Brekke, "Hydraulic Turbines: Design, Erection and Operation," *Norwegian University of Science and Technology (NTNU) publications,* 2001.

[9] M. K. Padhy and R. P. Saini, "A review on silt erosion in hydro turbines," *Renewable and Sustainable Energy Reviews,* vol. 12, pp. 1974-1987, 2008.

[10] R. Koirala, B. Thapa, H. P. Neopane, B. Zhu, and B. Chhetry, "Sediment erosion in guide vanes of Francis turbine: A case study of Kaligandaki Hydropower Plant, Nepal," *Wear,* vol. 362–363, pp. 53-60, 2016.

[11] M. Singh, J. Banerjee, P. L. Patel, and H. Tiwari, "Effect of silt erosion on francis turbine: A case study of Maneri Bhali stage-II, Uttarakhand, India," *Journal of Hydraulic Engineering,* vol. 19, pp. 1-10, 2013.

[12] H. K. Sharma, "Power generation in sediment laden rivers: The case of Nathpa Jhakri," *International Journal on Hydropower and Dams,* vol. 17, pp. 112-116, 2010.

[13] T. R. Bajracharya, B. Acharya, C. B. Joshi, R. P. Saini, and O. G. Dahlhaug, "Sand erosion of Pelton turbine nozzles and buckets: A case study of Chilime Hydropower Plant," *Wear*, vol. 264, pp. 177-184, 2008.

[14] O. G. Dahlhaug, P. E. Skåre, V. Mossing, and A. Gutierrez, "Erosion resistant coatings for Francis runners and guidevanes," *International Journal on Hydropower and Dams*, vol. 17, pp. 109-112, 2010.

[15] B. Chhettry, B. Thapa, and B. S. Thapa, "Assembly design to ease turbine maintenance in sediment-laden conditions," *International journal on hydropower and dams*, pp. 82-88, 2014.

[16] B. S. Thapa, B. Thapa, and O. G. Dahlhaug, "Current research in hydraulic turbines for handling sediments," *Energy*, vol. 47, pp. 62-69, 2012.

[17] B. S. Thapa, B. Thapa, M. Eltvik, K. Gjosater, and O. G. Dahlhaug, "Optimizing runner blade profile of Francis turbine to minimize sediment erosion," presented at the IOP Conference Series: Earth and Environmental Science, 2012.

[18] O. Reynolds, "On the action of a blast of sand in cutting hard materials," *Philos. Mag. (Fourth Ser.)*, vol. 46, pp. 337-343, 1873.

[19] I. Finnie, "Erosion of surfaces by solid particles," *Wear*, vol. 3, pp. 87-103, 1960.

[20] G. F. Truscott, "A literature survey on abrasive wear in hydraulic machinery," *Wear*, vol. 20, pp. 29-50, 1972.

[21] H. Brekke, "Design of hydraulic machinery working in sand laden water," in *Abrasive erosion and corrosion of hydraulic machinery*, C. G. Duan and V. Y. Karelin, Eds., ed London: Imperial college press, pp. 155-181, 2002.

[22] B. Thapa, "Sand erosion in hydraulic machinery," PhD thesis, PhD thesis, Norwegian University of Science and Technology, Faculty of Engineering Science and Technology, 2004.

[23] H. P. Neopane, "Sediment erosion in hydro turbines," Monoghraph, PhD thesis, Norwegian University of Science and Technology, Faculty of Engineering Science and Technology, 2010.

[24] M. Eltvik, "Sediment erosion in Francis turbines," PhD thesis, Norwegian University of Science and Technology, Faculty of Engineering Science and Technology, 2013.

[25] K. Gjosater, "Hydraulic Design of Francis Turbine Exposed to Sediment Erosion," Masters Thesis, Norwegian University of Science and Technology, 2011.

[26] B. S. Thapa, "Hydraulic design of Francis turbine to minimize sediment erosion," Masters Thesis, Kathmandu University, 2012.

[27] S. Chitrakar, M. Cervantes, and B. S. Thapa, "Fully coupled FSI analysis of Francis turbines exposed to sediment erosion," *International Journal of Fluid Machinery and Systems*, vol. 7, pp. 101-109, 2014.

[28] B. Rajkarnikar, D. H. P. Neopane, and B. S. Thapa, "Comparative study of sediment erosion on alternative designs of Francis runner blade," *International Journal of Fluid Machinery and Systems*, vol. 8, pp. 183-192, 2015.

[29] H. Brekke, "The influence from the guide vane clearance gap on efficiency and scale effect for Francis turbines," in *Proc. 14th IAHR Symposium on Progress within Large and High-Specific Energy Units*, pp. 825-837, 1988.

[30] B. Chhetry and K. Rana, "Effect of Sand Erosion on Turbine Components: A Case Study of Kali Gandaki "A" Hydroelectric Project (144 MW), Nepal," *Hydro Nepal: Journal of Water, Energy and Environment*, vol. 17, pp. 24-33, 2015.

[31] R. Koirala, B. Zhu, and H. P. Neopane, "Effect of guide vane clearance gap on Francis turbine performance," *Energies*, vol. 9, 2016.

[32] X. Chen, "Theoretical and experimental study of flow through the double cascade of a Francis turbine," PhD thesis, Norwegian University of Science and Technology, Faculty of Engineering Science and Technology, 1992.

[33] S. Eide, "Numerical analysis of the head covers deflection and the leakage flow in the guide vanes of high head Francis turbines," 2004.

[34] IEC, "Hydraulic turbines, storage pumps and pump-turbines – Model acceptance tests 2nd edn 1999-11," in *IEC 60193*, ed: The International Electro technical Commission, 1999.

Part II

Papers

Main Papers

Papers A-E

Paper-A

Sediment erosion in hydro turbines and its effect on the flow around guide vanes of Francis turbine

Biraj Singh Thapa, Ole Gunnar Dahlhaug and Bhola Thapa

Published in Journal of Renewable and Sustainable Energy Reviews, Vol 49 (2015), 1100-1113

(doi:10.1016/j.rser.2015.04.178)

Sediment erosion in hydro turbines and its effect on the flow around guide vanes of Francis turbine

Biraj Singh Thapa [1]; Ole Gunnar Dahlhaug [1]; Bhola Thapa[2]

[1]Department of Energy and Process Engineering, Norwegian University of Science and Technology, Norway

[2]Department of Mechanical Engineering, Kathmandu University, Nepal

Abstract

Erosion of material surface due to collision of solid particles has been a challenge to several fields of engineering. Despite of centuries of investigations and research, the exact phenomenon of erosion of surface by the solid particles has not been fully understood. Increasing number of hydropower plants are being built in the regions where rivers are heavily loaded with sediments. This induces material erosion in hydro turbines, leading to change in flow pattern, losses in efficiency, vibrations and even final breakdown of turbine components. To overcome sediment erosion related failures, development of erosion resistant alloys, coatings of the components, and optimization of hydraulic design of the components, are the important practices. In Francis turbines, erosion causes increase of clearance gap between guide vanes and facing plates and cross flow occurs from this increased gap. This cross flow together with other secondary flows disturbs the velocity profile at the runner inlet. Change in velocity profile at the inlet causes additional erosion damage and other undesired effects in the turbine runner. Most of the past studies in Francis turbine were focused to understand the flow phenomenon inside the turbine components and to analyze their effects on design improvements. There is still a need of further fundamental research to understand the effects of sediment erosion of turbine components on the flow phenomenon, and developing better designs of hydro turbines to minimize those effects.

Keywords: Sediment erosion, Francis turbine, Guide vane, Secondary flow, Efficiency

1. Introduction

Global primary energy consumption will increase about 1.5 fold, from 11,743 Mtoe in 2010 to 17,517 Mtoe in 2035 [1]. Fossil fuels account for about 90% of primary energy consumption at present. Due to its unsustainability, and environmental and health effects, alternative and clean resources of energy have to be tapped further more in future. With

about 15% of global electricity supply, hydropower serves as the major contributor of renewable and sustainable source. The theoretical reserve of hydro energy is 39,097 TWh/yr, with a technical availability about 14,653 TWh/yr and an economic availability about 8,728 TWh/yr [2]. By 2007, the installed capacity of economically available hydropower resources worldwide has crossed 35%, with Europe and North America having highest degree of development equaling 71% and 65% respectively. **Figure 1** shows the distribution of total hydropower potential across the different region of world. Most of the untapped hydro energy resources lies South Asian and South American countries, where demand of energy is the highest and will keep growing for some decades as huge population is in the transition phase of poverty and development [3]. However, both of these regions suffer from soil erosion due to weak geological formation and heavy precipitation in short time interval causing floods. In the central Himalaya and Ganges plain, more than 80% of annual rainfall occurs during the Indian summer monsoon season (May–October) [4]. This causes drastic increase of sediment concentration in rivers every year.

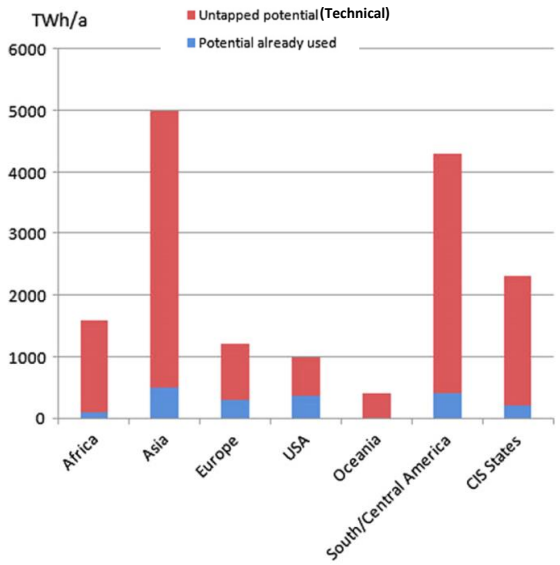

Figure 1. Hydropower potential, untapped and already uses power. Adapted from [3]

Run off the river hydropower projects across these region suffers several operational and maintained challenges, which are often associated with financial losses. The concentration of sediments in the rivers during extreme conditions can reach up 57,000 ppm and the amount of hard minerals in sediments is as high as 80% [8]. Loss of turbine efficiency in a power plant in Nepal, due to sediment erosion damage, has been measured to be 4% and 8% respectively in full load and part load conditions, within the short operational period of 01 September to 11 November, 2003 [8]. Sediment monitoring in the same period have

indicated that approximately 6900 tons of sediment had passed through this unit during the test period.

Similar cases of sediment erosion of turbine components and associated losses have been reported from power plants from India [9], Bhutan [10] and also from South American continents [7]. **Figure 2** shows typical damages of hydro turbine components from different power plants operating under heavy sediment load. Comparable patterns of turbine erosion, operational challenges and performance losses have been observed from different power plants, operating in sediment environment, across the continents.

48 MW*3 Francis turbine at Kaligandaki Power plant, Nepal [5]

250 MW*6 Francis turbine at Nathpa Jhakri Power plant, India [6]

23 MW*2 Francis turbine at Chawa Power plant, Peru [7]

Figure 2. Sediment erosion in Francis turbine runners from various Power plant

Several methods have been developed and implemented to stop or reduce sediments reaching and damaging the turbine components. Important and conventional ones include, prevention of sedimentation in the catchment areas [11], tapping sediments at intakes [12], applying preventative coatings on the turbine components exposed to high velocity water [13] and also shutting down the power plant in excessive sediment loads intakes [14]. Despite of these efforts erosion damage of turbine components has remained as a major challenge of hydropower development under the Himalayan and Andes basins. This has generated much interest among the researchers to find the alternative and sustainable solution to this age-old problem. A new method of manufacturing Francis turbine has been developed to allow protective coatings to be applied on all the surfaces of runner and guide vanes [15]. The components of turbine runner are fabricated separately and are bolted together after high velocity oxy-fuel (HVOF) coating has been applied very precisely. This technique has shown better performance compared to the conventional methods in 42 MW Chawa hydropower plant in Peru.

Recent studies have shown that the geometric profile of runner blade of Francis turbines can be optimized to reduce relative velocity of water and hence sediment erosion of the blades itself [16]. Analytical tool has been developed and several design options were

investigated. It has been proposed that with the new design methods, sediment erosion in Francis runner blades can be reduced by 30%. However, from numerical studies it was also found such design concepts will accelerate erosion in guide vanes due to change in flow around guide vanes [17]. Hence, there is still need of further investigation for reducing sediment erosion damage in Francis turbine components by design optimization.

2. Erosion wear in engineering materials and hydro turbines

References to scientific studies on abrasion of hard minerals by sand particles can be found from 1873 [18]. A comprehensive work on erosion of surfaces by solid particle has been published by Finnie on 1960 [19]. This work includes literature review of past research followed by theoretical and analytical analysis of the erosion with experimental validations. He categorized his studies to two main types of material behavior, ductile and brittle. It was observed that the ductile materials will undergo weight loss by the process of plastic deformation in which material is removed by the displacing or cutting action of the eroding particle. In a brittle material, on the other hand, material will be removed by the intersection of cracks, which is caused by the impact of the eroding particle. Based on this theory and also from earlier studies it was concluded that in general ductile material will have maximum erosion at the jet angle close to 30° and that for brittle materials that will occur at the jet angle close to 90°. Analytical equations were also developed to predict the erosion in both ductile and brittle materials and experiments were conducted on standard engineering materials for comparison. In latter publication Finnie [20] has summarized his understandings on the mechanisms of material removal in ductile and brittle solids. He has also discussed the erosion behavior for the materials in brittle-ductile transition in this work. **Figure 3** shows the erosion resistance of various engineering materials (grams of abrasive per mm^3 of base material removed) as the function of their hardness. It can be observed that for the softer materials, hardness has significant effects on erosion rates, but there is no general correlation for material with Vickers hardness above 200 kg/mm^2. Similar studies have also been conducted by Tilly [21] to study the effects of size of eroding particles on erosion rates. He found that engineering materials exhibit an initial increase in erosion with particle size until the onset of a saturation plateau, and then it is independent of size. The onset of the plateau is itself dependent upon flow velocity. **Figure 4** shows influence of particle size on erosion of different materials and plastics.

An intensive study on abrasive wear in hydraulic machinery in general has been conducted by Truscott [22] and was published in 1972. It reviews findings from most of the peer and earlier researchers to identify the various types of wear and the factors affecting them. The properties of the solid particles, the construction materials and the flow intensity were also investigated in details. He has come to following conclusions:

- Erosion is correlated to the velocity of solid particle, as erosion $\propto$ velocity^n, where the value of exponent ‘‘n’’ varies with material and other operating conditions.

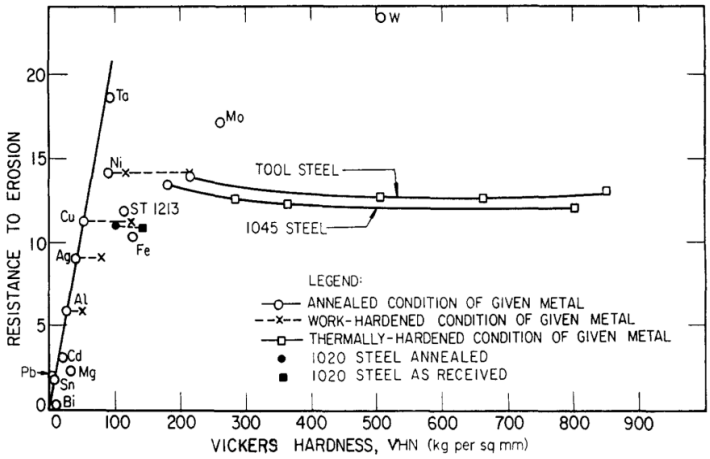

Figure 3. Resistance to erosion as a function of the VHN of the material before erosion. Adapted from Finnie [20]

- Wear increases rapidly when the particle hardness exceeds that of the metal surface being abraded.
- Wear increases generally with grain size, sharpness and solids concentration. Metal hardness is not an absolute criterion of wear. A reasonable resistance appears to be achieved above about 300 HB. The very hard alloys (e.g. tungsten carbide) and surface treatments are extremely resistant.
- Soft rubber appears generally more resistant than hard ones. Plastics coatings do not appear very promising for erosion resistance. Ceramics are very wear resistant, but their use has been limited by brittleness and susceptibility to thermal shock.
- Impact angle has a marked effect on wear; metals and rubbers behave in opposite ways.
- Good hydraulic design, particularly by avoiding rapid changes in flow direction, decreases wear.
- Rubber lining can give a much-increased life compared to that for metal, provided that the solids are not large or sharp, bonding is good, and operating head is relatively low.

- Soft-packed shaft glands require grease or clean water flushing supply for protection against sediment erosion.
- No outstanding new construction materials, suitable for commercial application to a wide range of machine sizes, have been reported to the date.

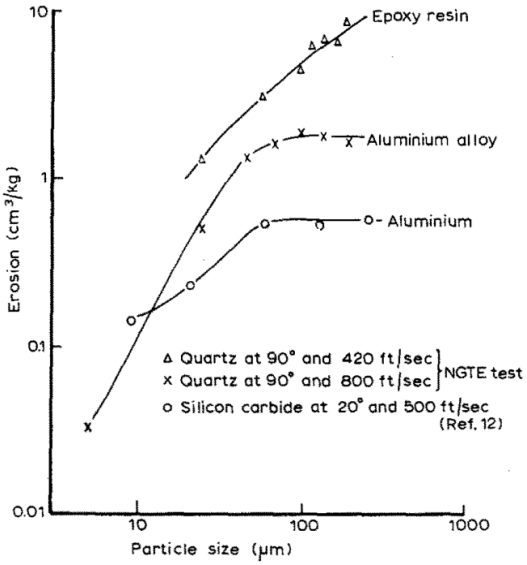

Figure 4. Influence of particle size on erosion. Adapted from Tilly [21].

Brekke [23] has made a very detailed investigation of sediment erosion in Hydraulic turbines. Cases of erosion in several hydropower plants were investigated and theoretical discussions were made. He has categorized the sediment erosion of hydraulic machinery into: (i) micro erosion due to fine particles (<60 μm) at high velocity (ii) secondary flow vortex erosion caused by obstacles or secondary flow (iii) erosion due to acceleration of large particles (> 0.5mm). He found that nozzle, needle and buckets are most affected components of Pelton turbine. Similarly, runner, guide vanes, facing plates and labyrinth seals are most affected components of Francis turbine. It has been proposed the basic design criteria for Pelton runners operating in sand laden water as, buckets with largest possible curvature and size, lowest number of jet and largest hydraulic radius. Similarly for Francis turbines smooth acceleration in guide vane, stay vane outlet angle to keep guide vane at neutral position in normal operation condition are important design criteria. It was also recommended that, to minimize effect of sand erosion, Pelton turbines should be preferred to Francis in overlapping zone of turbine selection diagram, lowest number of units and lowest possible speed should be selected.

A systematic study of sediment erosion in hydro turbines and components has been done in a PhD studies by Thapa [24]. Sediment samples from all the major basins in Nepal were collected and processed. Analysis was done to identify particle size distribution, type, and amount of hard particle distribution in samples. Laboratory tests were conducted in a high-velocity test rig to quantify erosion rates of different samples on different turbine materials and coatings. **Figure 5** shows the test rig used for this study. Baskarp-15 foundry sand with mean size of 0.15 mm was used as erosive particles in the tests. Flow rate was varied within the range of 20 m/s to 80 m/s and sediment concentration 0.38% (by volume) to 0.75% respectively. It was found that Turbine steel 13Cr4Ni and duplex steel SAF-2304 shows better erosion resistance in all operating condition. Turbine steel 13Cr1Ni has shown poorest erosion resistance, and turbine steel 16Cr5Ni have shown relatively higher erosion rate than 13Cr4Ni and duplex steel. He has also made field observations and measurement, which concluded that, due of sand erosion, the largest drop in efficiency for the Francis turbine is at part load, and that in Pelton turbine is at the best efficiency point.

Padhya [25] has conducted review of sediment erosion in hydro turbines including major theoretical investigations, experimental studies and case studies published till 2008. After detail investigations, she concluded that sediment erosion in hydro turbines cannot be avoided completely, but can be reduced to an economically acceptable level. She has also found that despite of design changes in the turbine components and providing different materials and coatings to the turbine blades, the improvement in most cases are not quite significant.

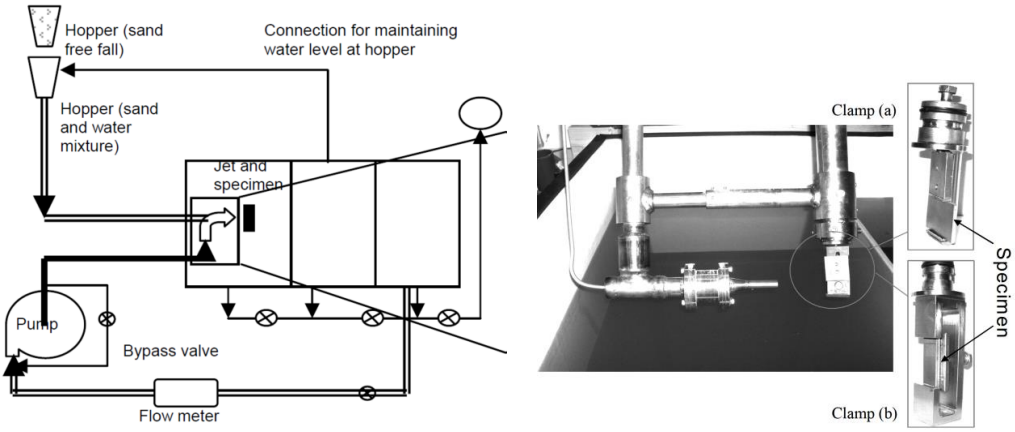

Figure 5. High velocity jet erosion test rig. Adapted from Thapa [24]

An attempt to develop empirical relations to quantify sediment erosion and consequent efficiency loss in Francis turbine has been done by Thapa [26]. He has reviewed the previous works on erosion models for hydraulic machineries. Based on the findings from

earlier studies and erosion models presented in IEC-62364 codes [27], an improved erosion model to estimate erosion rate in turbine runner blades and annual loss in runner efficiency, has been proposed as follows.

$$E_r = C \cdot K_{hardness} \cdot K_{shape} \cdot K_m \cdot K_f \cdot a \cdot (size)^b \quad \textbf{(mm/yr)} \quad \textbf{Eq. 1}$$

$$\eta_r = c \cdot (E_r)^d \quad \textbf{(\%/yr)} \quad \textbf{Eq. 2}$$

Where the symbols are defined as:

a,b	*empirical constants:* *a = 351.35, b = 1.4976 for quartz content of 38%, a = 1199.8, b = 1.8025 for quartz content of 60%, a = 1482.1, b = 1.8125 for quartz content of 80%.*
c,d	*empirical constants c = 0.1522 and d = 1.6946*
η_r	*loss in runner efficiency per year due to erosion alone*
size	*Median diameter d_{50} of particles, mm*
C	*silt concentration, kg/m^3*
K_f	*factor that characterizes how the abrasion relates to the water flow around each component*
$K_{hardness}$	*fraction of particles harder than the turbine material*
K_m	*factor that characterizes the abrasion relates to the material properties of the base material*
K_{shape}	*shaper factor of particle*

The improved erosion model estimated drop in efficiency of the runner alone for Jhimruk Hydroelectric Center in Nepal to be 1% per year, which was found to be consistent to the results of field measurements.

Relation between sediment erosion and cavitation erosion in hydraulic turbines has been studies by Thapa [28]. An experimental setup named as rotating disc apparatus (RDA) was developed to simulate a submerged body moving with the speed of around 39 m/s, with and without sediments. Cavitation inducers were installed at equidistant circumferential points in the disc half coated with Tungsten-Carbide coating (86WC-10Co-4Cr) using

HVOF methods. Cases of pure cavitation, pure sand erosion and combine cavitation and sand erosion were observed and analyzed. Painted disc with cavitation inducers were used for observation of pure cavitation, controlled amount of sand without cavitation inducers were used for pure sand erosion observation, and both sand and cavitation inducers were used for observation of combined effects. **Figure 6** shows the progressive erosion pattern due to combined effect of sand erosion and cavitation in uncoated region for a total test period of 4.5 hours with the sand of sieve size ranging from 90-212 micron. It was found that a synergic effect of cavitation and sand erosion is stronger than the individual effects. It was also observed that cavitation was less significant on HVOF coated parts but the combined effect of sand erosion and cavitation was significant. A good review paper on studies of cavitation on hydro turbines has been is published by Kumar [29]. Another review paper on combined effect of cavitation and sediment erosion in hydro turbines has been published by Gohil [30].

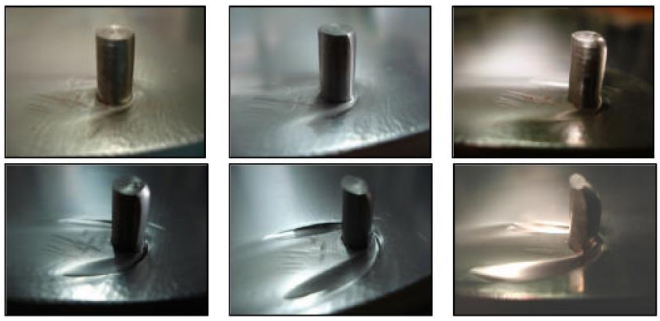

Figure 6. Progressive erosion pattern caused by combined sand erosion and cavitation in uncoated region of test disc with total test duration of 4.5 hours with measurements at 30 Min, 45 Min, 60 Min, 90 Min, 180 Min, 270 Min. Adapted from Thapa [28]

Several methods and setups for experimental investigations of sediment erosion on turbine materials in general have been developed, a good example is set by Abouel-Kasem [31]. However, there has been very less laboratory experiments on real turbine components. Rajkarnikar [32] has developed a more realistic method and setup to compare effects of sediment erosion in alternative designs of Francis runner blades. Especially casted specimens of the scaled model of Francis runner blades were bolted in a rotating disc at the angle representing actual inlet flow conditions. **Figure 7** shows the design of the test setup with the runner blades mounted on the rotating disc. The disc is placed in a closed housing with water and sediment mixture and is driven by motor up to the speed of 1400 rpm. Patterns of erosion on the blades were observed by removal of painted surface on the blade after an operation time of 30 minutes. The rate of material removal due to sediment erosion

was estimated by the measurement of weight loss from the blades after successive time intervals. Two alternative designs of the runner blades developed from separate studies were tested. **Figure 8** shows the observation of erosion pattern on the blades. The location of paint removal was found to be identical to the pattern of wear observed in the turbines operating in the real cases and also close to that predicted by CFD simulations. **Figure 9** shows the eroded blades after 350 minutes of operation. Some defects in casting of blades were also detected. Higher erosion in reference design can be observed than that in the optimized design. **Figure 10** shows the measurements of the erosion rate of the both designs of runner blades from this test setup. It can be seen that optimized design has considerably low erosion rates than the reference design. Thapa [33] has published a comprehensive documentation of similar research activities at Kathmandu University, Nepal over a period of a decade for understanding the causes, and minimizing the effects of sediment erosion in hydro turbines.

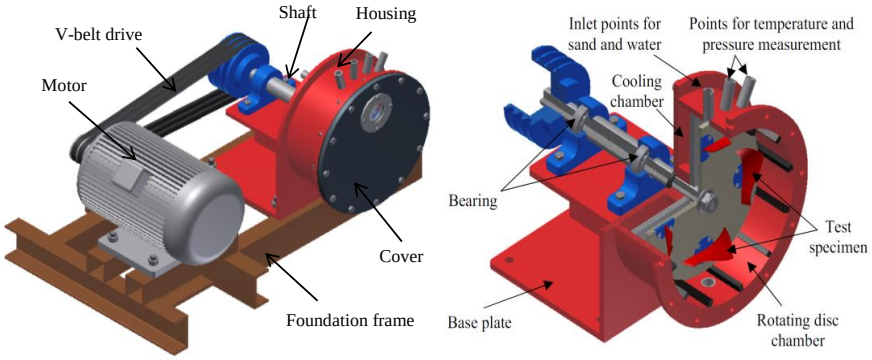

Figure 7. Test setup for study of sediment erosion on Francis runner blades. Adapted from Rajkarnikar [32]

Application of preventive coatings on material surface to avoid erosion, cavitation, corrosion and their combination has been practiced in several field of engineering. Application of such protective coatings in hydro turbines are immerging technologies and advanced form of those are also referred to as the "Nano Technology" [34]. An intensive investigation of the behavior of various compositions and morphologies of coatings, applied with alternative different processes, in erosion and erosion-corrosion environments has been done by Levy [35]. A study on more specific application of protective coatings to avoid cavitation and erosion damage in hydraulic turbine components is conducted by Singh [36]. This work reviews the base material properties and performance of various types of protective coatings on hydro turbines components in the cavitation and sediment environment. It has been reported that the performance of the coatings is dependent on

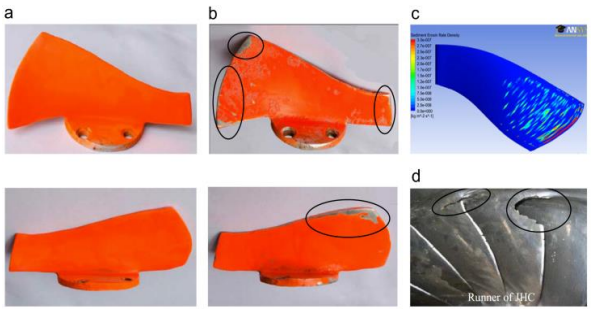

Figure 8. Observation of erosion patterns (a) Test specimen before test. (b)Test specimen after 30min. (c) Result of CFD analysis. (d) Eroded runner of JHC. Adapted from Rajkarnikar [32]

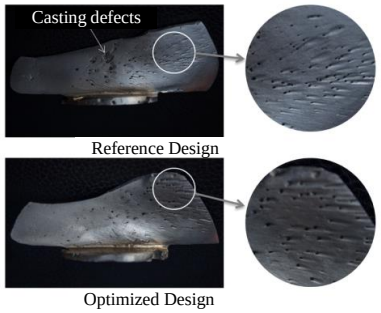

Figure 9. Observation of eroded surface after 130 mins. Adapted from Rajkarnikar [32]

several parameters, such as ratio of the size of coating particles to the erodent, relative hardness, shape of the erodent, and conditions of the flow. Both metallic (e.g. composite carbid based Ni, Cr, and Co coatings) and nonmetallic coatings (e.g. polyurethane elastomers, epoxy resin and polymer coatings) have shown better performance in turbine materials. Thermal spray based methods, such as arc plasma spraying, detonation gun, and high velocity oxy-fuel, have been commercially used to apply coatings on the components of hydro turbines. He has also observed that the combination of hardness and toughness in the Tungsten-carbide coating (80WC-20CrC) by HVOF methods led to the superior performance of 13Cr-4Ni stainless steel against both erosion and abrasion. However, coatings applied by the conventional methods as has several physical interphases, which are considered weak areas where mechanical, and electrochemical failures may originate. It has been outlined that the failures of coatings by micro-cracking, dis-bonding, and the dig-out of embedded ceramic are the present challenges to improve performance of coatings in sediment environment.

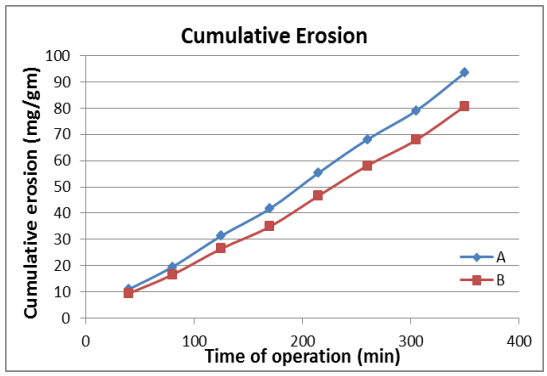

Figure 10. Measurements of erosion rates on alternative designs. Adapted from Rajkarnikar [32]

Thapa [24] has ranked erosion resistance of ceramic coatings in term of volume loss per unit striking particle as (75Cr3C2-25NiCr) > (86WC-10Co-4Cri) > (86WC-6Co-8Cr). It was also found that Polymers and Elastomer coatings are not appropriate for hydropower

turbine components. A thorough experimental investigation on HVOF sprayed WC coating has been done by Goyal [37]. WC-10Co-4Cr and Al_2O_3+13TiO_2 coatings were deposited on CF8M turbine steel by HVOF spray process and studied with regard to their performance under slurry erosion conditions. High speed erosion test rig was used for these tests and effects of parameters including average sediment size, speed and concentration on the erosion of these materials were investigated. It was found that the bare steel and Al_2O_3+13TiO_2 coating followed ductile and brittle mechanisms respectively under slurry erosion, whereas the WC-10Co-4Cr coating exhibited mixed behavior (mainly ductile). WC-10Co-4Cr coating was found to be useful to increase the sediment erosion resistance of steel.

These studies have shown that erosion damage of surfaces due to sediment particles is very difficult to predict, and despite of great efforts have been made to develop the erosion/cavitation resistant materials and coatings, the problem of cavitation/sediment erosion in hydro turbine components yet remains unsolved.

3. Design and sediment erosion of guide vanes of Francis turbines

Francis turbine is a reaction machine, which converts both pressure energy and kinetic energy in fluid to the mechanical energy at the runner. The conversion of a part of this pressure energy in the fluid into the kinetic energy is done by guide vanes (GV). Guide vanes, which are also called as wicket gates, also direct the fluid on to the runner blades at an angle appropriate to the design, imparting a tangential velocity and hence an angular momentum to the water before it enters to the runner. Moreover, the GV are pivoted and can be controlled by using a suitable governing mechanism to regulate the flow while the load in the generator changes.

General design criteria of GV are mainly based on, correct flow angles with minimum resistance, low governing forces and stable at full opening position incase disconnected with governing system. Basic design principles and dimensioning criteria of GV for high head Francis turbines are discussed by Wei [38]. Often NACA airfoils are good choice for shaping of GV however, optimization of profiles and dimensions are often done to maximize the overall design efficiency and facilitate the operational constraints. Design of GV is usually combined together with the design of stay vanes and both components as a single unit in a reaction turbine is often called as the distributor system. Alnaga [39] has developed an automatic iterative procedure for optimal design of Francis turbine distributors. This procedure is based on the geometry parameterization of the distributor to facilitate the fully automatic generation of the design by modifying the geometry parameters. Evolutionary algorithms in optimization techniques were applied to define the best design parameters using the optimal functions evaluated from CFD simulations. Three parameters were identified to define the objective function of design optimization.

The first parameter is related to the energetic losses computed as the inlet/outlet total pressure variation. The second parameter, related to flow disturbance, is the outlet angle variation. And the third parameter, related to the geometry cost, corresponds to the spiral casing surface. Optimization method was applied to two examples of Francis turbine distributors, with a specific speed (n_q) equal to 81 and 48. Two new geometries with best efficiency were obtained and performance was compared with the initial ones. The results from this optimization process showed that turbine efficiency improvement was approximately 1.5%, while spiral casing surface reduced by (3-5) % and energetic losses were limited to (1-2) %.

For a reaction machines the ratio of drop of pressure energy across runner to the net available energy is often called as the reaction ratio. Normally Francis turbines are designed with a reaction ratio of 0.5. In such designs, the available pressure energy in fluid at spiral casing is converted into 50% kinetic energy before entering the runner. Thus, a huge acceleration of fluid from inlet to outlet of GV can be expected. **Figure 11** shows the velocity distribution along an ideal streamline inside a Francis turbine unit operating for the best efficiency output. It shows that the highest velocity and acceleration occurs at the GV. Such higher velocities will cause flow instabilities and secondary flows around guide vanes. Consequences of such high velocity and instabilities can cause rapid erosion of guide vanes and facing plates due to sediments and cavitation or both. **Figure 12** shows the typical damage of GV and facing plates from a unit of 1500 MW hydropower project in India. Due to high flow velocity and heavy sediment load in flow severe damage in GV and deep grooves in facing plates can be observed.

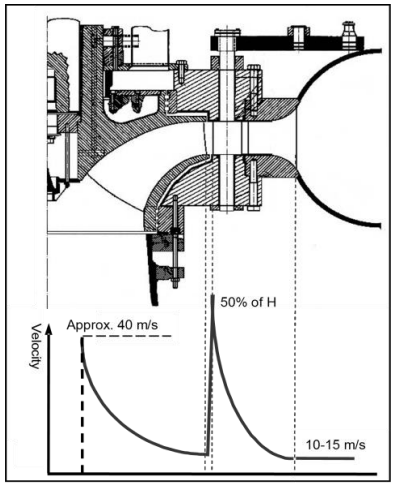

Figure 11. Velocity distribution inside Francis turbine. Adapted from Thapa [24]

General principles of hydraulic design of Francis turbines and the effects of reaction ratio has been discussed by Brekke [40]. He shows the strong influence of reaction ratio on the shaping of blade profile and also on relative velocities at runner outlet. As relative velocity has a strong influence on sediment erosion, hence the reaction ratio can be considered as an important parameter for design optimization against sediment erosion. Mette [17] has explored this issue in details in her PhD studies. She has used analytical tools to develop alternative designs of Francis turbines with different reaction ratios and have applied numerical methods to investigate flow and sediment erosion patterns. It was found that by reshaping Francis runner by lowering reaction ratio would reduce relative velocity in blades

and hence the sediment erosion in runner will be minimized. However, on the other hand it was also found that lowering the reaction ratio will also increase the absolute velocity in GV and hence it escalates the erosion in GV. It was concluded that the further study by combining the design optimization for runner and GV together with the objective of minimum erosion in both components was necessary.

Figure 12. Sediment erosion damage in GV and facing plates. Adapted from Alam [6]

Mack [41] has conducted studies to predict sediment erosion in guide vanes and in labyrinth seals in Francis turbines by Numerical methods. Lagrangian particle tracking methods and *k-ε* turbulence model with Finnie erosion model was applied. The flow equations were solved by finite volume method to simulate 3D flow around GV with a clearance gap. By comparison with actual cases, it was concluded that Numerical methods are capable to simulate the flow behavior and erosion in GV.

It is often difficult to classify the erosion in GV. Depending upon the design and operational characteristics, different power plants have different mechanism, location and intensity of erosion in GV. A detailed investigation of sediment erosion in Francis turbines components has been done by Brekke [23]. He has also outlined some of the design and operational methods to reduce sediment erosion in GV and other components of Francis turbines. The classification of the erosion in GV, based on the cause behind them, is done as follows.

a. ***Turbulence erosion*** at the outlet region and facing plate due to high velocity of fine grain sand.

b. ***Secondary flow erosion*** at the corner between GV and facing plates due to fine and medium size particles, which makes horse shoe grooves in the facing plates following contours of GV.

c. ***Leakage erosion*** at the clearance between GV and facing plate due to local separation and horse shoe vortex in the suction side. The leakage also cause local separation and turbulence at the pressure side at inlet and suction side at outlet of GV causing even a deep groove at the bottom and top of the GV.

d. ***Acceleration erosion***, caused by separation of large particles from the streamlines of main flow due to rotation of water in front of runner. The acceleration of particle is normal to streamline and strikes GV surface causing severe erosion, and it also creates secondary flow causing erosion at the corner between GV and facing plates by fine particles.

Most of these erosion mechanisms in GV can be observed in **Figure 12**.

The most common and measureable erosion in GV is the increase of clearance gap across the face of GV and facing plate. Increase of the clearance gap has serious consequences by creating the secondary and cross flows, often called as leakage flow. These unwanted flows disturb the main flow at the inlet of runner and initiate/accelerate the flow instabilities. For a typical high head Francis turbines, the clearance gap is maintained between 0.1 mm to 0.3 mm by the design. It has been reported from Nepal [5, 8, 24] that, due to sediment erosion the clearance gap in Middle Marsyangdi hydroelectric power plant was measured to 1.6 mm. Similarly, at Jhimruk hydroelectric center the horseshoe shape of erosion grooves at lower facing plate was with depth of about 4 mm. In Modikhola hydropower project the clearance gap was up to 2 mm and that in Kali Gandaki-A hydropower plant it was as high as 5 mm. Heavy erosion damage in the runners were also observed. Comparative flow analysis at the outlet of GV with and without erosion and increased clearance gap would helpful to identify their effects and intensity of additional damage in runner due to flow distortions.

4. Flow analysis around guide vanes of Francis turbines

Guide vanes direct flow at an appropriate angle to the runner imparting the flow an angular momentum or spin. This makes GV positioned such that at two points, along the same chord length, are located at different radii. Thus, despite of uniform airfoil structure GV will have a high pressure side and a low pressure side. Flow with spin and that with pressure difference across the surfaces will induce leakage flow from the GV clearance gap, and wakes and vortices from the GV trailing edge [42]. These wakes further interacts with pressure field between runner blades and creates non-uniform flow field in which the runner blades will rotate. **Figure 13** shows such non-uniform flow at the inlet of Francis runner due to flow distortion. This non-uniform flow field further interacts with rotating runner as each blade passes GV. This effect, also called as rotor-stator interaction, causes vibrations and pressure pulsations in runner, and affects the performance of the turbine. Chen [43] has reported high vortices and pressure fluctuations in GV leading to cavitation with temperature rise up to 600°C in the GV of Three Gorges turbines. It was identified to be caused by poor design of GV, which was later corrected.

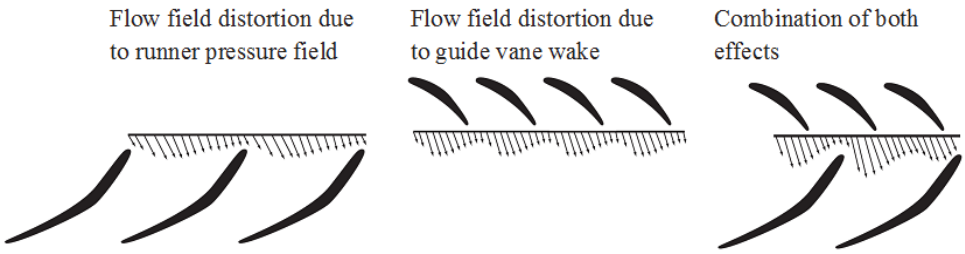

Figure 13. Flow field at inlet of Francis runner displaying runner and guide vane effects on flow velocity and angles. Adapted from Ruchonnet [42].

A very detailed study of flow field around GV of Francis turbines has been done by Chen [44]. An experimental set up with a cascade of stay vanes and GV simulating actual flow in Francis turbine was developed. Effects of leakage flow, wakes on the velocity distribution between adjacent GV and also at outlet of GV were studied. **Figure 14** and **Figure 15** show the test setup and results from this study. Flow visualization through leakage between GV face and facing plates was done by releasing die from the GV faces towards covers (injection streak line method), and the flow visualization across the space between adjacent GV was done by fixing cotton tufts on nylon strings to form a mesh network between two neighboring guide vanes (tuft grid method). Pressure across the GV surface and GV faces were measured by placing pressure taps at 17 locations, which were connected to the pressure transducer through pressure switch. Laser Doppler Velocimetry (LDV) method was used to capture velocity profile in 7 different cross-sectional planes located at the inlet, the middle part, and the outlet of the cascade and 5 test sections from the front facing plate to the middle height of the GV. The clearances between the guide vanes and the facing plates were 0.4 mm and 1.0 mm. It was found that the exit flow field of the guide vane cascade indicates the combined influence from of the leakage flow and the wake flow, which reduces the homogeneity of the flow field at the inlet of runner. It was concluded that the exit flow from the guide vane cascade is neither uniform in circumferential direction, nor in span wise direction. Higher turbulent stress in the corner between the suction side of the GV and facing plate was measured. This indicates that secondary flow induced by leakage flow, horseshoe vortex, and passage cross flow transports the higher turbulence energy fluid towards this corner, thus higher sediment erosion in this area can be expected. The same setup was latter modified by Antonsen [45] to study connection between the design of GV and the dynamic load on the runner due to rotor stator interaction. Both symmetric and asymmetric profiles of GV were tested to estimate the wake at the exit of the guide vanes. **Figure 16** shows the results from LDV measurements of flow velocity at increasing distance past the GV trailing edge. A very clear pattern of wake can be observed. The velocity defect of the wake, due to viscous effects, was found to be proportional to the distance from the trailing edge to the power of

-0.5. So the velocity defect rapidly deteriorates. However, the wake will still exhibit a non-uniform pressure field and is transported through hydraulic channel to the runner blades as shown in **Figure 17**. This effect was also captured by Kobro [46] during his onboard Francis model runner pressure measurements.

Flow Visualization by Tufts (on the surface of the facing plate)

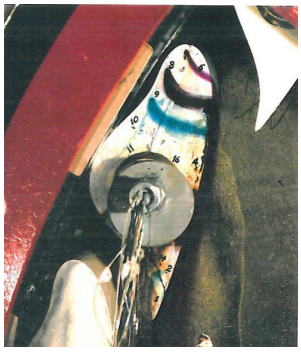

Visualization or Leakage Flow on the Guide Vane's face (C_r=0.0024)

Figure 14. Flow visualization around GV. Adapted from Chen [**44**]

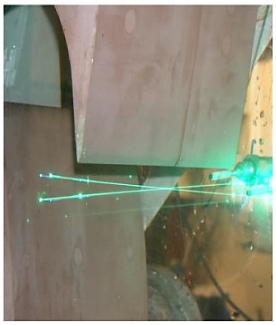

LDV Measurement

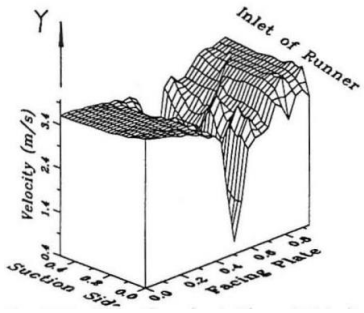

Three-dimensional View of Velocity distribution at the exit of the guide vanes

Figure 15. Test setup for study of flow field around GV of Francis turbines. Adapted from Chen [44]

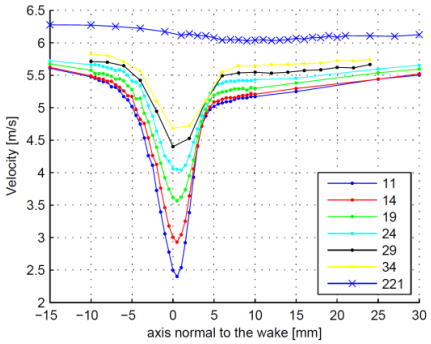

Figure 16. Wake at different downstream positions. Adapted from Antonsen [45]

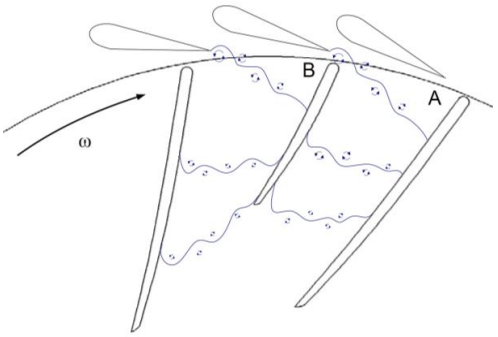

Figure 17. Transport of guide vane wake. Adapted from Kobro [46].

Zobeiri [47] has studied effect of hydrofoil trailing edge shape on the wake dynamic and flow induced vibrations at high Reynolds number (5E+5–2.9E+6). NACA 0009 hydrofoils with blunt and oblique (30 degree) trailing edges were tested. The velocity field was surveyed with the help of LDV, and Particle Image Velocimetry, (PIV). Flow induced vibration measurements and high-speed visualization were also performed in phase locked average of the wake velocity. **Figure 18** shows the results for this study. It was found that geometry of trailing edge has a very significant effect on vortex generation. Remarkable reduction of vortex induced vibration occurred with the oblique trailing edge compared to that from blunt trailing edge. It was investigated that the oblique truncation leads to a thickening of the core of upper and lower vortices as well as a disorganization of the alternate shedding in the near wake. It was concluded that the collision between upper and

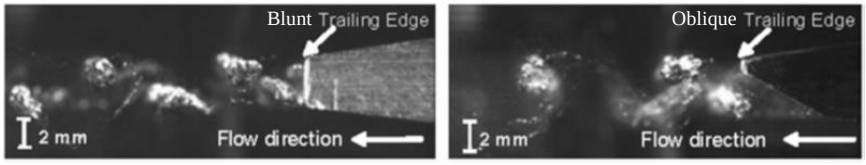

High speed visualization of the wake dynamic (side view)

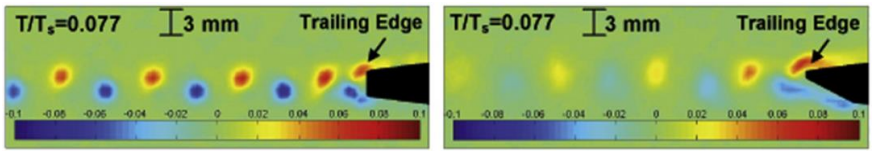

Wake visualization by PIV, normalized vorticity

Figure 18. Wake profiles for airfoils with truncated and oblique geometry of trailing edge. Adapted from Zobeiri [47].

lower vortices and the resulting vorticity redistribution is the main reason of the wake reduction obtained with oblique trailing edge.

A very detailed measurement of flow field around guide vane of Francis turbine has been done by Qian [48] in her PhD studies. The experiments were conducted in two stages called configuration 1 and configuration 2. Configuration 1 consisted of a guide vane installed in a water channel, tested at Reynolds numbers 1.1E+5, 1.8E+5, 2.2E+5 and 2.8E+5 and angles of attack: α= 0°, 5°,10°,15° and 20°, which are similar to those, encountered in standard model Francis turbines. The flow data obtained include instantaneous velocity vector maps (x/c) as well as averaged results regarding stream wise velocity profiles (U/U_c), stream wise velocity fluctuations (U'^2/U_c^2) and Reynolds shear stresses ($u'v'/U_c^2$). For the same conditions, the head losses due to the guide vane were also measured and compared. Configuration 2 corresponds to the distributor section of an actual model of Francis turbine with a specific speed (nq) = 46.2, provided by GE. The 5 operation points at Q_{11}/Q_{11n}=0.55, 0.65, 0.75, 1.0 and 1.08 with the corresponding GV opening α=11°, 13°, 15°, 20° and 22° are selected for all the measurements. Instantaneous results such as velocity vector maps and average results such as velocity fluctuation and velocity magnitude contours were presented. The pressure distribution around the pressure side and suction side of the two neighboring guide vanes was measured with 10 miniature piezo-resistive pressure sensors with a specially designed mounting method on the surfaces without any geometry alteration. Based on the measurements, the effects of operation points on the flow behavior were analyzed. **Figure 19** shows the results from configuration 1. Effects of boundary layer flow as well as disturbance in flow past tailing edge due to formation wake and recirculation can be observed. Higher velocity fluctuation and turbulent stresses in the flow past trailing edge can also be identified. Head loss created by the guide vane was measured to increase with the angle of attack. A particularly large head loss occurring between α=10° and α =20°, in agreement with the flow field measurements, shows that separation occurs intermittently at α =15° and systematically at α =20°.

Figure 20 shows the results from configuration 2. It was observed that the flow at the exit of the stator is strongly non-uniform for all operation points. At full-load, the flow is more uniform in the middle of the inter-GV channel, but the velocity fluctuation and the velocity gradient are stronger along the guide vane surfaces compared to light overload. The velocity fluctuation is much stronger at the part load condition. It was also observed that the pressure fluctuation between the pressure side and suction side reduces below 3% near the best efficiency point. It was concluded that the conventional design of GV can guide the flow correctly the at the best efficiency point and light overload points only and further research is needed to better GV to minimize unwanted flow distortions.

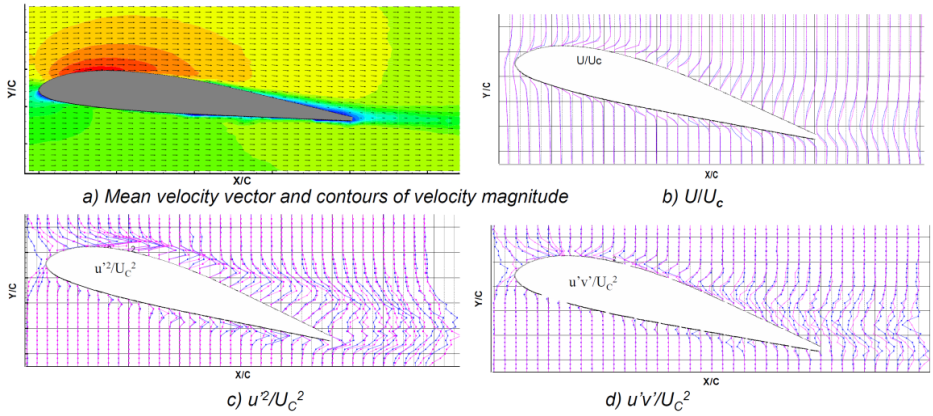

a) Mean velocity vector and contours of velocity magnitude b) U/U_c

c) u'^2/U_c^2 d) $u'v'/U_c^2$

Mean Flow fields around the guide vane

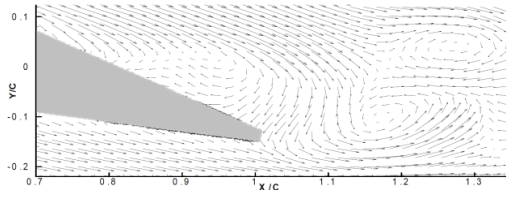

Instantaneous velocity field at α = 15°

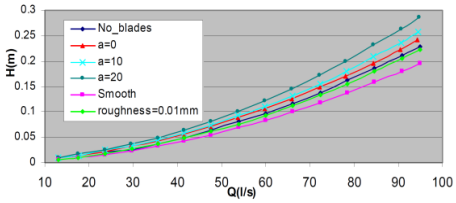

Head loss vs. angle of attack

Figure 19. Flow visualization and measurements from configuration 1. Adapted from [48]

Sohn [49] has done an experimental studies with NACA airfoils by using the smoke-wire technique to produce visible streak lines and images captured and analyzed by PIV methods. The free-stream velocity was 26.0 m/s, and the corresponding Reynolds number was 4.12E+5. **Figure 21** shows wing tip vortices visualizations for the half-wing model with the square-cut wing tip configuration. The planform and the profile views show the formation of tip vortex and its disturbance in flow downstream of trailing edge. The cross sectional view of wing tip vortices, which was illuminated by 3 W Ar-ion laser beams at the distance of chord length from the trailing edge, shows the circulatory motion of the wing-tip vortex with its expanding nature as it goes downstream. It was also observed (not shown here) that the wing-tip vortices at different angles of attack has a distinct formation and structure characteristics with increasing tip vortex for increasing angle of attack.

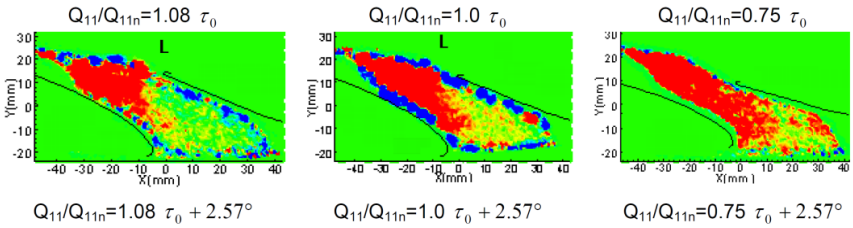

Velocity magnitude fluctuation contours for different operation points

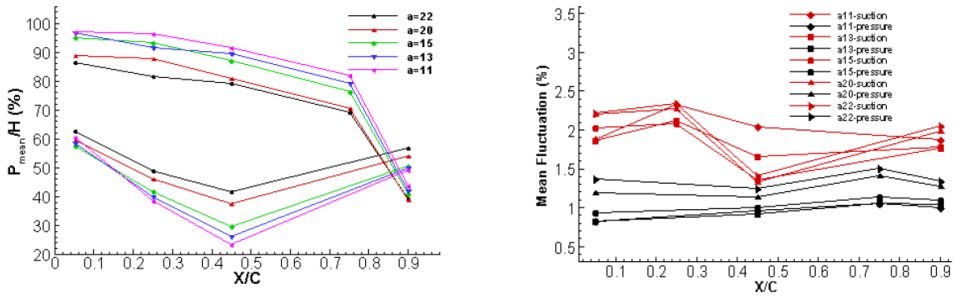

Static components of pressure and mean pressure fluctuation around GV

Figure 20. Flow visualization and measurements from configuration 2. Adapted from Qian [48]

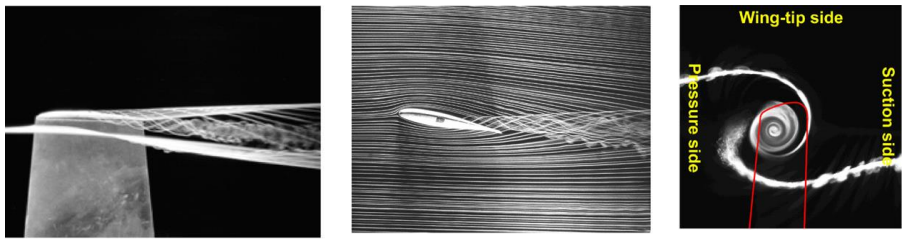

Planform view Profile view Cross-sectional view

Figure 21. Wing tip vortices visualizations for α=10°. Adapted from Sohn [49]

Tallman [50] has done a very thorough theoretical investigation on the effects of the tip clearance height on the leakage flow, vortex, and associated secondary flows. A pressure-correction based, three-dimensional, Navier-Stokes CFD code has been used to simulate and study the effects tip clearance height and the associated flow physics in a linear turbine cascade in stationary condition. This also represents the clearance flow from the guide vanes. **Figure 22** shows fluid path lines for the tip clearance gap equaling 1 percent of blade

span (0.186 m) with inlet flow velocity of 13.82 m/s and air as working medium. Gap entrainment leakage flow producing the leakage vortex core can be clearly observed. This leakage vortex has been categorized into three types corresponding to three different types of leakage vortex roll-up phenomenon. The type 1 vortex, which forms the innermost core of the leakage vortex, starts to roll at approximately 30 percent axial chord and aid in the roll-up of the leakage vortex core. The type 2 vortex occurs in fluid pathlines that cross the gap at its upstream half and near to the outer casing, and will resist rolling into the leakage vortex. These fluid pathlines are gradually entrained around the outside of the leakage vortex downstream of the trailing edge, but do not roll up inside the passage. The type 3 vortex consists of fluid that exits the gap from its downstream half and tends to wrap around the leakage vortex as a group. Thus, the vorticity is rather convected with the flow due to roll up of fluid path lines through the small clearance gap, than by as classical explanation of leakage jet/passage flow shearing. However, due to the greater leakage jet mass flow and inertia in the larger tip clearance case, leakage jet/passage flow shearing appears responsible for creating vorticity. It was also observed (not shown here) that at the passage exit, the leakage vortex flow occupies roughly half of the blade spacing near the casing in the 2.5 percent case, compared with roughly a third of the blade spacing in the 1.0 percent case.

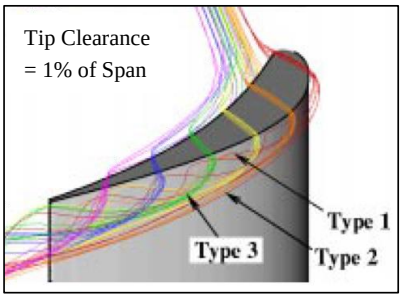

Figure 22. Tip leakage flow path lines. Adapted from Tallman [50]

These studies show that flow around GV of Francis turbine is highly non-uniform both in magnitude and in direction and that in both cross-sectional as well as span wise plane. Acceleration and continuous change in direction as flow moves from spiral casing to runner starts the flow distortions. These distortions are further enhanced by viscous effects as wakes, and boundary layer effects as turbulence and shear stresses. Clearance flow induced vortex by mixing of cross flow makes the flow past GV even more unstable. Such flow with high sediment load can cause severe damage of turbine components.

5. Effects of guide vane erosion on turbine performance

There has been very less studies so far to estimate the effects of flow from eroded guide vanes on turbine erosion or its performance. Past studies suggest that the increase of clearance gap between facing plate and GV face is the most crucial damage of GV erosion. Flow studies also show this effect have significant consequences on the inlet flow at the runner.

Brekke [51] has studied the influence of the guide vane clearance gap on turbine efficiency for different specific speeds. Tests were made by changing the clearance gap in two different prototype and model turbines followed by the measurements of efficiency. Three different magnitude of clearance gap of 0.3 mm 0.5 mm and 1 mm were induced by inserting the steel seams underneath the bottom cover flange of same turbine (P= 315 MW, H=520 m) within a short time interval of operation. Thermodynamic efficiency measurements were done in the power plant and model test were done in laboratory condition with similar magnitude of clearance gap to study its effects on efficiency as well as leakage flow. **Figure 23** shows the results from this study. It was observed that the clearance gap has a high influence on overall efficiency of Francis turbine. Decrease of 0.5% efficiency at BEP was measured in prototype with 0.5 mm clearance gap compared to the original runner with 0.3 mm clearance gap. Similarly for 1 mm clearance gap the decrease in turbine efficiency was measured to be 0.8%. Model tests with results showed that the loss in efficiency being larger than the increase in leakage flow (in percentage of total turbine flow) form the clearance gap. The disturbance of flow in the runner from vortex lines formed by the leakage, which increases the GV wake, was thought to be the reason for this. Chen [44] has also reported that the turbulent stresses increases much more in the corner between the suction side of the GV and facing plate than in the corner between the pressure side and the facing plate.

Investigations to understand the effects of GV erosion on the flow phenomenon and its interaction with the pre-existing flow instabilities in turbine components seem to be lacking. It can be logically deduced from past studies that the erosion in GV will have considerable effects on overall turbine performance and also on erosion rates of runner parts. However, detailed scientific studies are required to make quantitative analysis of this fact.

6. Summary and Future Direction

Future developments of hydropower projects will be escalating in Asian and South American continents. Several power plants across these basins have reported severe cases of material erosion from turbine components due to high sediment load in the flow. Presence of hard particles as quartz in sediment removes the base material of turbine gradually. Effects as progressive loss in turbine efficiency, increase of noise level, and vibrations in components are the common consequences of the sediment erosion damage. Most of the bigger turbines manufactures have developed their turbine designs for the projects with lesser problems of sediments. Consequently, a proper solution to this age long problem in the other parts of world has not been found so far.

Studies to understand and minimize problems due to solid particle collisions have started back in 19th century. Most of the researches then were focused to the applications for cutting

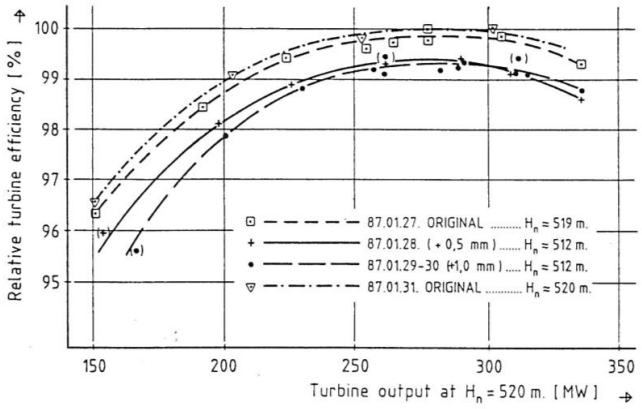

Thermodynamic efficiency measurement of turbines

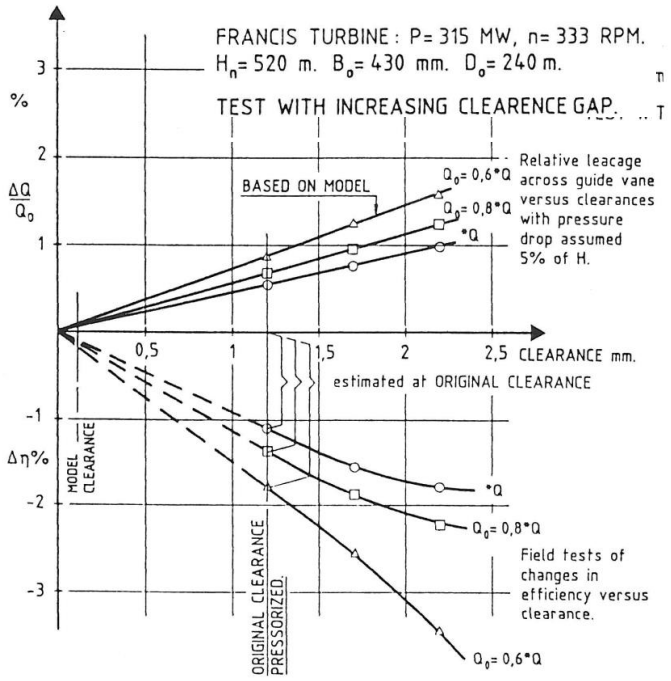

Leakage flow and efficiency drop

Figure 23. Prototype and model tests with variations in GV clearance gap. Adapted from Brekke [51]

industries and slurry transport phenomenon. Research on sediment erosion of hydro turbine components accelerated only on late 20^{th} centuries and most of the publications on this area are found from the last decade. Thus, there is still need of further investigation in this subject to generate knowledge for better technology.

Several independent researches done at different times have established the factors effecting sediment erosion rate as: factors associated with operating conditions (velocity, acceleration, impingement angle, flux rate, medium of flow and temperature), factors associated with eroding particles (size, shape, hardness and material) and factors associated with base material (chemistry, material property and morphology). More some advanced studies have shown that each of these factors have different effects on intensity of damage depending upon specific applications and flow behavior. Thus, a general model of erosion cannot be established.

In hydraulic machineries, erosion due to sediment is found to have synergic effects with cavitation and corrosion. Effects of corrosion have been minimized with the development of stainless steels, but the combined effects of cavitation and sediment erosion in hydro turbines is still a challenge. Tungsten Carbide based HVOF coating on 13Cr4Ni stainless steels have shown a very good resistance to erosion and cavitation, but its performance is heavily dependent on quality of coating layers. Due to intricate shapes, it is often difficult to coat all the parts with uniform thickness.

The increase in level of understanding of flow inside Francis turbine components has added valuable information to the studies of sediment erosion in these machines. Experimental data and field measurements, together with the advancements in numerical tools has given better understating of causes and effects of sediment erosion in hydraulic turbines. Recent studies have shown that the flow inside Francis turbine is highly non-uniform. Being a reaction machine and due to more complex design of components, the flow inside these turbines are infused with instabilities as wakes, vortices and pressure pulsations before the flow enters the runner. These instabilities not only affect the turbine performance but also accelerate the sediment erosion damages.

Currently practiced methods to control sediment erosion in turbine components as, prevention of sedimentation in the catchment areas, tapping sediments at intakes, and applying preventative coatings on the turbine components exposed to high velocity water have not shown successful results in most of the cases. Thus, there is still a need for further research to find better solutions to prevent turbine damage from sediments. Future study on minimizing sediment erosion damage in Francis turbine components needs to be focused on following:

- Design optimization of the turbine components to reduce flow instabilities and minimize relative velocities should be considered as an additional field of

investigation to the currently practiced methods to control sediment erosion in Francis turbine components.

- Surface coatings by erosion resistant materials and their procedures should be further investigated. Better coating particles to retain properties in physical interphases have to be developed. Particularly, coating on Francis turbine components has to be further improved by better assembly/manufacturing design of parts, so that coatings can be applied more uniformly and to all the parts.

- Observation of actual erosion damage in turbine components and studies on flow behavior around those components should be better correlated to link the erosion damage with the design of the components. The causes of flow instabilities inside Francis turbine components should be further investigated and design improvements to minimize them should be done.

- Several studies have shown that the flow instabilities in Francis turbines originate from the guide vanes. Eroded guide vanes and with increased clearance gap contribute to further increase of these flow instabilities. Experimental and numerical studies have verified the negative effects of flow from the clearance gap, and measurements in power plants have shown direct loss in turbine efficiency due to increased clearance gap. Better understanding of this phenomenon has to be made and effective methods to minimize the consequences have to be explored.

References

[1] Matsuo Y, Yanagisawa A, Yamashita Y. A global energy outlook to 2035 with strategic considerations for Asia and Middle East energy supply and demand interdependencies. Energy Strategy Reviews. 2013;2:79-91.

[2] Jia J, Punys P, Ma J. Hydropower. In: Chen W-Y, Seiner J, Suzuki T, Lackner M, editors. Handbook of Climate Change Mitigation: Springer US; 2012. p. 1355-401.

[3] Darmawi, Sipahutar R, Bernas SM, Imanuddin MS. Renewable energy and hydropower utilization tendency worldwide. Renewable and Sustainable Energy Reviews. 2013;17:213-5.

[4] Bookhagen B. Appearance of extreme monsoonal rainfall events and their impact on erosion in the Himalaya. Geomatics Nat Hazards Risk. 2010;1:37-50.

[5] Chhettry B, Thapa B, Thapa BS. Assembly design to ease turbine maintenance in sediment-laden conditions. International journal on hydropower and dams. 2014:82-8.

[6] Sharma HK. Power generation in sediment laden rivers: The case of Nathpa Jhakri. International Journal on Hydropower and Dams. 2010;17:112-6.

[7] Neopane HP. Sediment erosion in hydro turbines [Monoghraph]: PhD thesis, Norwegian University of Science and Technology, Faculty of Engineering Science and Technology; 2010.

[8] Pradhan PMS, Dahlhaug OG, Joshi PN, Støle H. Sediment and Efficiency Measurements at Jhimruk Hydropower Plant – Monsoon 2003. Report from HydroLab, Nepal; 2004.

[9] Singh M, Banerjee J, Patel PL, Tiwari H. Effect of silt erosion on francis turbine: A case study of Maneri Bhali stage-II, Uttarakhand, India. Journal of Hydraulic Engineering. 2013;19:1-10.

[10] Dorji U, Ghomashchi R. Hydro turbine failure mechanisms: An overview. Eng Fail Anal. 2014;44:136-47.

[11] Alam S. Essential design features for efficient sediment management. International Journal on Hydropower and Dams. 2005;12:80-3.

[12] Pandit HP, Shakya NM, Stole H, Garg NK. Sediment exclusion in Himalayan rivers using hydrocyclone. Journal of Hydraulic Engineering. 2008;14:118-33.

[13] Thapa B, Upadhyay P, Dahlhaug OG, Timsina M, Basnet R. HVOF coatings for erosion resistance of hydraulic turbines: Experience of Kaligandaki-A Hydropower Plant. Second Int Symposium on Water Resources and Renewable Energy Development in Asia. Danang, Vietnam, 2008.

[14] Bishwakarma MB, Støle H. Real-time sediment monitoring in hydropower plants. Journal of Hydraulic Research. 2008;46:282-8.

[15] Dahlhaug OG, Skåre PE, Mossing V, Gutierrez A. Erosion resistant coatings for Francis runners and guidevanes. International Journal on Hydropower and Dams. 2010;17:109-12.

[16] Thapa BS, Thapa B, Eltvik M, Gjosater K, Dahlhaug OG. Optimizing runner blade profile of Francis turbine to minimize sediment erosion. 26th IAHR Symposium on Hydraulic Machinery and Systems. Beijing2012.

[17] Eltvik M. Sediment erosion in Francis turbines: PhD thesis, Norwegian University of Science and Technology, Faculty of Engineering Science and Technology; 2013.

[18] Reynolds O. On the action of a blast of sand in cutting hard materials. Philos Mag (Fourth Ser). 1873;46:337-43.

[19] Finnie I. Erosion of surfaces by solid particles. Wear. 1960;3:87-103.

[20] Finnie I. Some reflections on the past and future of erosion. Wear. 1995;186-187:1-10.

[21] Tilly GP. Sand erosion of metals and plastics: A brief review. Wear. 1969;14:241-8.

[22] Truscott GF. A literature survey on abrasive wear in hydraulic machinery. Wear. 1972;20:29-50.

[23] Brekke H. Design of hydraulic machinery working in sand laden water. In: Duan CG, Karelin VY, editors. Abrasive erosion and corrosion of hydraulic machinery. London: Imperial college press; 2002. p. 155-81.

[24] Thapa B. Sand erosion in hydraulic machinery: PhD thesis, Norwegian University of Science and Technology, Faculty of Engineering Science and Technology; 2004.

[25] Padhy MK, Saini RP. A review on silt erosion in hydro turbines. Renewable and Sustainable Energy Reviews. 2008;12:1974-87.

[26] Thapa BS, Thapa B, Dahlhaug OG. Empirical modelling of sediment erosion in Francis turbines. Energy. 2012;41:386-91.

[27] IEC. Hydraulic machines - guide for dealing with abrasive erosion in water. IEC-62364 Ed 102009.

[28] Thapa B, Chaudhary P, Dahlhaug OG, Upadhyay P. Study of combined effect of sand erosion and cavitation in hydraulic turbines. International Conference on Small Hydropower-Hydro Sri Lanka2007. p. 24.

[29] Kumar P, Saini RP. Study of cavitation in hydro turbines - A review. Renewable and Sustainable Energy Reviews. 2010;14:374-83.

[30] Gohil PP, Saini RP. Coalesced effect of cavitation and silt erosion in hydro turbines - A review. Renewable and Sustainable Energy Reviews. 2014;33:280-9.

[31] Abouel-Kasem A, Abd-elrhman YM, Emara KM, Ahmed SM. Design and performance of slurry erosion tester. J Tribol. 2010;132:1-10.

[32] Rajkarnikar B, Neopane HP, Thapa BS. Development of rotating disc apparatus for test of sediment-induced erosion in francis runner blades. Wear. 2013;306:119-25.

[33] Thapa BS, Thapa B, Dahlhaug OG. Current research in hydraulic turbines for handling sediments. Energy. 2012;47:62-9.

[34] Li Y, Ma J, Yu W. Aplication of nanotechnology on hydraulic turbine abrasion and erosion. 2010 International Conference on Power System Technology2010. p. 1-3.

[35] Levy AV. The erosion-corrosion behavior of protective coatings. Surface and Coatings Technology. 1988;36:387-406.

[36] Singh R, Tiwari SK, Mishra SK. Cavitation erosion in hydraulic turbine components and mitigation by coatings: Current status and future needs. J Mater Eng Perform. 2012;21:1539-51.

[37] Kumar Goyal D, Singh H, Kumar H, Sahni V. Slurry erosion behaviour of HVOF sprayed WC-10Co-4Cr and Al 2O 3+13TiO 2 coatings on a turbine steel. Wear. 2012;289:46-57.

[38] Wei Z, Finstad PH, Olimstad G, Walseth E, Eltvik M. High Pressure Hydraulic Machinery. In: Publication N, editor. Compendium 2009.

[39] Alnaga A, Kueny J-L. Optimal design of hydraulic turbine distributor. WSEAS Transactions on Fluid Mechanics. 2008;3:10.

[40] Brekke H. Hydraulic design strategy for Francis turbines. International Journal on Hydropower and Dams. 1996;3:38-42.

[41] Mack R, Drtina P, Lang E. Numerical prediction of erosion on guide vanes and in labyrinth seals in hydraulic turbines. Wear. 1999;233–235:685-91.

[42] Ruchonnet N, Nicolet C, Avellan F. One-dimensional modeling of rotor stator interaction in Francis pump-turbine. Proceedings of the 23rd IAHR Symposium on Hydraulic Machinery and Systems2006.

[43] Chen T, Li SC. Numerical investigation of guide-plate induced pressure fluctuations on guide vanes of three gorges turbines. Journal of Fluids Engineering, Transactions of the ASME. 2011;133:10.

[44] Chen X. Theoretical and experimental study of flow through the double cascade of a Francis turbine, : PhD thesis, Norwegian University of Science and Technology, Faculty of Engineering Science and Technology; 1992.

[45] Antonsen Ø. Unsteady flow in wicket gate and runner with focus on static and dynamic load on runner: PhD thesis, Norwegian University of Science and Technology, Faculty of Engineering Science and Technology; 2007.

[46] Kobro E, Nielsen TK, Dahlhaug OG. Data analysis from onboard Francis model runner pressure measurements. Honolulu2010. p. 98-103.

[47] Zobeiri A, Ausoni P, Avellan F, Farhat M. How oblique trailing edge of a hydrofoil reduces the vortex-induced vibration. J Fluids Struct. 2012;32:78-89.

[48] Qian R. Flow field measurements in a stator of a hydraulic turbine 2008.

[49] Sohn MH, Chang JW. Visualization and PIV study of wing-tip vortices for three different tip configurations. Aerosp Sci Technol. 2012;16:40-6.

[50] Tallman J, Lakshminarayana B. Numerical simulation of tip leakage flows in axial flow turbines, with emphasis on flow physics: Part I- Effect of tip clearance height. Journal of Turbomachinery. 2001;123:314-23.

[51] Brekke H. The influence from the guide vane clearance gap on efficiency and scale effect for Francis turbines. Proc 14th IAHR Symposium on Progress within Large and High-Specific Energy Units1988. p. 825-37.

Paper-B

Design and development of guide vane cascade for a low specific speed Francis turbine

Biraj Singh Thapa, Chirag Trivedi and Ole Gunnar Dahlhaug

Published in Journal of Hydrodynamics, Ser. B., Vol 28 (2016), 676–689

(doi: 10.1016/S1001-6058(16)60648-0)

Design and development of guide vane cascade for a low speed number Francis turbine

Biraj Singh Thapa, Chirag Trivedi, Ole Gunnar Dahlhaug

Department of Energy and Process Engineering, Norwegian University of Science and Technology, Norway

Abstract

Guide vane cascade of a low speed number Francis turbine is developed for the experimental investigations. The test setup is able to produce similar velocity distributions at the runner inlet as that of a reference prototype turbine. Standard analytical methods are used to design the reference turbine. Periodic walls of flow channel between guide vanes are identified as the starting profile for the boundary of the cascade. Two alternative designs with three guide vanes and one guide vane, both without runner, are studied. A new approach, for the hydraulic design and optimization of the cascade test setup layout, is proposed and investigated in details. CFD based optimization methods are used to define the final layout of the test setup. The optimum design is developed as a test setup and experimental validation is done with PIV methods. The optimized design of cascade with one guide is found to produce the similar flow conditions as that at the runner inlet of a low speed number Francis turbine.

Keywords: Guide vanes; Francis turbine; Cascade; Optimization; CFD; PIV

1. Introduction

Increase in demand of clean energy is promoting further explorations of renewable energy sources. Hydropower is one of the oldest and most reliable sources of clean energy to meet electricity demand. It contributes more than 20% of the global electricity generation. However, more than 80% of feasible hydropower resources are still untapped [1]. In recent years large scale of new hydropower plants are under construction, particularly in Asia and South America. Thus, hydropower sector will receive more attention and investments in future. It also demands research and development activities to address several technical and operational challenges brought by environmental issues and market prices [2].

Hydraulic turbine is an important component of a hydropower plant. The turbine converts available hydraulic energy into mechanical energy, which is then converted to electrical energy by the generators. Francis type of hydraulic turbines are widely used for this energy conversion, as it can meet the real time demand with its ability to maintain high efficiency

even in fluctuating load. Single unit of these turbines are capable to generate power up to 1000 MW [3]. During the operation of Francis turbines, the guide vanes (GV) control the discharge to the runner according to power requirement. Water usually accelerates when it passes through the GV and is directed to the runner at an appropriate inlet angle. In a conventional Francis turbine, about 50% of pressure head is converted to velocity head as the flow accelerates through the GV [4]. For the high head Francis turbines, this accelerated flow causes unstable flow conditions contributing to vortex shedding, high amplitude pressure pulsation, flow separation and sometimes cavitation [5]. Non-uniform pressure and velocity distribution significantly affects the turbine operation and induce dynamic load on runner affecting the operating life of the turbine [6]. Operating conditions with sediment-laden flows add additional challenges and escalates the problems with the eroded surfaces due material removal [7].

Minimizing the rotor stator interaction and achieving uniform velocity distribution at the runner inlet is one of the challenging tasks for a turbine designer. Some of the researchers have attempted to investigate and improve the flow conditions in the flow passages of the GV and runner blades to address this issue. Ruchonnet [8] has developed a mathematical model and studied the rotor stator interaction in a Francis pump turbine. He has studied the role of Eigen frequencies on hydraulic systems experiencing high amplitude pressure fluctuations. Larsson [9] has conducted experimental and theoretical analysis of inlet flow of a Francis turbine runner. He has used LDA methods to measure the characteristics of velocity distribution in vane less space and found that the velocity fluctuations in a GV passage can be up to 15% of theoretical value due to the rotor stator interaction. Qian [10] has used PIV methods to measure the pressure and velocity distribution around the pressure side and suction side of the two neighboring GV in a model Francis turbine. It was found that both radial and tangential components of velocity between the GV fluctuate significantly. Kobro [11] has measured the effects of such velocity fluctuations on the dynamic load in runner blades in a model Francis turbines. He found that fluctuations of stresses inside the runner blades were highest for 50-70% of nominal discharge. Xiao [12] has conducted CFD predictions of pressure pulsations in a Francis pump turbine with misaligned GV. It was found that the misaligned GV significantly reduce the pulse amplitudes in the stationary parts of the turbine but increases the pulse amplitudes within the rotating runner blade passages. These works show that the unsteady flow is inherent from the GV and cause to several undesirable effects on turbine parts. Comprehensive study of unsteady flow around the GV of Francis turbines to identify its correlation with secondary flow fields and with the design of GV profile would contribute to further research in this field of study.

For a more detailed and specific investigation of flow field inside a turbine, a stationary cascade system can also produce reliable results. Cascade setup considers only a section of turbine and hence reduces flow requirements inside the test rig. Furthermore, the

components in the cascade can be designed to have a better excess to measuring instruments and physical observations. Such method however, does not include the effects of runner in the flow field, and also assumes the periodic symmetry in flow over the cascade boundary. Despite of these limitations, researchers have obtained reliable and useful results using the cascade setup. Bario [13] has used a single GV cascade to measure the boundary layer on the pressure and suction sides of a turbine inlet GV. Schabowski [14] has developed a test set up with cascaded vanes to test alternative geometries to reduce tip losses in unshrouded axial gas turbines. He also used the results to verify CFD codes for such cases of flow. Zobeiri [15] has also used single GV cascade setup to investigate the effects of hydrofoil trailing edge shape on the wake dynamics and flow induced vibration. He identified the vortex redistribution phenomenon as the cause of vibration reduction in oblique shaped trailing edge. Finstad [16] has further investigated this vortex redistributing phenomenon behind the trailing edge of airfoils for reducing rotor stator interaction in hydraulic machineries. He has also used a single GV cascade setup for the measurements and has tested effects of different shapes of vortex generators mounted on the rear section of suction side of GV. Most of these measurements have been supported by CFD analysis for predicting the flow behavior under applicable boundary conditions. However, none of these measurements was conducted with the same magnitude of velocity and pressure as that is observed in a prototype turbine. It is challenging to develop laboratory setup, which can reproduce similar pressure and velocity distribution as that observed in prototypes.

Main objective of the presented work is to develop a cascade of GV passages, which will be able to produce steady state flow conditions from the stay vane outlet to the runner inlet of a low speed number Francis turbine. The design goal is to acquire quite similar flow conditions as that observed in a prototype turbine. The purpose of this setup is to examine the effects of leakage flow around GV on the velocity and pressure distribution at the runner inlet. The setup isolates the effects of runner on the flow field and hence allows precise study of effects of leakage flow. The paper discusses the analytical and numerical techniques applied to develop the GV cascade starting from the preliminary design to the final optimization and its experimental validation.

2. Analytical design and optimization

2.1 Reference turbine

Jhimruk Hydroelectric Center in Nepal is considered as the reference case for this study. The power plant has three units of Francis turbine and each produces 4.2 MW at the best efficiency point (BEP). These are low speed number splitter bladed Francis turbines defined by **Eq. 1** [17].

$$\Omega = \boldsymbol{\omega} \cdot \sqrt{\boldsymbol{Q}} / (\boldsymbol{2g} \cdot \boldsymbol{H})^{\boldsymbol{3/4}} \qquad \textbf{(-)} \qquad \textbf{Eq. 1}$$

The power plant represents a typical case of projects operating under large sediment load in Himalayan basin [18]. Several academic studies [19-21] have been conducted to improve hydraulic design of this turbine to handle large sediment load. Design and drawings of the installed prototype are not available therefore an in-house tool named as "*Khoj*", was developed to design a reference turbine with the aim to replace with the existing one [20]. Extensive investigations were carried out on this reference turbine for optimizing hydraulic design to minimize sediment erosion without compromise in efficiency [22-26]. Understanding the consequences of erosion on GV and investigating its effects on velocity distribution at runner inlet was identified as the further works.

The "*Khoj*" has been updated to estimate velocity component at different sections of the reference turbine. These sections include center of spiral casing, inlet and outlet of stay vanes, inlet and outlet GV and inlet of runner. Separate codes are developed to compute the free vortex flow lines at the required sections of flow passages, starting from the center of spiral casing to the middle of runner blade. **Table 1** presents the relevant analytical values for the reference turbine at BEP. With head exceeding 200 m and speed number 0.32 these turbine can be considered as a case of high head Francis units. **Figure 1** shows the major dimensions of the actual turbine. It can be observed that the main dimensions from the analytical design are similar to that of actual turbine. **Figure 2** shows the flow velocities at different sections of the actual turbine. It can be observed that the highest velocities inside the turbines is at the outlet of GV, which exceeds 40 m/s at part load conditions. Relative velocity at the runner outlet also reaches close to 40 m/s at the full load condition. Such

Table 1. Reference turbine analytical design values

Parameters	**Symbol**	**Unit**	**Value**
Net head	H	m	201.5
Flow rate per unit turbine	Q	m^3/s	2.35
Rotational speed	n	rpm	1000
Speed number	Ω	-	0.32
Number of blades in runner	Z_Blades	#	17
Inlet diameter of runner	D_1	m	0.89
Outlet diameter of runner	D_2	m	0.54
Number of GV	Z_gv	#	24
Chord length of GV	L_gv	m	0.14
Profile of GV surface	-	-	NACA 0012

high velocities causes flow instability and also severe erosion of respective components under high sediment load.

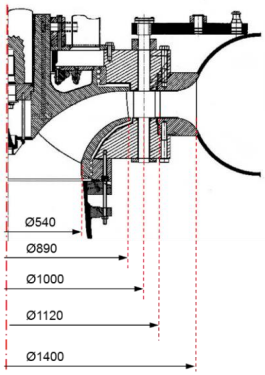

Figure 1. Dimensions of prototype turbine [18]

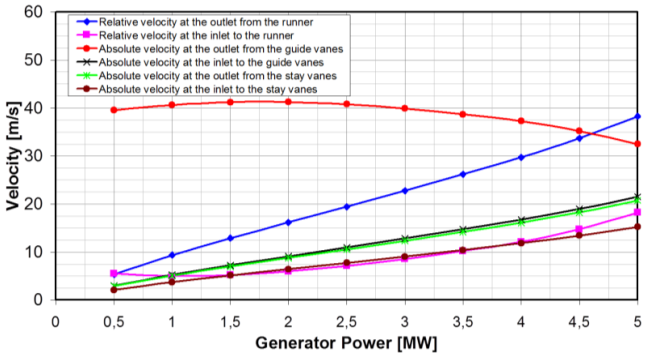

Figure 2. Velocities in prototype turbine [18]

2.2 Design of flow cascade

A symmetric section of reference turbine forms the flow cascade. Some of the researchers have considered a straight channel with GV, while others have considered a section of prototype or model turbine to investigate the passage flow conditions. Choice of channel profile depends upon objectives and requirements of the measurements. For the present study, five GV with four flow passages out of 24 passages of the GV is considered as a reference case. Two outer GV forms as walls of cascade and three inner GV guides flow in the channel as in the case of prototype turbine. Similar design of test setup has also been developed by the past researchers to investigate the unsteady flow in the stator part of Francis turbine [9, 27]. It is expected that such configuration with multiple GV would avoid the effects of walls on the flow field around the central GV. With the present study, an alternative design of test setup with a single GV is also done, and its performance is compared with that of the case of three GV cascade.

Figure 3 shows the layout of reference turbine and the section considered for the reference (3 GV) cascade. Five GV located at the end section of spiral casing (SC) are considered for this design. The choice of GV at the end section of SC will minimize the overall size of test setup. **Figure 4** shows the profile of walls within the cascade with the selected five GV. For the reference case, walls defined by the profile of free vortex flow is considered from the center of spiral casing to the inlet of GV, from the outlet of GV to the inlet of runner and from the inlet of runner to the middle of runner blade. Profile of wall upstream of center of spiral casing up to the inlet of cascade is designed to give same distribution of tangential and radial component of velocity at the center of spiral casing from the completely axial

flow at the inlet of cascade (**Figure 6**). Stay vanes are not included as the part of cascade, as they are mainly for strengthening spiral casing and do not play significant role for hydraulic design [28]. Circular portion of spiral casing is replaced with flat plates with the same height as that of the span of GV. Thus, section from inlet to outlet of cascade is embedded between two flat plates. This makes the design relatively simple and easy for manufacturing. However, such simplification would affect the flow conditions and hence the optimization of walls' profile is necessary. Optimization techniques are applied to redesign the profile from the inlet of cascade to the center of spiral casing, and from the inlet of runner to the outlet of cascade until the satisfactory flow conditions are obtained.

Table 2 lists the parameters and the target velocity, which are used to govern the optimization process. Tangential and radial components of velocity obtained from the analytical design of reference turbine are used as the control parameters. The difference in tangential component of velocity at the inlet and outlet of runner is proportionate to the hydraulic efficiency of the runner (**Eq. 2**). Hence, this velocity component is identified as the most important parameter to govern the optimization process. **Figure 5** shows the respective velocity components inside the turbine for the parameters listed in Table 2. Details of design techniques and calculation methods adopted for the analytical design of the complete turbine and estimation of the respective velocity components has been presented in [22, 28]**.**

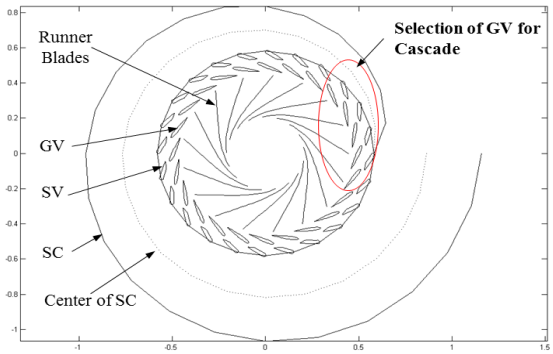

Figure 3. Analytical design and section for cascade

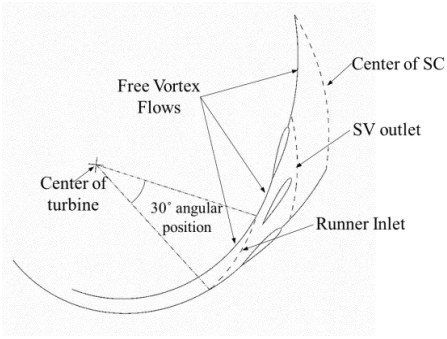

Figure 4. Wall profile for cascade flow

Table 2. Control parameters for design optimization

Control Parameters	Symbol	Unit	Value
Absolute velocity at runner inlet	C1	m/s	41.86
Tangential component at runner inlet	Cu1	m/s	40.72
Radial component at runner inlet	Cm1	m/s	9.7
Tangential component at SV outlet	CuSVo	m/s	13.81
Radial component at SV outlet	CmSVo	m/s	7.26
Absolute velocity at SV outlet	CSVo	m/s	15.6

$$\eta_h = \frac{Cu1 \cdot U1 - Cu2 \cdot U2}{gH} \qquad \textbf{Eq. 2}$$

Symbol 1 & 2 represents the parameters at the inlet and the outlet of runner respectively.

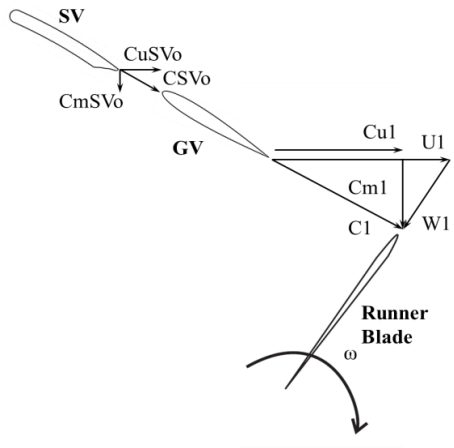

Figure 5. Velocity Components in Turbine

CFD analysis is conducted to validate the respective control parameters for the optimized designs. Equally spaced control points along the circumferential direction along the outlet of stay vane and along the inlet of runner are used for plotting the velocity profiles (**Figure 4** & **Figure 19**). Three GV cascade has 50 control points within its 60 degrees of angular position between the flow channel walls as shown in **Figure 4**. Similarly, one GV cascade has 22 control points within its 30 degrees of angular positions between the flow channel walls. **Figure 6** shows the reference layout of 3 GV cascade and different sections identified for the design optimization process. The geometries of sections upstream of center of spiral casing (1, 2) and downstream of runner inlet (3-5), as shown in **Figure 6**, are optimized to get the optimum velocity distributions along the control points. Geometry of sections defined by free vortex flow (6-8) are not changed throughout the optimization process.

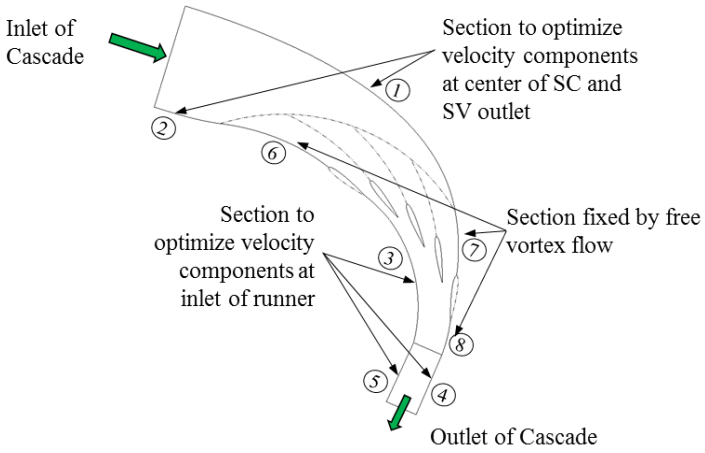

Figure 6. Reference design and sections for optimization

The overall optimization process is summarized with the flow chart in **Figure 7**. Same procedure is applied for optimization of the both 3 GV and 1 GV cascade. Different cases of optimized design of cascade are developed and CFD studies of each alternative design are conducted to evaluate the properties of the control parameters along the control points. The sections upstream of center of the spiral casing (1, 2) are adjusted to control velocity components at the outlet of stay vanes. The sections downstream of the runner inlet (3-5) are adjusted to control velocity components at the inlet of runner. Particularly it is observed that among others, section 1 and section 3 (**Figure 6**) are very sensitive to velocity distribution at the outlet of stay vanes and at the inlet of runner respectively. Both of these

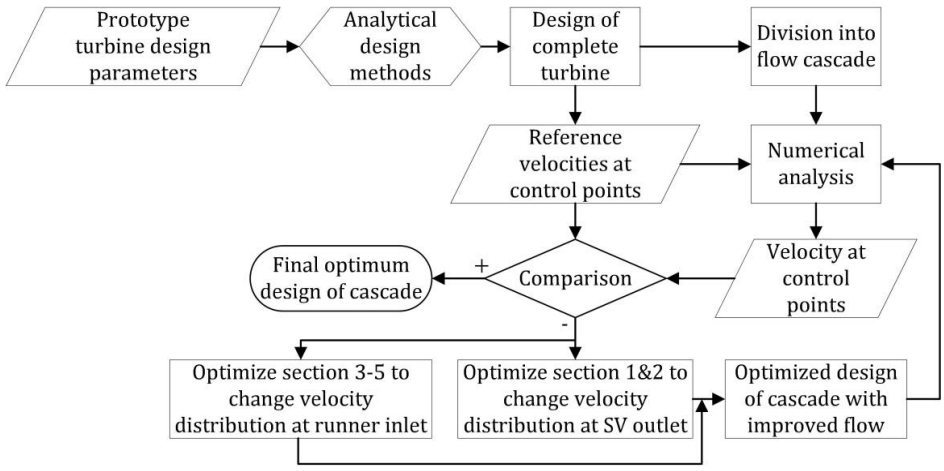

Figure 7. Design optimization flow chart

sections being a longer curvature impart higher angular momentum to flow. This would lead to change in distribution of total velocity into its components as the flow progresses inside the channel.

Comparison of tangential velocity, obtained from the analytical design of turbine with that for alternative design of cascades, is the basis to accept or reject the alternative designs. Results of each successive optimization process are used to form hypothesis to develop the next optimized design. The final optimum design of the cascade test setup is identifed as the one, which yeilded the minimum differnece in tangential velocity component at the runner inlet position.

3. Numerical Model

Academic version of Ansys 15.0 is used for the numerical modelling, meshing, and simulation. Primary objective of the numerical study is to evaluate the flow field inside the GV cascade. For the mesh validation, velocity profiles at the stay vane outlet and runner inlet sections are compared with the velocity profiles available by analytical solution. Geometry and shape of the test section are optimized with coarse mesh (nodes < 3 million). Then, more detailed validation of the optimum design of cascade is conducted with fine mesh (nodes > 10 million), and with different turbulence models. The geometry of cascade is prepared in Creo Parametric, refined with Ansys CAD model and then exported to meshing module. **Figure 8** and **Figure 9** show the CAD model of the GV cascade created for three GV and one GV case respectively. Around the GV, geometrical shape is similar to the existing turbine. To obtain uniform flow distribution, inlet section is extended by 5 times of inlet pipe diameter. Similarly, to avoid the influence of downstream boundary condition, outlet section is also extended by 5 times of outlet pipe diameter.

The coarse mesh is generated with Ansys Meshing module. Created mesh density, quality, and selected flow physics, are shown in Table 3. Total 2.34 million and 1.38 million nodes are created in the computational domain of 3 GV and 1 GV, respectively. The computational domains include both hexahedral and quad elements. This combination allowed to create relatively fine mesh around the GV, where the expected flow velocity is high and boundary layer is thin. Smooth transition of 5 layers of inflation with growth rate of 1.2 is prescribed for capturing the effects of walls on the boundary layer flow. Features as “proximity and curvature”, “patch conformal” and “topology checking” are also applied. Patch conformal hybrid mesh with high grid density in the region of control points is obtained for the coarse mesh CFD studies. Quality of mesh obtained thus satisfies the necessities of the numerical simulation in Ansys CFX [29]. Mass flow inlet and pressure outlet boundary conditions are prescribed during the simulations. Total 11 simulations are performed for 3 GV cascade and 5 simulations are performed for 1 GV cascade. **Figure 10** and **Figure 11** show the parts of coarse mesh around the control points for 1 GV and 3 GV cascade respectively. In both the cases high density mesh is generated around the GV. It can also be observed that the

transition of hexahedral mesh between different densities is patch conformed by creating prism and pyramids mesh elements.

Table 3. Mesh statistics for coarse mesh study

Parameter	**Value (3 GV/ 1 GV)**
Nodes (Mil)	2.34/1.38
Total elements (Mil)	2.23 /1.29
Hexa elements (Mil)	2.22/1.29
Max edge length ratio	51.5/11.1
Skewness	0.14/0.14
Orthogonal quality	0.96/0.96
Aspect ratio	2.94/2.75
Turbulence	SST
Fluid type	Water at 25˚C
Simulation type	Steady state
Inlet condition	Uniform mass flow (kg/s) 391.67/195.83
Outlet condition	Average static pressure (atm) 7/8
Convergence criteria	RMS<1E-04
Advection scheme	High Resolution
Total simulations	11/5

Fine mesh in 1 GV cascade is created after the optimization of the cascade using coarse mesh. The cascade of fine mesh includes complete hexahedral mesh of 10 million nodes. **Figure 12** shows the part of mesh generated for this study. The mesh quality is better than the quality obtained with coarse mesh. Dimensionless node position (y^+) from the boundaries is varying from less than one to 300. The node position is adjusted according to the Reynolds number in the corresponding subdomains of the cascade. Since the flow is accelerating around the GV, the maximum fine mesh is required around the GV. Similar methods of mesh generation is discussed in detailed in previous works by the authors [30].

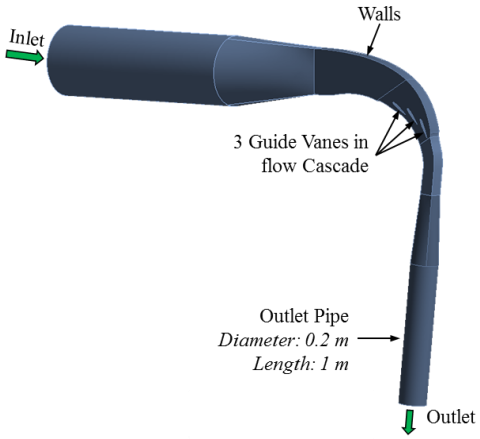

Figure 8. Flow domain for 3 GV cascade

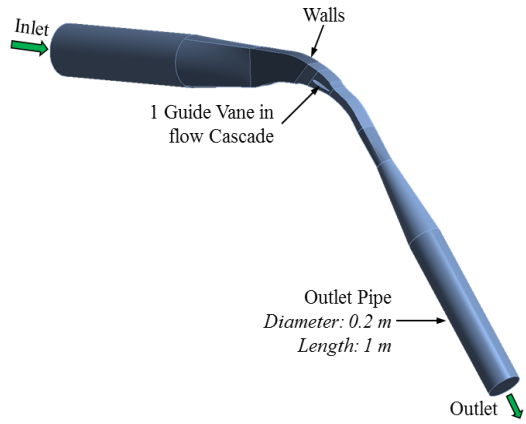

Figure 9. Flow domain for 1 GV cascade

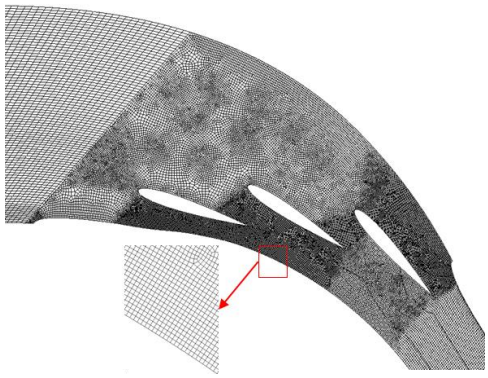

Figure 10. Coarse mesh for 3 GV cascade

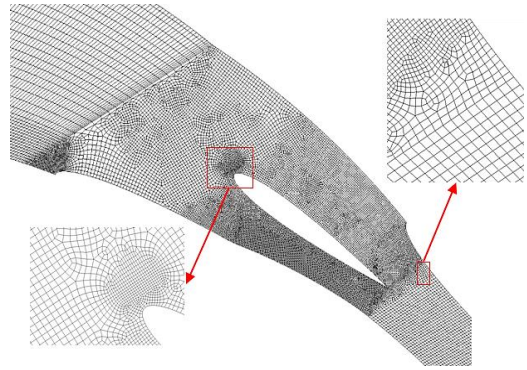

Figure 11. Coarse mesh for 1 GV cascade

To investigate the flow field in detail, six turbulence models and two discretization schemes are tested. Geometry of optimized design of 1 GV cascade is used for this study and also for the grid independency tests. The turbulence models namely, RNG k-ε, standard k-ε, k-ω, SST k-ω, eddy viscosity transport, and Reynolds stress model are used. High resolution and second order advection schemes are used for the discretization. Mathematical expressions of the turbulence models and discretization schemes are extensively discussed in the literatures [31], therefore it is not discussed in this paper. **Figure 13** shows tangential component of velocity at the control points of runner inlet (Cu1) and stay vane outlet (CuSVo) respectively for different cases of turbulence mode. The numerical values of

tangential velocity (Cu), at the stay vane outlet and runner inlet sections are compared with the ideal analytical values. Ideal velocity profile assumes tangential velocity of 14 m/s and 40.8 m/s at the stay vane outlet and the runner inlet, respectively. Trend of the numerical velocity distribution is found to be similar for all turbulence models. Velocity profile at the runner inlet shows sudden drop of velocity at the GV trailing edge from the maximum velocity of 43 m/s. This could be attributed to the wake flow leaving the GV. The standard *k-ε* model showed velocity drop of 3 m/s whereas the Reynolds stress model showed drop less than 1 m/s. By comparing the results of high resolution and second order discretization schemes, both schemes showed almost similar variation across the width of the cascade. Velocity distribution at the stay vane outlet is almost same for all selected turbulence models. No major difference among the turbulence models is observed except velocity profiles near the boundary (wall). RNG *k-ε* model showed lower velocity than the SST and *k-ω* models.

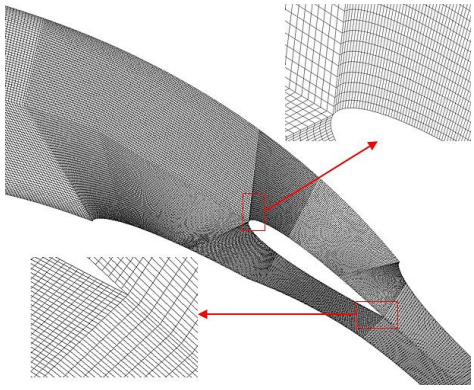

Figure 12. Fine mesh for 1 GV cascade

After comparing the different turbulence models, it is found that the simulation conducted with eddy viscosity transport equation and high resolution advection scheme showed quite better results, for this flow conditions. The basis of comparison is the flow field along the position of stay vanes outlet and along the position of runner inlet. Velocity profile along the runner inlet with the wake from trailing edge of the GV is found to be the most sensitive case to compare between different turbulence models. Some of the models have over predicted the trailing edge wake and some of them under predicted the wake effect. Eddy viscosity model showed better resolution of the flow field and wake, therefore this turbulence model is considered for further validation of the numerical model.

To perform mesh independency tests, a hexahedral mesh with five densities is created starting from 1 million to 10 million nodes. Quality of the mesh is maintained uniform for all densities as stated in Table 3. Initially mesh is created with one million nodes, then two million by increasing the scale factor of 2 and so on for successive mesh densities. **Figure 14** shows the velocity profiles at the runner inlet position for different cased of mesh densities. All the gird density, except for the case of 1 million nodes, predicts the similar velocity profile. It is evident that 1 million node density is not sufficient enough to capture the wake phenomenon. Velocity profile at the stay vane outlet is almost same for all densities of the mesh indicating that there is minimum effect of spatial discretization on the

upstream flow field. It is concluded that mesh with 2 million node is found suitable for this study.

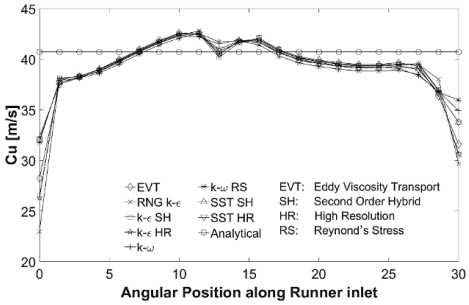

Figure 13. Turbulence model test at runner inlet

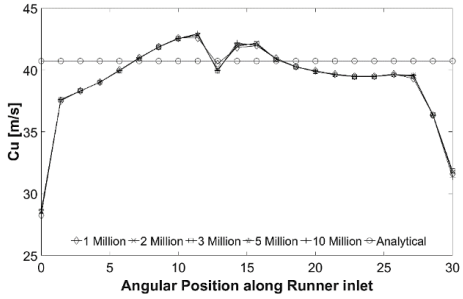

Figure 14. Mesh density test at runner inlet

4. Results and Discussions

Results of numerical simulations of the flow inside the alternative designs of cascade at the control points, as defined in section 2.2, is compared with that of the analytical values. For cross verification of final design, the numerical results from current study are compared with that from other experimental and CFD studies of similar nature. Results from the experimental study of the flow inside the optimum design of cascade is also presented as the validation of this study.

4.1 Optimization for 3 GV cascade

The numerical study of the alternative designs of 3 GV cascade is done with the coarse mesh as discussed in section 3.1. Only the results for the reference and the final optimized designs are discussed in this paper. Most of the results for intermediate designs fall in-between that of reference and optimized design. **Figure 15** shows the velocity distributions along the inlet of runner for reference design of 3GV cascade. It can be observed that total velocity (C1) is lower than the analytical value towards the inner wall from the mid span of flow channel and higher than the analytical value towards outer wall from the mid span of flow. It can also be noticed that tangential component of velocity (Cu1) is major contributor to this skewed velocity distribution. **Figure 16** shows the velocity distributions along the outlet of stay vane. Similar pattern of skewed velocity distribution along the inlet of runner can also be observed at the outlet of stay vanes. Simplification in design of spiral casing and the channel downstream of runner inlet are the probable causes for this deviation. It is hypothesized that increasing the curvature of inner walls and reducing the same for outer walls can counter effect this skewed velocity distribution. Different curvatures for the walls and their combinations are introduced for changing the geometry of the inner and outer walls to come up with the final optimized design.

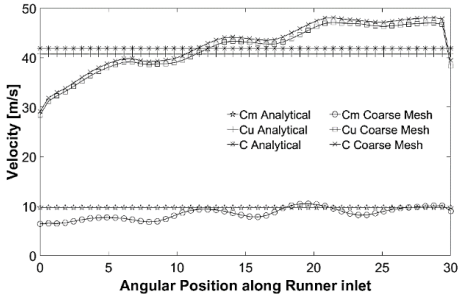

Figure 15. Runner inlet velocities for 3 GV reference design

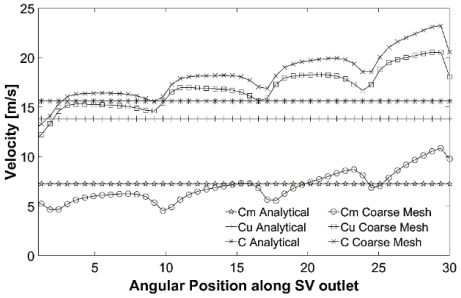

Figure 16. Stay vane outlet velocities for 3 GV reference design

Figure 17 and **Figure 18** show the velocity distributions along the inlet of runner and along the outlet of stay vanes respectively for the optimized design. It can be observed that skewed velocity distribution for both runner inlet and stay vane outlet position is normalized. The velocity components for the runner inlet position are lower than the analytical values and it is higher than the analytical values for stay vane outlet position. It is likely that viscous effects and frictional losses in the walls might have caused lower velocities at runner inlet compared to that of analytical values, which is for the ideal flow conditions. Alteration of geometries at the inlet section of cascade for desired velocity profile at the position of runner inlet, have effected flow area and hence the velocities at the stay vane outlet. Variation in the velocity at the control points 16, 28, and 41 correspond to the effect of GV leading and trailing edge. Velocity and pressure contours have shown large pressure gradient on the leading and trailing edge.

Figure 19 shows the contours for the velocity distribution along the section of reference design of 3 GV cascade. Regions of velocity higher than 45 m/s covers area downstream of runner inlet and the velocity upstream of stay vane outlet is below 20 m/s. Such velocity distribution requires high accelerated flow and hence demands the consecutive pressure distribution as shown in **Figure 20**. It is observed that pressure in the region upstream of stay vane is greater than 10 bars, which is the limiting capacity of the laboratory. The pressure in the region downstream of runner inlet is lower than the atmospheric pressure, which induces the chances of cavitation in the region where the measurements are to be taken. These results further justify the need of design optimization of the cascade.

Figure 21 and **Figure 22** show the contours for the velocity distribution and the contours of pressure distribution along the section of optimized design of 3 GV cascade respectively. It can be observed that both velocity and pressure distributions have improved significantly. It satisfies the laboratory constraints while avoiding the cavitation in the regions where measurements have to be conducted. Flow field around the middle GV may be considered

as actual flow field in the turbine because flow around this GV is not largely affected by the boundaries.

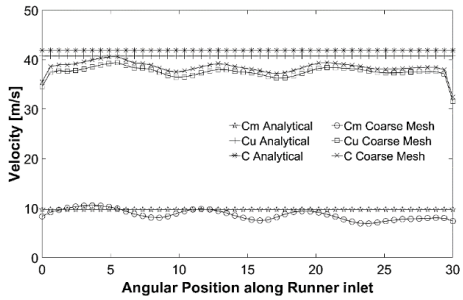

Figure 17. Runner inlet velocities for 3 GV optimized design

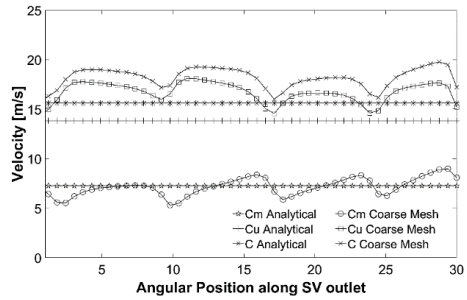

Figure 18. Stay vane outlet velocities for 3 GV optimized design

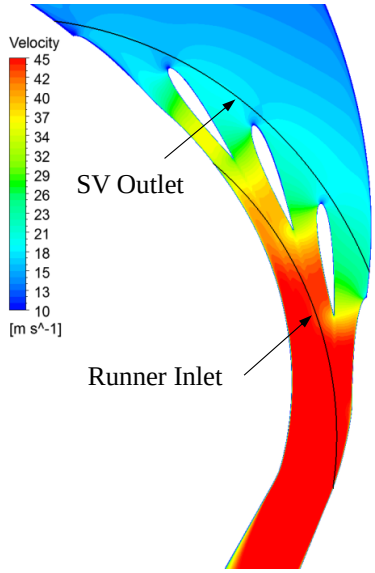

Figure 19. Velocity profile for reference 3 GV design

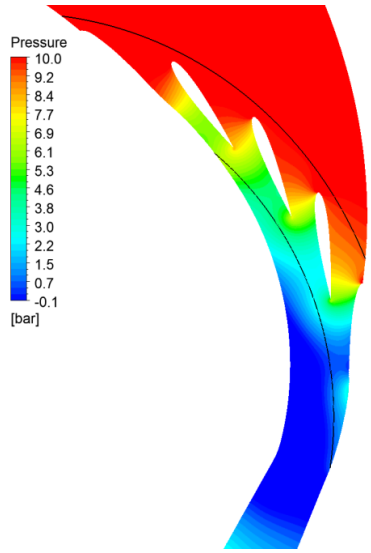

Figure 20. Pressure profile for reference 3 GV design

4.1 Optimum design of 1 GV cascade

Similar design methods as for 3 GV cascade is used to develop the reference design of 1 GV cascade. Similar methods as for 3 GV is also used to optimize its geometry for desired velocity distributions along the control points. Coarse mesh is used to analyze alternative design options. The final optimized design is analyzed by fine mesh for cross verifications

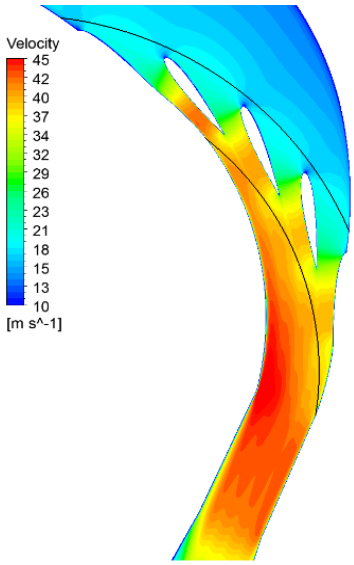

Figure 21. Velocity profile for optimized 3 GV design

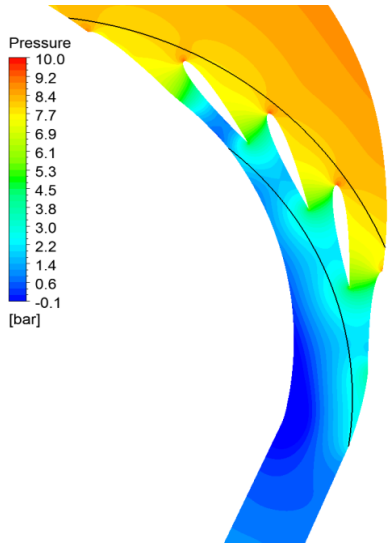

Figure 22. Pressure profile for optimized 3 GV design

of the results. Only the results of final (optimum) design for 1 GV cascade is discussed in this paper. **Figure 23** and **Figure 24** show the velocity and pressure fields of the final design of 1 GV cascade. It can be seen that both velocity and pressure distribution has the matching profile with the theoretical distributions. **Figure 25** compares tangential velocity (Cu) distribution for the optimum design of 1 GV cascade obtained by both coarse and fine mesh with that of analytical values. It can be observed that both coarse mesh and fine mesh study show that velocity distribution along the control points are close to that of analytical values. As expected, fine mesh study predicts boundary wall effects and wake flow more precisely than that of coarse mesh. Accuracy in such effects as wakes and boundary layer flow etc. may not be necessary for the study of the effects of change in cascade geometry on the velocity distribution. This study shows that the results from coarse mesh study can be accepted for the analysis of design optimization of test setup as intended for this study.

Difference between the original design of cascade (3 GV setup) without any optimization, and the optimum design of cascade (1 GV setup) can be made by comparing **Figure 15** and **Figure 25**. It can be observed in **Figure 15** that the original 3 GV design has higher difference in tangential component of velocity between the adjacent GV at runner inlet. However, optimum 1 GV design (**Figure 25**) gives the almost constant tangential component of velocity at runner inlet from the adjacent GV.

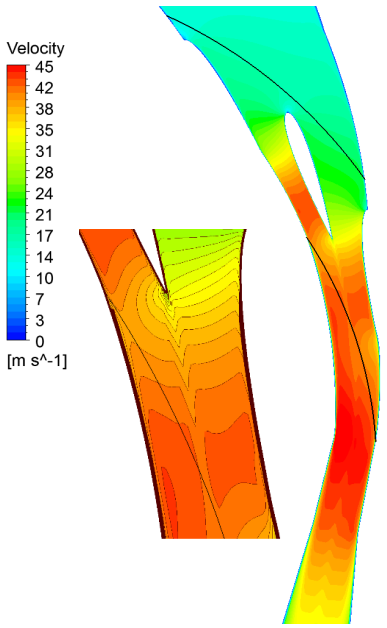

Figure 23. Velocity profile for optimum design of 1 GV cascade

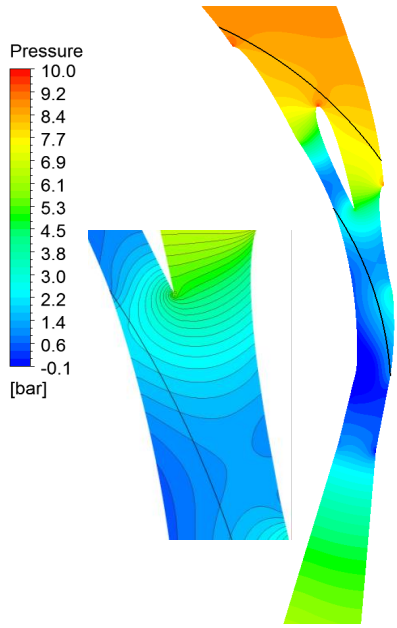

Figure 24. Pressure profile for optimum design of 1 GV cascade

This analysis supports the argument that 1 GV cascade is able to produce the velocity profile at the position of inlet of runner comparable to that of an actual Francis turbine, excluding the rotor-stator interaction. However, with 1 GV cascade the correct flow conditions can be achieved only for a single operating point. Thus, all the measurements have to be done only at one operating point. For this study, best efficiency point (BEP) is considered for the design of cascade and for the consequent measurements.

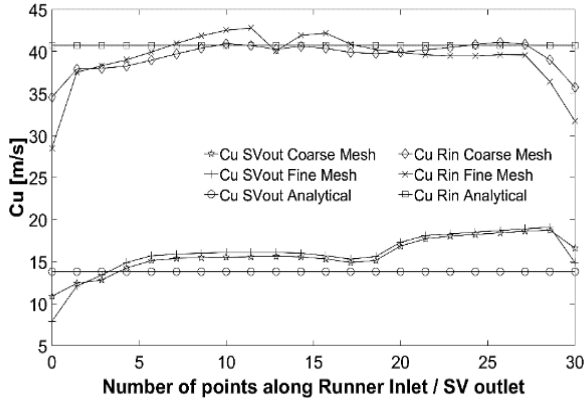

Figure 25. Velocity components for 1 GV optimum design from different methods

4.2 Experimental validation

Development of the experimental test setup is based on the layout of optimum design of 1 GV cascade. The main aim the test setup is to measure the change in velocity and pressure distribution at the inlet of runner due to increasing leakage flow around GV. Particle Image Velocimetry (PIV) methods is applied for capturing velocity field, from the position of stay vane outlet to the position of runner inlet. For the convenience of manufacturing, assembly and testing, the setup is divided into several parts as shown in **Figure 26**. The test section contains the test GV inside a plexi-glass flow channel. The cover plates of test section have openings for excess to the laser sheet and camera exposure for PIV images as shown in **Figure 27**.

Experimental validation of the test setup is conducted at the facilities of the Waterpower laboratory in NTNU. The test setup is mounted in a closed loop system consisting of pump, flow meter, and a pressure tank. The reference test condition for this measurements is the total velocity (C) at the runner inlet being 12.45 m/s. Flow rate of 58.2 liter per second is necessary to build this velocity. Results from the PIV measurement of velocity distribution at position of outlet of GV and at the inlet of runner is compared to that from the fine mesh CFD results for the same operating conditions. The PIV measurements is performed with a Dantec system. The pulsed light sheet with a thickness of 2 mm, is generated by two double-cavity Nd-YAG lasers providing 120 mJ by pulse. The lighted field is visualized by a HiSense 2M CCD PIV cameras, with a series of paired images acquired at 150 μs and 4 Hz. Alignment of laser and camera with respect to the measurement plane is achieved with separate laser pointers. Fluorescent seeding particles, with a density of 1.016 kg/m^3, refractive index of 1.52 and mean diameter of 55 μm are used during the measurements. The camera resolution is 1280x1024 pixels for a 350x400 mm spatial domain. The camera exposition and its synchronization with laser and the image processing is done with a Dantec DynamicStudio 3.40 PIV specific processor. The image processing is carried out with 32-pixel resolution cross-correlation technique with 50% overlap. **Figure 28** shows the shows the field of view of the test section and circular position of turbine components. Velocity vectors are obtained along the mid span of the test setup from the PIV measurements, with the time-averaged value for 100 image pairs. **Figure 29** shows the comparison between results from PIV measurements with that of CFD simulations for similar flow conditions. Tangential velocity distribution along the circular section of GV outlet and runner inlet, as shown in **Figure 28**, is used as basis for this comparison. It can be observed that CFD results at GV outlet position is very close with that of PIV results. However, as expected, CFD over predicts the wake with respect to PIV measurements. At the runner inlet position as well, CFD results is close to that of PIV measurements. Effects of wall due to 1 GV cascade, and also measurements being conducted at lower velocities, could be the reasons for the velocity form PIV measurements, at the runner inlet, being less uniform with respect to the analytical velocity profile as shown in **Figure 29**. With these

PIV results, it can be inferred that 1 GV test setup can produce the velocity conditions comparable with the prototype turbine.

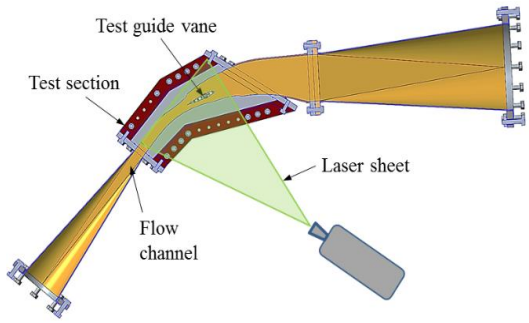

Figure 26. Cross section view of 1 GV test setup

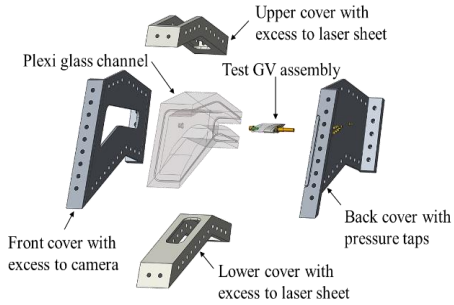

Figure 27. Exploded view of the test section

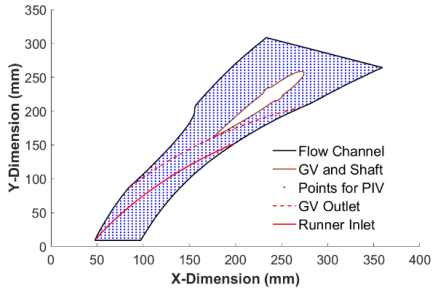

Figure 28. Test Section and measurement points for PIV

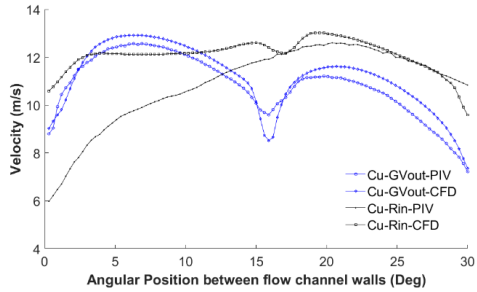

Figure 29. Comparison between PIV and CFD results

4.3 Comparison with similar studies

There are some past studies for the flow analysis with the use of cascade GV setup. Comparison with the methods adopted for the design of such setup could not be done as the available literatures does not discuss the design methods in detail. Most of studies are focused on the measurements of wake behind the GV and on the prediction of rotor-stator interaction. Antonsen [32] has conducted measurements of wake flow in a 5 GV cascade setup for a high head Francis turbine. He has also compared the results with the CFD study. **Figure 30** shows comparison of LDA measurements and CFD studies of wake behind the GV of a Francis turbine from his study. The measurements were done along the direction normal to the wake and not along the runner inlet as for this study. The

profile of wake from his study can be compared with that estimated by CFD simulations for optimized design of 1 GV cascade. The constant velocity contours in zoomed section (**Figure 23**) shows the formation and dissipation of wake behind the GV that also matches to the results from Antonsen (**Figure 30**).

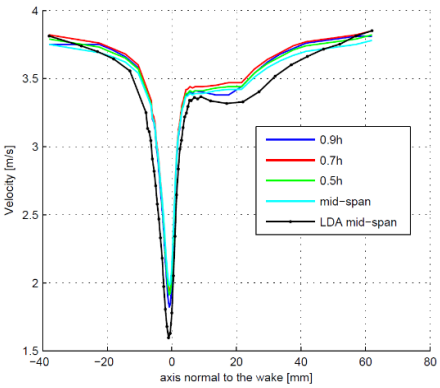

Figure 30. LDV and CFD study of wake behind guide vane [32]

Larsson [9] has conducted the measurement of velocity components along the circular section in the vane less gap between the outlet of GV and the inlet of runner. He has also compared the experimental results with different numerical simulations. **Figure 31** shows the distribution of tangential velocity along the vane less gap for one GV pitch in circumferential direction. He has verified this result with the actual measurements of velocity in vane less space in a model turbine. His CFD simulations, both with coarse mesh and fine mesh, were not able to predict the wake flow accurately. It can be observed that the profile of tangential velocity at GV outlet measured by Larsson is similar to that predicted for 1 GV cascade with the PIV measurements and CFD study shown in **Figure 29**. Simulations with the coarse mesh for pressure distribution in the vane less space done by Larsson is presented in **Figure 32**. Profile of pressure distribution obtained from his result is comparable with that for the optimum design of 1 GV cascade for this study, as presented in **Figure 24**. Due to difference in pressure along the pressure side and suction side of GV, runner experiences marginal increase in pressure as it passes from suction side of one GV to the point of wake interactions, and again experiences marginal reduction in pressure as it reaches to the suction side of adjacent GV. This pressure fluctuation also has its effects on velocity profile along the inlet of runner from the suction side of one GV to another. Hence, runner passes through the contours of different velocity magnitudes as it crosses one GV to another. This phenomenon can be observed in **Figure 23**, **Figure 13** and **Figure 14**. Thus, it can be accepted that the velocity profiles created by 1 GV cascade at the runner inlet is much closer to the prototype Francis turbine operating at BEP.

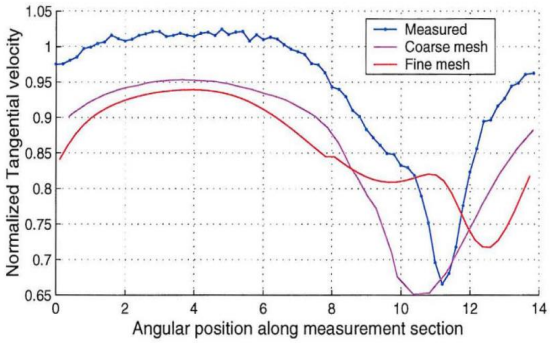

Figure 31. LDA and CFD measurements of velocity component behind GV [9]

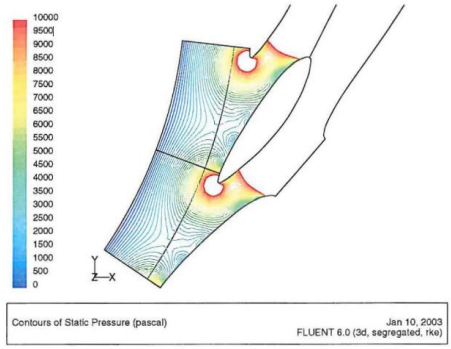

Figure 32. CFD study of pressure distribution behind GV [9]

5. Conclusions

This paper suggests an approach to design a cascade setup for investigating the flow in stator part of low speed number Francis turbines. Several researchers have conducted theoretical, numerical and experimental studies to investigate flow phenomenon inside Francis turbine with different objectives. Stationary cascade with single or multiple guide vanes is often used to study flow in the stator part of Francis turbine. Details of design methods adopted for development of such test setups are not found to be published in available literatures. It is also perceived that none of the measurements in laboratory setup has been done for the prototype operating conditions.

This paper discussed the details of the methods used to design and optimize a cascade test setup for studying the effects of leakage flow between guide vanes and its walls in a low specific speed Francis turbines. Analytical methods are used to design a complete reference turbine. Flow cascade with three guide vanes and one guide vane at the end section of spiral casing are selected as alternative design options. Computed velocity profiles through analytical method are compared with the CFD results to identify the best design option. The design optimization is carried out using coarse mesh and total 11 and 5 simulations are conducted for 3 GV and 1 GV cascade respectively. Furthermore, to investigate effects of spatial discretization and turbulence models, detail mesh independency study are also conducted. It is found that the mesh with two million nodes and eddy viscosity transport equation and high resolution discretization scheme provide good results. Final simulation of the optimum design of test setup is conducted using the verified numerical model. The optimum design is fabricated and experimental validation of flow conditions with respect to CFD and analytical calculations are made.

With this study, it is concluded that optimized design of both 3 GV and 1 GV cascade can create the similar flow conditions at the position of inlet of runner as that in the case of

actual turbine. Due to manufacturing and testing easiness, 1 GV cascade is selected for the development of test setup. Results of measurements from this setup can be compared directly to the case of prototype turbine at BEP conditions. It is also concluded that, for flow analysis and design optimization of problems, CFD studies with relatively coarse mesh can give reliable results.

Acknowledgments

Authors would like to thank Mr. Frode Kjøsnes for his supports in CFD study with fine mesh, and Ms. Linda Haugvaldstad for her support in stress analysis in the test section of the setup.

References

[1] Darmawi, R. Sipahutar, S. M. Bernas, and M. S. Imanuddin, "Renewable energy and hydropower utilization tendency worldwide," Renewable and Sustainable Energy Reviews, vol. 17, pp. 213-215, 2013.

[2] R. Sternberg, "Hydropower's future, the environment, and global electricity systems," Renewable and Sustainable Energy Reviews, vol. 14, pp. 713-723, 2010.

[3] E. Flores, L. Bornard, L. Tomas, J. Liu, and M. Couston, "Design of large Francis turbine using optimal methods," in IOP Conference Series: Earth and Environmental Science, 2012, p. 022023.

[4] H. Brekke, "Hydraulic design strategy for Francis turbines," International Journal on Hydropower and Dams, vol. 3, pp. 38-42, 1996.

[5] X. Yexiang, W. Zhengwei, Y. Zongguo, and Z. Jin, "Experimental and numerical analysis of pressure pulses characteristics in a Francis turbine with partial load," in IOP Conference Series: Earth and Environmental Science, 2010, p. 012023.

[6] M. V. Magnoli and R. Schilling, "Numerical Simulation of Pressure Pulsations in Francis Turbines," in Advances in Hydroinformatics, P. Gourbesville, J. Cunge, and G. Caignaert, Eds., ed: Springer Singapore, 2014, pp. 389-403.

[7] B. S. Thapa, O. G. Dahlhaug, and B. Thapa, "Sediment erosion in hydro turbines and its effect on the flow around guide vanes of Francis turbine," Renewable and Sustainable Energy Reviews, vol. 49, pp. 1100-1113, 2015.

[8] N. Ruchonnet, C. Nicolet, and F. Avellan, "One-dimensional modeling of rotor stator interaction in Francis pump-turbine," in Proceedings of the 23rd IAHR Symposium on Hydraulic Machinery and Systems, 2006.

[9] C. Larsson, Experimental and theoretical analysis of inlet flow of a Francis turbine runner: PhD thesis, Norwegian University of Science and Technology, Faculty of Engineering Science and Technology, 2003.

[10] R. Qian, "Flow field measurements in a stator of a hydraulic turbine," PhD thesis, Laval University, Faculty of Science and Engineering, 2008.

[11] E. Kobro, A. Gamboa, R. Bloch, and T. Nielsen, "Onboard pressure measurement in high head Francis prototype runners," in 3rd IAHR International Meeting of the WorkGroup on Cavitation and Dynamic Problems in Hydraulic Machinery and Systems, Czech Republic, 2009, pp. 14-16.

[12] Y.-x. Xiao, Z.-w. Wang, J. Zhang, and Y.-y. Luo, "Numerical predictions of pressure pulses in a Francis pump turbine with misaligned guide vanes," Journal of Hydrodynamics, Ser. B, vol. 26, pp. 250-256, 2014.

[13] F. Bario and C. Beral, "Boundary layer measurements on the pressure and suction sides of a turbine inlet guide vane," Experimental Thermal and Fluid Science, vol. 17, pp. 1-9, 1998.

[14] Z. Schabowski and H. Hodson, "The Reduction of over tip leakage loss in unshrouded axial turbines using winglets and squealers," Journal of Turbomachinery, vol. 136, 2014.

[15] A. Zobeiri, P. Ausoni, F. Avellan, and M. Farhat, "How oblique trailing edge of a hydrofoil reduces the vortex-induced vibration," Journal of Fluids and Structures, vol. 32, pp. 78-89, 2012.

[16] P. H. E. Finstad, M. Kjeldsen, and R. E. Arndt, "Characterizing Rotor-Stator interaction-RSI in hydrofoil wake using CFD and experimentally obtained wake flow fields," in 14 th International Symposium on Transport Phenomena and Dynamics of Rotating, 2012.

[17] H. Brekke, "Hydraulic Turbines: Design, Erection and Operation," Norwegian University of Science and Technology (NTNU) publications, 2001.

[18] P. M. S. Pradhan, O. G. Dahlhaug, P. N. Joshi, and H. Støle, "Sediment and Efficiency Measurements at Jhimruk Hydropower Plant – Monsoon 2003," Report from HydroLab, Nepal2004.

[19] K. Gjosater, "Hydraulic Design of Francis Turbine Exposed to Sediment Erosion," Masters Thesis, Norwegian University of Science and Technology, 2011.

[20] B. S. Thapa, "Hydraulic design of Francis turbine to minimize sediment erosion," Masters Thesis, Kathmandu University, 2012.

[21] M. Eltvik, "Sediment erosion in Francis turbines," PhD thesis, Norwegian University of Science and Technology, Faculty of Engineering Science and Technology, 2013.

[22] B. S. Thapa, M. Eltvik, K. Gjøsæter, O. G. Dahlhaug, and B. Thapa, "Design Optimization of Francis Runners for Sediment Handling," in Fourth International Conference on Water Resources and Renewable Energy Development in Asia, Thailand, 2012.

[23] B. S. Thapa, K. Gjosater, M. Eltvik, O. G. Dahlhaug, and B. Thapa, "Effects of turbine design parameters on sediment erosion of Francis runner," Dhaka, 2012, pp. 167-171.

[24] B. S. Thapa, B. Thapa, M. Eltvik, K. Gjosater, and O. G. Dahlhaug, "Optimizing runner blade profile of Francis turbine to minimize sediment erosion," in IOP Conference Series: Earth and Environmental Science, 2012, p. 032052.

[25] S. Chitrakar, M. Cervantes, and B. S. Thapa, "Fully coupled FSI analysis of Francis turbines exposed to sediment erosion," International Journal of Fluid Machinery and Systems, vol. 7, pp. 101-109, 2014.

[26] B. Rajkarnikar, H. P. Neopane, and B. S. Thapa, "Development of rotating disc apparatus for test of sediment-induced erosion in francis runner blades," Wear, vol. 306, pp. 119-125, 2013.

[27] X. Chen, "Theoretical and experimental study of flow through the double cascade of a Francis turbine," PhD thesis, Norwegian University of Science and Technology, Faculty of Engineering Science and Technology, 1992.

[28] Z. Wei, P. H. Finstad, G. Olimstad, E. Walseth, and M. Eltvik, "High Pressure Hydraulic Machinery," in Compendium, N. Publication, Ed., ed, 2009.

[29] ANSYS, Ansys 16.0 Release Documentation, Theory and Modelling Guide. ANSYS Inc., Southpointe, 2600 ANSYS Drive, Canonsburg, PA 15317, USA, 2015.

[30] C. Trivedi, M. J. Cervantes, O. G. Dahlhaug, and B. K. Gandhi, "Experimental Investigation of a High Head Francis Turbine During Spin-No-Load Operation," Journal of Fluids Engineering, vol. 137, pp. 061106-061106, 2015.

[31] J. H. Ferziger and M. Perić, Computational methods for fluid dynamics vol. 3: Springer Berlin, 2002.

[32] Ø. Antonsen, "Unsteady flow in wicket gate and runner with focus on static and dynamic load on runner," Doctoral Thesis, PhD thesis, Norwegian University of Science and Technology, Faculty of Engineering Science and Technology, 2007.

Paper-C

Flow measurements in the distributor of Francis turbine: *A PIV approach*

Biraj Singh Thapa, Ole Gunnar Dahlhaug and Bhola Thapa

Submitted to Journal, Renewable Energy, 2016

Flow measurements in the distributor of Francis turbine: *A PIV approach*

Biraj Singh Thapa [1]; Ole Gunnar Dahlhaug [1]; Bhola Thapa[2]

[1]Department of Energy and Process Engineering, Norwegian University of Science and Technology, Norway

[2]Department of Mechanical Engineering, Kathmandu University, Nepal

Abstract

A guide vane cascade is developed for the study of flow in the distributor of a low specific speed Francis turbine. Velocity and pressure measurements are done with Reynold's number 1.15E+07, at 80% of BEP flow as in a reference prototype turbine. This work illustrates the development of test setup and focuses on investigation of PIV methods applied for the velocity measurements. Techniques developed for 'in-situ' calibration of PIV setup and methods applied for image processing are discussed in details. Approach to estimate total uncertainty in PIV measurements and minimum no of image pairs required for statistical convergence of velocity field is presented. Reference measurements are done along the plane of chord, from guide vane wall to its mid-span. Flow velocity exceeding 35 m/s, at the runner inlet of Francis turbine, is reported for the first time from such an experimental study. Flow phenomenon inside Francis turbine distributor are characterized and comparison are done with the cases for prototype turbines. The cascade setup is found to reproduce the flow conditions inside a Francis turbine distributor, except the rotor-stator-interaction. PIV methods are generalized for the cases of similar measurements and the results will be applicable to validate numerical studies.

***Keywords*:** Francis turbine; Guide vane; Cascade; PIV; Uncertainty; Velocity triangle

1. Introduction

Since the first installation of hydroelectric power plant in 1827, this green energy technology has undergone several innovations and capacity enhancements. At present hydropower sector produces more than 1211 GW electricity worldwide, which is about 20% of total electricity supply [2]. As thermal energy is not associated with hydropower system, the efficiency of this technology may reach100% in theory [3]. In practice, up to 93% efficiency is possible, which makes hydropower one of the most efficient and economic energy resources. Two third of technically feasible hydropower resources are

still undeveloped. More than 80% of the undeveloped hydropower resources lie in Asia, South America and Africa [4]. Hence, future of hydropower developments will be more localized in these regions.

Energy conversion process in a hydropower system occurs in several intermittent stages. Major stages include conversion of potential energy stored in reservoir to kinetic and pressure energy in the penstock, then to mechanical energy in the turbine, and finally to electrical energy in the generators. The most complicated energy conversion occurs inside the turbines, where water transfers its hydraulic energy and exits out from the system. The turbines are mechanical components, which include runners that are driven by hydraulic energy of water. Depending upon nature of flow parameters and mechanism of energy conversion, the hydro turbines are classified into several types. Francis type of turbines, which harness both kinetic and potential energy in water, are most commonly used in hydropower systems due to its high efficiency and flexibility [5].

Figure 1 shows cross section of a Francis turbine with flow velocities at respective components. Spiral casing (SC), stay vanes (SV) and guide vanes (GV), together, are often called as the distributor part of turbine. Flow accelerates inside the distributor and normally 50% potential energy is converted to kinetic energy before water enters into runner. GV regulates the flow into runner and gives it correct tangential velocity

Nomenclature	
C	total flow velocity, m/s
C_m	meridional component of C, m/s
C_u	tangential component of C, m/s
E	specific hydraulic energy, jkg^{-1}
g	acceleration due to gravity, m/s^2
H	height of runner, m
H_n	net/effective head to turbine, m
n	rotational speed of runner, s^{-1}
N_{QE}	specific speed,-
Q	discharge through turbine, m^3/s
S	span, m
U	runner peripheral velocity, m/s
W	relative velocity, m/s
β	runner inlet angle, deg
ε	uncertainty, %
η_h	hydraulic efficiency,-
ω	runner angular speed, rad/s
Subscripts	
in, o	inlet and outlet of respective parts
int	instantaneous
red	reduced
rep	repetition
sys	systematic
t	total
Abbreviations	
BEP	best efficiency point
GV	guide vane
GVds	guide vane downstream
IA	interrogation area
IEC	international electrotechnical commission
R	runner
RSI	rotor-stator-interaction
PIV	particle image velocimetry
PP	periodic position
SC	spiral casing
SV	stay vane
TGV	test guide vane

required for the energy conversion process. Water leaves runner with a high relative velocity and exits through draft tube.

Francis turbines are normally designed with the aim to maximize hydraulic efficiency, minimize size and avoid cavitation [6]. These conditions demands high flow velocity and high blade loading inside runner. Such conditions induce several undesirable effects, particularly at off design operating points. Secondary flows originating from distributor, and pressure pulsations originating from draft tube, are identified as the most undesirable phenomenon inside Francis turbines [7]. Furthermore, the rotating runner interacts with static distributor and produces periodic disturbance in flow, called as rotor-stator-interaction (RSI). High velocity in distributor produces wake, which further interacts with RSI and downstream flow. These phenomenon cause non-uniform pressure and velocity distribution inside turbine and induce dynamic load on runner [8]. Performance and effective life of a Francis turbine is highly dependent on minimization of such undesirable phenomenon. Operating condition with sediment-laden flow and cavitating flows add additional challenges. Problems induced by the eroded surfaces due material removal are often associated with such operating conditions [9].

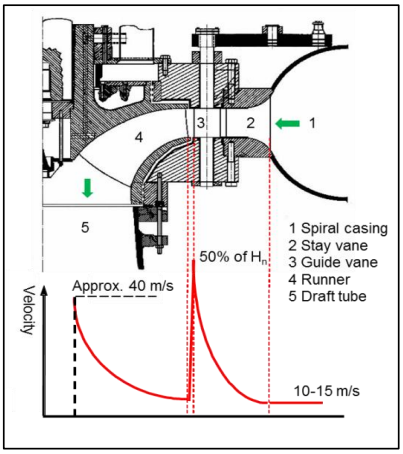

Figure 1. Velocity distribution inside Francis turbine [1]

Different approaches to design and optimize Francis turbine for specific design requirements have been proposed by several researchers [10-12]. Traditional designs methods are specifically developed for the clean water operation and hence such turbines are not operating satisfactorily in sediment-laden projects [13]. There has been some attempts for design improvements of Francis turbines for operation in high sediment load, but necessity of further research has been identified for technological advancement [14]. In the future, development of hydropower will occur in across the region, where problem of sediment erosion of mechanical components has been a major challenge [4]. Hence, the optimization of design procedures, to include sediment erosion as one of the design parameters appears as a research gap at present.

The presented work is a part of a study to identify the effects of sediment erosion of guide vanes on the performance of Francis turbine. The goal of the study is to optimize the design methods of the guide vanes for sediment-laden projects. A guide vane cascade has been developed to reproduce the flow inside Francis turbine at the prototype operating conditions, with the flexibility of PIV measurements. Pressure and velocity measurements

have been conducted to study flow characteristics inside the distributor system. This paper discusses the procedures used to develop the cascade, methods used for PIV measurement technique, and the results for the reference case. The presented results will be used to compare with the cases of eroded guide vanes and optimized designs of guide vanes. The experimental data will also be made available to validate numerical modelling for similar studies.

2. Development of test setup

2.1 Reference turbine

Jhimruk Hydroelectric Centre in Nepal is considered as the reference case for this study. The power plant has three units of Francis turbine, each producing 4.2 MW at BEP. These are splitter bladed Francis turbines as with specific speed 0.086, as defined in equation (**Eq. 1**) by IEC guidelines [15].

$$N_{QE} = \frac{n \cdot Q^{0.5}}{E^{0.75}} \qquad (-) \qquad \textbf{Eq. 1}$$

Where, N_{QE} is specific speed, n is speed of runner (s^{-1}), Q is discharge through turbine (m^3/s) and E is specific hydraulic energy of turbine (Jkg^{-1}).

This power plant also represents a typical case of projects operating under large sediment load in Himalayan basin [1]. Design and drawings of the prototypes are not available. An in-house tool named as "*Khoj*", was developed to design a reference turbine with the aim to replace with the existing one [16]. Extensive investigations have been carried out on this reference turbine for optimizing hydraulic design of runner to resist sediment erosion [16, 17]. Current studies focus on optimization guide vanes for the same reference turbine.

Table 1 presents the relevant analytical values for the reference turbine at BEP. These parameters are used to develop the test setup for this study.

Table 1. Reference turbine analytical design values

S.N.	Parameters	Symbol	Unit	Value
1	Net head	H_n	m	201.5
2	Flow rate per unit turbine	Q	m^3/s	2.35
3	Rotational speed	n	s^{-1}	16.67
4	Specific speed	N_{QE}	-	0.086
5	Number of blades in runner	Z_{blade}	-	17
6	Inlet diameter of runner	*D-Rin*	m	0.89

7	Number of Guide vanes	Z_{GV}	-	24
8	Chord length of GV	L_{GV}	m	0.14

2.2 Design and optimization of flow cascade

A symmetric section of reference turbine forms the flow cascade. Some of the researchers have considered a straight channel with single guide vane [18], while others have considered a section of model turbine to investigate the passage flow conditions [19]. Choice of cascade profile depends upon objectives and requirements of the measurements. For the present study, three GV with two flow passages out of the 24 GV passages is considered as periodic flow channel. This configuration has a single test guide vane (TGV) inside the flow channel. Two outer GV forms as part the boundary wall of cascade and middle GV guides flow in the channel. This layout of the test setup is named as one GV test setup. The purpose of this setup is to examine flow conditions around the distributor of low specific speed Francis turbine. The setup isolates the effects of runner on the flow field and hence allows precise study of flow characteristics in distributor part of Francis turbine. **Figure 2** shows the layout of cascade designed for the BEP operation. Cascade boundary walls, from inlet to outlet, including positon center of SC, GV and runner inlet can be seen. SV are not included as part of cascade, as they are mainly for strengthening spiral casing and do not play significant role for hydraulic design [20]. Circular portion of SC is replaced with flat plates, with the same height as that of the span of GV. Thus, section from inlet to outlet of cascade is embedded between two flat plates. This makes the design relatively simple and easy for manufacturing. However, such simplification would affect the flow conditions and hence the optimization of geometry of the cascade's periodic walls is necessary. CFD based optimization techniques are applied to redesign the profile from the inlet of cascade to the center of spiral casing, and from the inlet of runner to the outlet of cascade until the satisfactory flow conditions are obtained. The profile of the periodic wall upstream of the center of the spiral casing up to the inlet of cascade is re-designed to develop the required velocity components at the center of spiral casing from completely axial flow at the inlet of cascade (**Figure 2**). The criteria to satisfy the optimization goal are to have same tangential and meridional velocity at the position of runner inlet inside the cascade, as that observed in the case of reference prototype turbine. **Figure 3** shows the respective velocity components inside the reference Francis turbine that has been considered for this study. SVo and Rin represents stay vane outlet and runner inlet position respectively. Details of design optimization and CFD analysis is discussed in earlier work by the same authors [21].

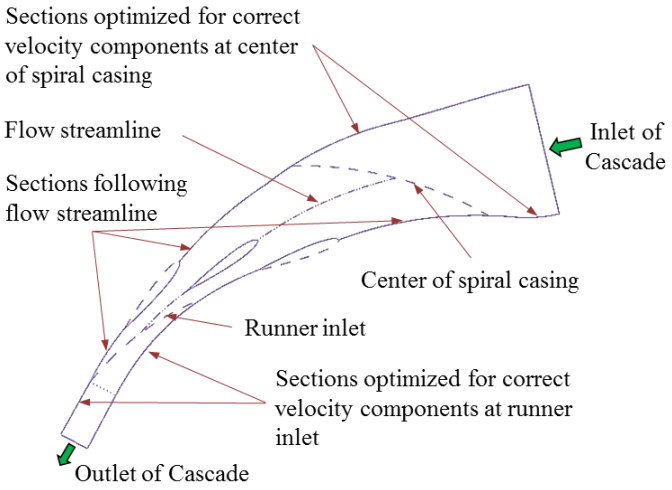

Figure 2. Reference design and sections for optimization

Development of the experimental test setup is based on the layout of optimum design as shown in **Figure 2**. This configuration represents the flow around one GV, between two periodic GV flow channels of a Francis turbine. Angular position covered by the periodic walls inside cascade is 30 degrees from the turbine center, which is 1/12th size of turbine in circumferential direction. **Figure 4** shows the cross section view of the test setup along the plane of the TGV chord. The test section contains the TGV inside the flow channel. **Figure 5** shows exploded view of the test section designed for PIV measurements. The flow channel is made by plexi-glass and is packed inside steel cover plates to hold the pressure up to 10 bars.

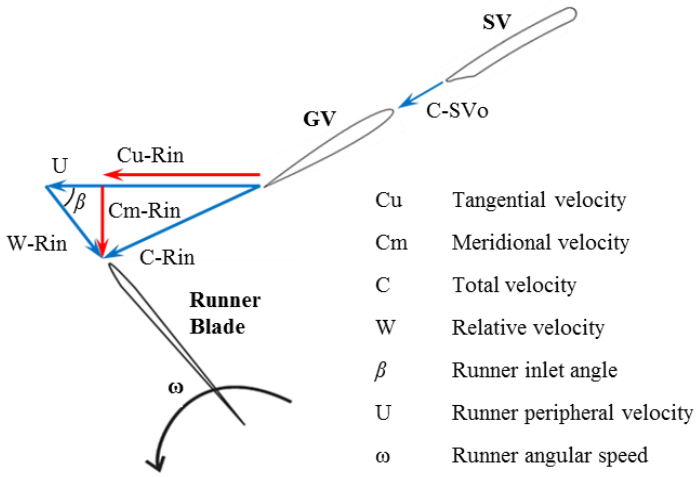

Figure 3. Velocity Components in Turbine

Cover plates are designed to give optical excess for laser and camera for PIV recording. The TGV has been designed as an assembly of parts made by plexi and aluminum. Plexi part of TGV imparts transmission of the laser sheet, allowing flow visualization inside the flow channel. Separate TGV are designed for velocity and pressure measurements to meet the specific requirements.

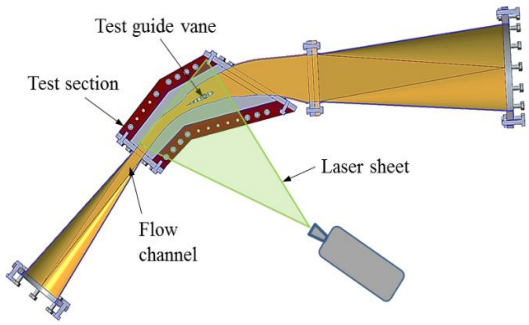

Figure 4. Sectional view of test setup along measurement plane

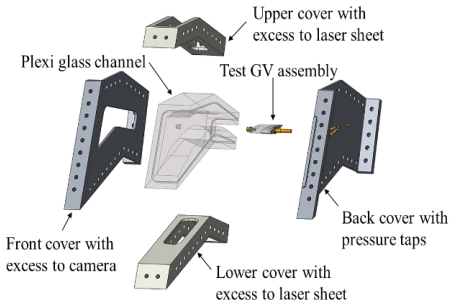

Figure 5. Test section components designed for PIV measurement

2.3 Flow conditions and measurements locations

The test setup is installed at the facilities of the Waterpower Laboratory at NTNU. The setup is mounted in a closed loop system consisting of pump, flow meter, and a pressure tank. The flowmeter is calibrated with volumetric methods as per IEC guidelines [15] and the total uncertainty is found to be below ± 0.15%.

Table 2 shows the comparison of flow conditions inside cascade with the prototype turbine at BEP. Equivalent turbine head for cascade is calculated for the same reduced velocity (**Eq. 3**), as for the prototype, defined by Brekke [6]. Reynold's number for runner and GV is calculated as defined by IEC [15]. All the measurements for this study are conducted with flow rate of 0.155 m^3/s. This is close to 80% of design flow for the same flow area in the prototype at BEP. The close loop system is pressurized and maintained at eight bars to achieve this flow condition to avoid cavitation. With this flow rate, the average velocity obtained at the runner inlet position, is 33.29 m/s. For obtaining the prototype operating conditions inside the cascade, the maximum pressure inside test loop exceeded above ten bars. Due practical limitations, all the measurements for this study are conducted with the conditions listed in **Table 2**.

Pressure measurements are done along the TGV surface at test section wall, and separately at TGV surface along its mid-span. **Figure 6** shows the arrangements of surface pressure measurement at the TGV end span. Fourteen pressure taps are inserted in the test section cover plate to measure pressure around the TGV surface. One tap is located at TGV leading

edge and trailing edge respectively. Remaining twelve taps are located at six different symmetric positions along TGV chord at pressure side and suction side respectively.

Table 2. Operating conditions for prototype and cascade

Parameters	**Symbol**	**Unit**	**Prototype**	**Cascade**
Flow rate per channel	Qc	m^3/s	0.195	0.155
Total velocity at runner inlet	C-Rin	m/s	41.86	33.29
Equivalent turbine head	H	m	201.5	129.8
Shape of GV profile	-	-	NACA 0012	NACA 0012
Reynold's no for runner	Re-R	-	1.52E+07	1.15E+07
Reynold's no for GV	Re-GV	-	1.05E+06	8.58E+05

Figure 7 shows the arrangements for the pressure measurement along TGV mid-span. Eleven pressure taps are inserted along on the TGV surface. Taps are located at the same position along TGV chord as for the first eleven taps for surface pressure measurement, starting from the leading edge. The TGV parts for pressure measurements at mid-span are 3D printed to allow the taps to pass internally through TGV and come out of TGV shaft to be connected to pressure sensors. Each pressure tap is connected to piezo-resistive pressure transducer through a plastic pipe of 1.6 mm inner diameter. Pressure measurements from all the taps are conducted simultaneously with the same flow conditions as that for the PIV measurements. This insures direct comparison of pressure and velocity fields inside the test section for respective flow conditions. All pressure sensors are pre-calibrated against a dead weight calibrator. Measurement uncertainly was maintained to be below 0.05% at all the measuring points. An average of 2000 samples, for each pressure point, measured at 5 HZ, is considered for the pressure analysis.

3. PIV Methods

3.1 Introduction and approach

PIV is an optical and a nonintrusive technique for accurate, quantitative measurement of fluid velocity vectors. With its first application in 1980s, PIV has undergone many development phases. With modern equipment, it offers both spatial and temporal resolution sufficient to permit the computation of instantaneous fluid vorticity and rate of strain [22]. Due to its non-intrusive nature and planer or volumetric flow field measurements, PIV techniques is getting increasingly applied in hydro turbine research, to analyze from complex turbulent to two phase flows [23]. Unique methods have been devised for excess

of laser and camera inside the flow passage of rotating turbine blades for velocity measurements in the inter-blade channel of a hydraulic turbine [24].

A 2D PIV technique has been applied in this study. **Figure 8** shows the schematic procedures and elements used for this type of PIV measurement. Two double-cavity Nd-YAG lasers providing 120 mJ by pulse, forming a light sheet with the thickness (Δz_0) of 2 mm, are separated by adjustable time delay (Δt) of 75 μs. The pulse durations of laser is of 4 ns, which are short enough to freeze the image with the movement at sub-pixel level for the expected maximum velocity of 35 m/s in the flow channel. Fluorescent seeding particles, with a density of 1.016 kg/m^3, refractive index of 1.52 and mean diameter of 55 μm are used during the measurements. Average particle density in each interrogation area is maintained between 10 to 15. Scattered light from the same seeder particles in each laser pulse are captured and stored by camera in its first and second frames respectively. A CCD camera with resolution of 1280x1024 pixels and the pixel size of 7.4 μm is used to record image at 10 bits resolution of grey scale. Total 1103 grid points are equally spaced under the measurement area of 0.026 m^2. Unique velocity vectors are obtained by PIV for each grid point, which are separated by 4.7 mm in physical space. Multiple image pairs are captured at the trigger rate of 4 Hz to satisfy statistical convergence of flow vectors in each interrogation area. The camera exposition, its synchronization with laser and image processing are done with a Dantec DynamicStudio 3.40 PIV specific processor. The displacement of the particle images in each interrogation area is measured by cross-correlating the images of the first and second frames, to find the mean displacement that gives the maximum correlation. Displacement (Δx, Δy) over the time delay (Δt) gives 2D velocity vectors for each interrogation area. In-house post processing tools are developed for computation and display of relevant information of flow field.

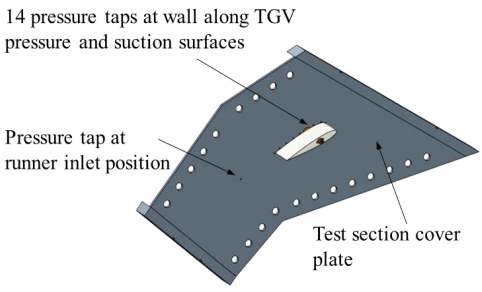

Figure 6. Pressure measurements along GV surface

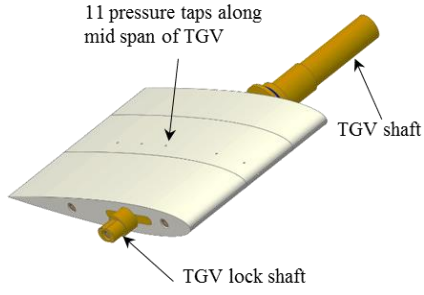

Figure 7. Pressure measurements at TGV mid-span

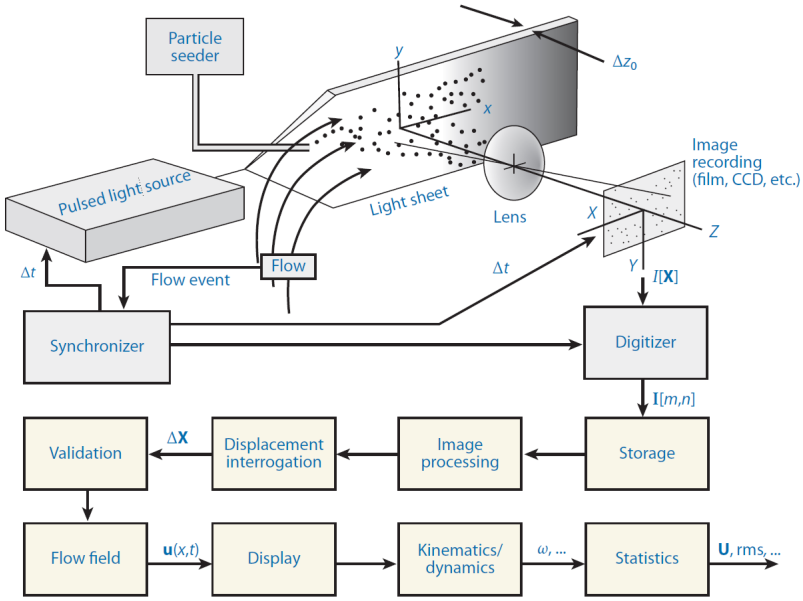

Figure 8. Procedures and elements for 2D PIV [25]

The laser sheet for PIV is positioned to capture the entire flow flied inside test section plexi channel along the plane of TGV chord (**Figure 4**). Geometry of test section allows measurement of velocity vectors from the position of SV outlet to the position of runner inlet. **Figure 9** shows the region of interest from PIV image along the plane of measurement. Position of respective turbine components from SV outlet to runner inlet, inside the flow channel, can be observed. Periodic position (PP) between the cascade walls represents 30 degree angular position in circumferential direction with respect to turbine center. It can be observed that the PP from 0% to 50% represents the pressure side of the flow and PP from 50% to 100% represents the suction side of the flow respectively.

The test section is designed to conduct PIV measurements from the TGV wall up-to the TGV mid-span. **Figure 10** shows the measurement span inside the test section with respect to position of runner blade in axial view. At runner inlet position, the measurement span covers the position between runner hub to the runner mid height. The PIV measurement is started from the plane of test section wall and is preceded towards TGV mid-span. Total 25 different measurement planes are distributed inside the measurement span with higher spatial resolution towards the wall. Starting from the wall, these measurement planes are separated by 0.25 mm for first 4 planes, and by 0.5 mm for next 8 planes. Similarly next 5 measurement planes are separated by 2 mm and last 6 measurement planes are separated by 5 mm respectively. It is expected that this spatial distribution of measurement planes is sufficient to capture the steady state flow field within the volume of measurement span.

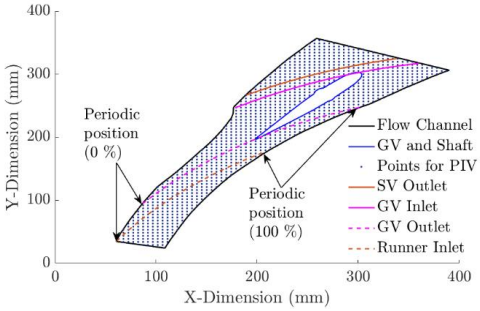

Figure 9. PIV measurement section and positons

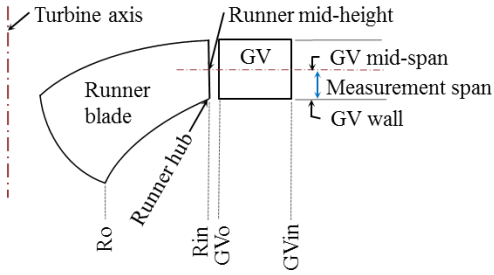

Figure 10. Measurement area relative to runner blade

3.2 Calibration and processing technique

A CCD camera used for PIV application digitizes the captured image and stores it inform of binary data for each pixel. The actual objects dimension depends upon the image dimension and focal length of camera lens, as defined by geometrical lens law. In practice the object dimensions are often calculated from the captured images as a multiple of a scale factor, defined by **Eq. 2.**

$$\boldsymbol{Object\ dimension = Scale\ factor * camera\ pixel\ size} \quad \textbf{[mm/pixel]} \quad \textbf{Eq. 2}$$

For a planar PIV, the scale factor is determined by estimating number of pixels covered by a known dimension in the imaging plane. A pin hole calibration method, which uses calibration target plate with multiple dots equally spaced in imaging plane is widely used, for calibration of planar PIV [26]. This method transforms the image using linear or polynomial functions such that control points in calibration image align with the known relative positions of these points in the physical world. Same calibration principle has been followed for this study.

As the measurements have been conducted in 25 different imaging planes, the scale factor for each plane is needed to be determined separately. A tailor made *'in-situ'* calibration method has been developed for this purpose. **Figure 11** shows the design of the calibration system for this study. Spot plates, replacing the conventional target plate, are designed to fit into the geometry of the test setup and be accurately positioned in the respective imaging planes. Sliding block is designed to be inserted inside the plexi glass flow channel. Base plate slides into the grooves of sliding block and carries two pairs of the spot plates at the known distance. Each spot plate has five white spots of 2 mm diameter at equi-distance of 20 mm from the central spot. Back spot plate pair is positioned at 5 mm behind the front spot plate pair. The spot plates are manually positioned to the correct imaging plane by guiding it against a pre-positioned scale on the sliding block. Unique scale factor is

calculated for all the 25 planes of measurement, averaging it from the front spot plate and back spot plate respectively. **Figure 12** shows the physical dimension of object in terms of number of pixels occupied by the image for different plane of measurements, calculated as per **Eq 2**. As the object plane closer to camera covers larger number of pixel, its corresponding scale factor and object dimensions both are smaller. It is estimated that the accuracy in positioning the spot plates on the measurement plane was ± 0.25 mm. This adds ± 0.02% of uncertainty for measurement of scale factor and can therefore be neglected owing to its insignificant influence on total uncertainty in velocity measurements.

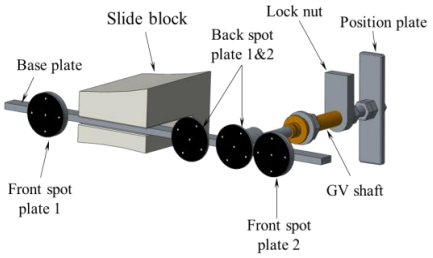

Figure 11. Design of calibration system for PIV

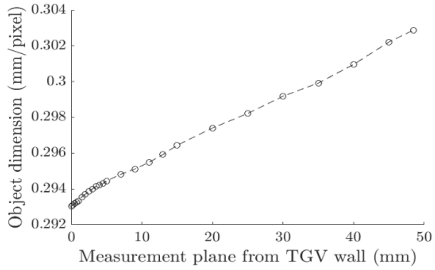

Figure 12. Scale factor for PIV measurement planes

Image processing of PIV data is done as per the standard methods and descriptions discussed in details in literatures [27, 28]. **Figure 13** summarizes the important steps for image processing considered for this study. Image acquisition settings are selected to minimize bad vectors and uncertainty in measurements. Seeding density, laser thickness and acceleration of flow in measurement area also contributes to the image acquisition settings. The frames are divided into interrogation area of 32x32 pixel resolution. Image processing tools relating with cross-correlation technique with 50% overlap are applied to locate the position of same particles in respective frames in each interrogation area. Overlapping of interrogation area by 50% increases the number of velocity vectors by twice but it also smooth the velocity gradients due to its relatively larger window size. Statistical convergence of flow vectors is done to determine the minimum number of image pairs required for steady velocity components. Post processing tools have been developed separately to extract the velocity field in desired locations and to display them in suitable format.

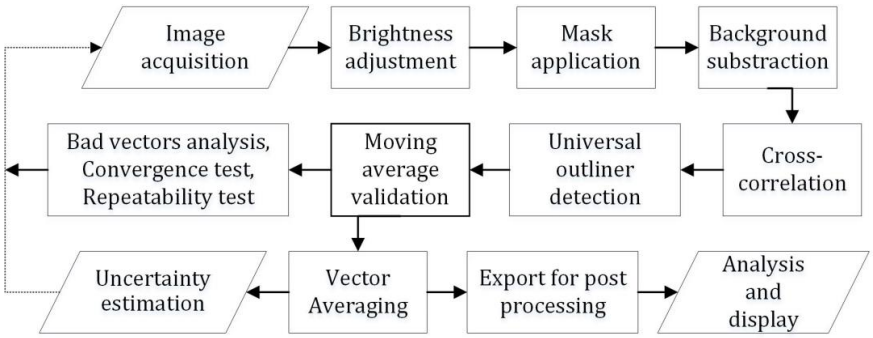

Figure 13. PIV image processing flow chart

3.3 Uncertainty and Repeatability

PIV methods include several variables and estimating the contribution of each variable to the measuring uncertainty could be complicated and challenging. Good choice of particles, image acquisition settings and image processing methods can give the total uncertainty less than 5% even in the most challenging flows [29]. For this study, methods are applied for the estimation of random uncertainty in PIV measurement. Past studies have shown than a typical systematic uncertainty (ε_{sys}) for the PIV setup, as used for this study, is up to $\pm$ 2% [28].

A study of position and density of bad vectors in each interrogation area (IA) has been done. Total 100 image pairs are captured and processed to compute instantaneous velocity vectors in each time step as per methods outlined in **Figure 13**. Standard methods relating to 'universal outliner detection' and 'moving average validation' as defined in literatures [27, 28] are applied to locate bad vectors in each instantaneous velocity field. Bad vectors, in each interrogation area, for all 100 instantaneous velocity field, are extracted and grouped. **Figure 14** shows the intensity and distribution of bad vectors at GV mid-span plane. Average bad vectors are estimated to be 11% with all 100 image pairs. It can be observed that most of the bad vectors are segregated in two specific locations. **Figure 15** shows the instantaneous image captured by the camera for this analysis. Strong shadows are seen in the same locations as that for high intensity of bad vectors. These shadows can be reduced by increasing the laser intensity, but cannot be eliminated. One way to reduce the uncertainty due to bad vectors is to estimate minimum number of good vectors needed to converse velocity in the desired area.

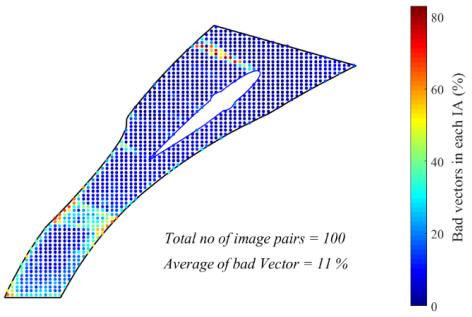

Figure 14. Distribution of bad vectors in flow field

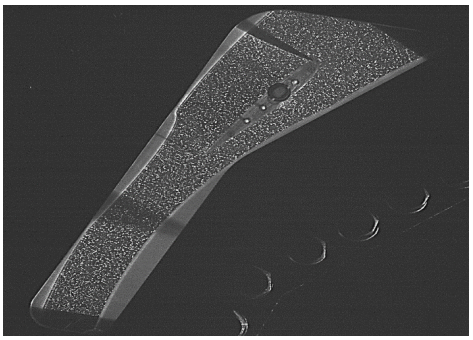

Figure 15. Unprocessed PIV image of flow field

Convergence tests are done to determine minimum number of good vectors to keep the time evolution of average velocity within the standard error of mean (SEM) limits of 95% confidence intervals. 200 image pairs are captured and bad vectors are removed. Analysis are done at 50% periodic position at the runner inlet (**Figure 9**). This position falls close to the center of region with the segregated bad vectors, at downstream of guide vane (**Figure 14**). **Figure 16** shows the time evolution of velocity and standard deviation of good vectors. Calculation of running average velocity ($\bar{C}$) and running standard deviation ($\bar{\sigma}$) is done as per the equations presented in **Table 3**. It is estimated that minimum 60 good vectors (N_{min}) are required to converse velocity and standard deviation (**Figure 16**). With maximum 40% bad vectors in this area, it can be assumed that 100 pairs of images will be sufficient to converge the velocity field in this area of interest inside the test section.

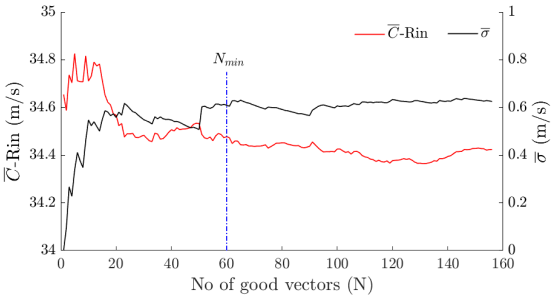

Figure 16. Convergence tests at runner inlet

Random uncertainty of PIV measurement is estimated as separate components. The first is component is named as uncertainty in instantaneous velocity measurement (ε_{int}). This estimates random uncertainty in instantaneous velocity, for each interrogation area, with respect to mean velocity of 100 image pairs, in respective interrogation area. The second component is named as uncertainty in measurement repetition (ε_{rep}). This estimates random uncertainty in average velocity from the different sets of measurements with the same flow conditions. Both uncertainties are estimated based on the equations presented in **Table 3**. The distribution of ε_{int} inside the flow channel is shown **Figure 17**.

The highest uncertainty being around upper part of TGV inlet section shows that shadow has strong effects on the good vectors as well. It can also be seen that elimination of bad vectors downstream of TGV has improved the average velocity field in this region. The maximum ε_{int} in this region, which is also the region of interest, is below ±1.5%. **Figure 18** shows estimated ε_{rep} based on five different sets of measurements on conducted at different dates, and with the same flow conditions. Velocity at runner inlet position, along the periodic position of cascade walls, is considered to check the repeatability, as this is the most important region of interest and also carries highest velocities within in the measurement area. The repetition of flow field also depends upon the ability of the test setup to produce the same velocity conditions for the different measurements. Hence, ε_{rep} represents uncertainty of repeatability of the entire measurement system. Higher ε_{rep} at the walls signifies presence of non-linear boundary layer flow close to walls, which can also be seen in **Figure 17**. Average ε_{rep} along the runner inlet position is estimated to be ±1.44%.

Table 3. Description of statistical methods

Parameter	Description
Average velocity	$C(x,y) = \frac{1}{N}\sum_{i=1}^{N} C(x,y,t_i)$
Standard deviation	$\sigma = \sqrt{\frac{1}{N-1}\sum_{i=1}^{N}(C(x,y) - C(x,y,t_i))^2}$
Standard error of mean (SEM)	$\delta = \pm(1.96 \cdot \frac{\sigma}{\sqrt{N}})$
% Random uncertainty of mean	$\varepsilon = \pm\frac{\delta}{C(x,y)} \cdot 100$
Running average velocity	$\bar{C} = \frac{1}{N}\sum_{i=1}^{N} C(x,y,t_0 + i\Delta t)$
Running standard deviation	$\bar{\sigma} = \frac{1}{N}\sum_{i=1}^{N} \sigma(x,y,t_0 + i\Delta t)$

The total uncertainty (ε_t) in PIV measurement is calculated as the root mean square of all ε_{sys}, ε_{int} and ε_{rep}. It is estimated that total uncertainty associated the velocity measurements

(ε_t) is below ±2.5%. This ε_t is accepted to fall within the limit of standard PIV methods for such applications as also reported by other researchers [30].

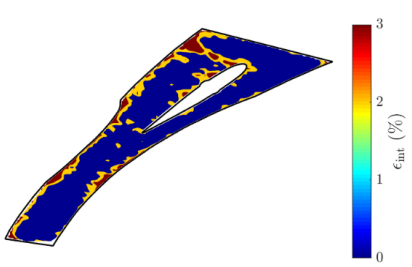

Figure 17. Uncertainty of PIV: instantaneous measurement

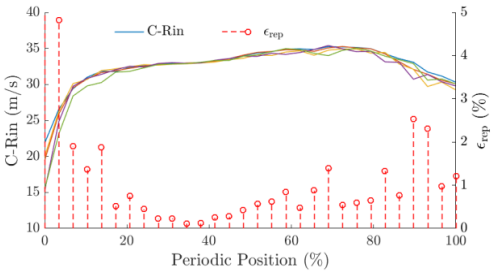

Figure 18. Uncertainty of PIV: measurement repetition

4. Measurement Results and Discussions

This article presents the results of pressure and velocity measurements with the flow conditions, as described in Table 2. Pressure measurements are done along the pressure and the suction side at the TGV wall and at the TGV mid-span, described in section 2.3. Velocity measurements are done at 25 different planes between the TGV wall and the TGV mid-span, described in section 3.

Figure 19 compares the pressure distribution along the TGV wall and the TGV mid-span. The highest pressure at the leading edge shows the stagnation point. A clear pattern of pressure and suction side can be observed as the flow progresses towards the trailing edge. Equal distribution of pressure up to 10% of the TGV chord from the leading edge shows angle of attack close to zero. As the TGV chord is located at different radius from the center of flow streamlines, a gradual development of pressure difference towards trailing edge is observed. Maximum pressure difference occurs at 75% of the chord length and pressure from the both surfaces equalize at the TGV trailing edge. Boundary layer flow at the test section wall causes lower velocities and hence lowers dynamic pressure at the walls. Thus, higher stagnation pressure is observed at the mid-span than that at the wall. Fairly equal pressure distribution at the wall and the mid-span, downstream of stagnation point, suggests equal of static pressure around the TGV surfaces in both planes of measurements. Observation of pressure measurements matches general behavior of symmetric guide vanes in Francis turbines, as reported by Antonsen [31].

Figure 20 shows velocity distribution inside the flow cascade obtained from PIV measurements along the plane of TGV mid-span. The basic flow phenomenon as stagnation point at the leading edge of TGV, development of flow around the pressure and the suction sides and formation of wake at the trailing edge can be observed in the velocity contour. A

lower velocity along the pressure side of TGV and higher for the suction side matches the results from the pressure measurements. At the trailing edge, flow from the pressure side has a negative pressure gradient and flow from suction side has a positive pressure gradient (**Figure 19**). This causes mixing of fluids with different pressure gradients at the trailing edge of TGV (**Figure 20**). Thus, velocity and pressure distribution along the circumferential direction at GV outlet in Francis turbine becomes non-uniform. Hence, even in the normal operating conditions, turbine runner passes through different gradients of velocity and pressure as it rotates between two GV. Slight increase in wall pressure compared to that in mid-span is observed at the suction side close to 60% of chord length (**Figure 19**). Since this is the region with the highest velocities, and accelerating flow experience retardation in this location, vortex is likely to originate and affect the pressure distribution in this area. It is observed in **Figure 20**, that the flow around the TGV is not identical with the flow around the GV that form the part of wall in flow channel. It is partly due to the nature of flow without runner and mainly due to single GV in the flow cascade.

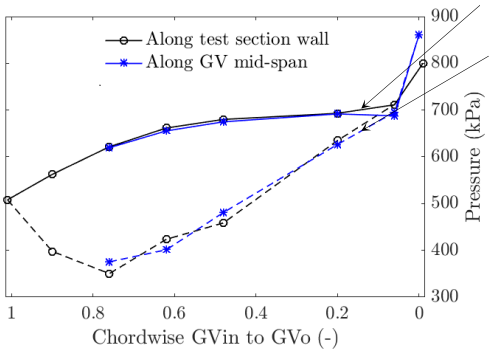

Figure 19. Pressure measurements along GV surfaces

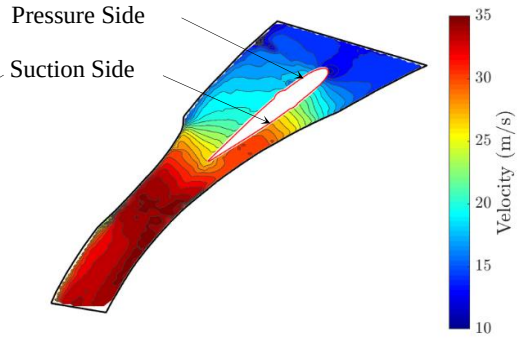

Figure 20. Velocity measurement inside flow channel

Figure 21 compares the development of tangential component of velocity (or swirl) inside the flow channel to that of the reference prototype turbine (**Table 1**). The velocity component for cascade is extracted from the PIV measurement and the velocity component for the prototype is adapted from the data presented in earlier work by Pradhan [32]. For the direct comparison, the velocity components at the respective position for both cases is reduced to a non-dimensional term defined by **Eq. 3.**

$$Cu_{red} = \frac{Cu}{\sqrt{2 \cdot g \cdot H_n}} \qquad (-) \qquad \textbf{Eq. 3}$$

Where, Cu_{red} is reduced tangential velocity, Cu (m/s) is tangential velocity at respective position, g (m/s^{-2}) is acceleration due to gravity and, H_n (m) net head acting on turbine.

It is observed that Cu_{red} inside cascade, at the TGV inlet position differs than that in prototype by 16%. Simplification in geometry at the cascade inlet section, by replacing spiral casing with flat plates can cause this difference. However, as the flow develops downstream from the TGV inlet, Cu_{red} for the cascade gets close to that for the prototype. The average difference in the swirl developed by the cascade and the prototype turbine, between TGV outlet to runner inlet, is 3.8%. This is the most important region of interest inside the cascade. In considerations of the simplicity in design and the effects of walls that form the periodic boundary of the cascade, this difference can be accepted.

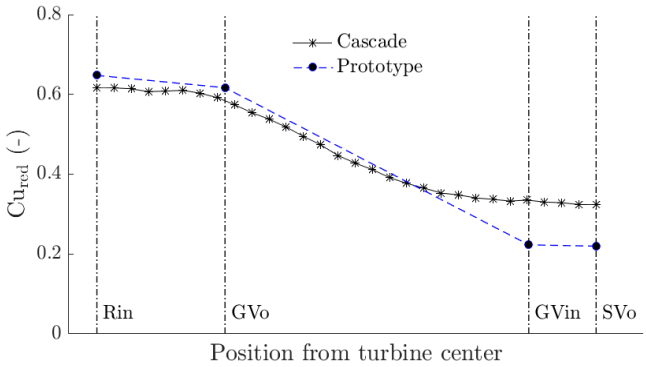

Figure 21. Reduced velocity inside cascade and turbine

Figure 22 shows velocity distribution from the TGV outlet to the runner inlet position in the casade. All the positions downstream of the TGV (GVds) are equally spaced concentric arc between the TGV outlet and the runner inlet in circumferential direction. Distribution of tangential velocity, downstream of the TGV suggest how the flow velocity developes from the TGV outlet to the runner inlet progressively. Presence of wake can be observed at the TGV trailing edge. At the TGV outlet, location of the wake is close to the TGV trailing edge. Two lobes on either side of the wake suggests non-uniform velocity distribution between adjacent GV in circumferential direction. Velocity profile towards the suction side of the TGV outlet has smaller peak than that towards the pressure side. Effect of periodic boundary walls on the flow is expected to cause this difference. As the flow progresses downstream of GV, wake appears to be dampened out gradually due to viscous effects. It can be clearly noticed that wake is moving towards suction side, as flow proceeds downstream of the TGV. At the runner inlet, wake appears to be negligible. This study shows that the transport of wake from GV to runner does not follow the flow in meridional direction. The location of wake moves towards the suction side, as flow develops from GV outlet to runner inlet. Flow with non-uniform pressure distribution in circumferential direction can cause the wake to be pushed towards the suction side of the flow.

Figure 23 shows the velocity distribution from GV outlet to runner inlet inside a high head Francis turbine. The data for this plot has been obtained from CFD investigations done by Tridevi [33]. It can be observed that the presence of runner in flow field changes the inlet flow conditions quite significantly. The cyclic fluctuation of velocity at runner inlet is identified as runner blades' interaction with flow, described as RSI in section 1. Similar patterns of GV wake being dampened out and moving towards the suction side, as observed in the cascade (**Figure 22**), is seen case of the turbine as well. Better symmetricity of flow at GV outlet in turbine than that for cascade is due to absence of periodic walls. RSI is the periodic effect and can be ignored to investigate the nature of main flow inside the distributor. Thus a simplified cascade setup, as developed in this study, can produce flow conditions inside Francis turbine distributor, while ignoring RSI. This setup will mainly be used to study the effects of sediment erosion on GV, and the role of GV design optimization to minimize such effects. Further part of this paper presents the results for measurements with the case without GV erosion. The results will be considered as the reference case for future studies with the cases of the eroded GV and the optimized design of GV.

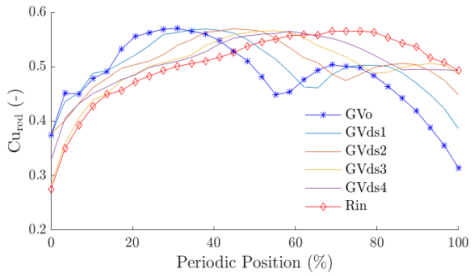

Figure 22. Velocity profile from GVout to Rin in cascade

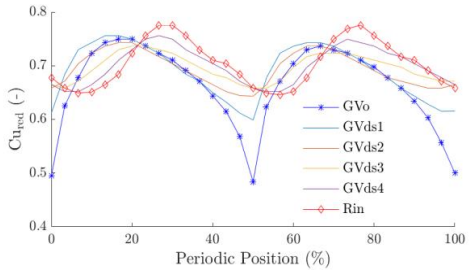

Figure 23. Velocity profile from GVout to Rin in turbine

Figure 24 shows the distribution of tangential velocity along the circumferential plane of the TGV outlet (**Figure 9**). The GV-Span represents measurement area from the test section wall up to the TGV mid-span as shown in **Figure 10**. The region of two higher velocities separated by a region of lower velocity suggests the wake along the trailing edge of TGV from the wall to the mid-span. Non-symmetricity in

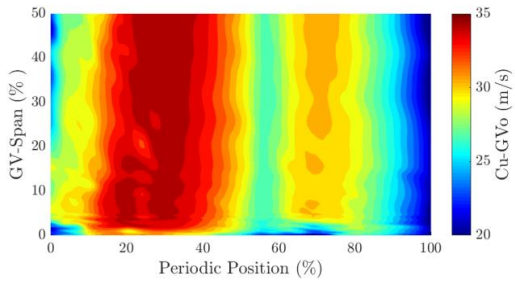

Figure 24. Distribution of Cu along GV outlet

velocity on either side of wake is due to the limitation of having only one GV between the cascade periodic walls, as discussed in earlier paragraph.

Figure 25 shows the distribution of tangential velocity along the circumferential plane of runner inlet. Height of runner at the inlet (Rin-Height) corresponds to the same measurement span as that of GV-Span, shown **Figure 24**. The distribution of meridional velocity at runner inlet for the same location is shown in **Figure 26**. It can be observed that at the runner inlet position, both Cu and Cm components are highly affected by the periodic walls of cascade. Ideally, both of these velocity components should remain constant along the circumferential direction. It can also be observed that both Cu and Cm components remains constant within the periodic position of 50% to 80%. This region can be considered as the PP inside the cascade, which is free from the effects of the periodic walls. Hence, only this region of PP will be considered to analyze velocity field inside the cascade. It can also be observed in both figures that Cu and Cm are uniform along the span wise direction except close to walls. This suggests that the test setup produces the uniform velocity field, at the position of runner inlet, from hub to mid height, at each position in circumferential direction.

Figure 27 and **Figure 28** show the distribution of runner inlet angle (β-Rin) and relative velocity at runner inlet (W-Rin) respectively. Definition of these terms can be seen in **Figure 3**. An ideal turbine runner rotating with a peripheral velocity at inlet (U-Rin) of 37.4 m/s is considered to calculate both the runner inlet angle and the relative velocity developed inside the cascade. The effects of wall is present up to 5% of flow from GV wall as also seen in previous cases. It can be observed that both the runner inlet angle and relative velocity remains fairly constant in circumferential and span wise direction. The runner inlet angle plays an important role for the design of blade geometry at inlet. Relative velocity does not have direct influence on turbine performance, but it plays a major role in sediment erosion of turbine components [9].

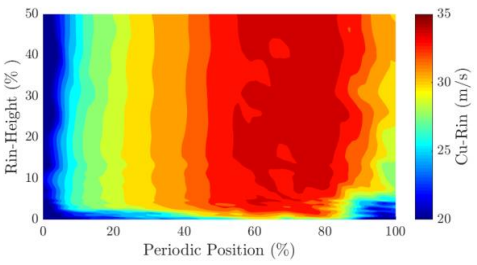

Figure 25. Distribution of Cu along runner inlet

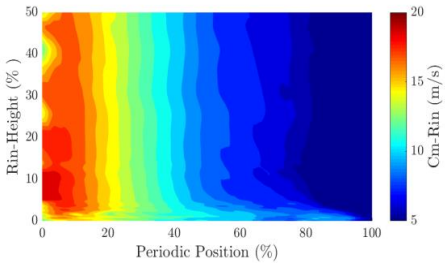

Figure 26. Distribution of Cm along runner inlet

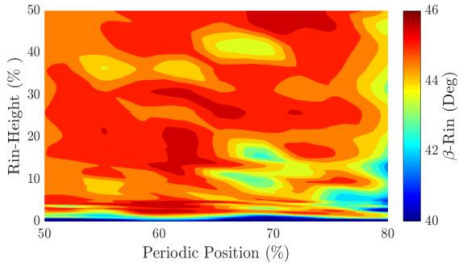

Figure 27. Distribution of runner inlet angle

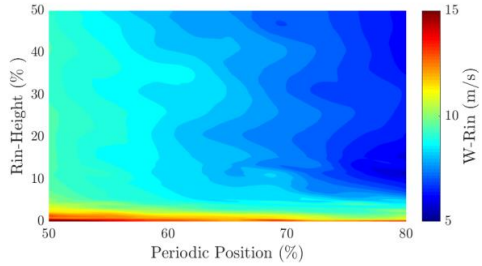

Figure 28. Distribution of relative velocity at runner inlet

Figure 29 shows velocity triangles at the runner inlet for the different circumferential position, with the ideal turbine runner. Velocity components are extracted from the PIV measurements (**Figure 26-Figure 28**) at the position of runner mid height. Velocity triangles are obtained for three periodic positions inside the region with stable flow (50% to 80% periodic position). Velocity triangle for the ideal turbine, operating under the same flow conditions is also computed, based on analytical design methods as described in literature [20]. It can be observed that the velocity triangles at the runner inlet for the cascade, at the different circumferential positions, are close to each other. The analytical velocity triangle is proportional to that for the cascade, but bears significant differences in respective velocity components. **Table 4** lists the average difference in respective velocity component at runner inlet between the cascade and that from the analytical calculations. It can be observed that the tangential velocity (Cu-Rin) in cascade is 13.3% lower than that of the analytical design. The meridional velocity (Cm-Rin) increases by 17.5% to compensate the reduction of Cu-Rin. The differences in Cu-Rin and Cm-Rin make cause the highest deviation on the relative velocity (W-Rin), to satisfy the triangle law. The analytical design does not consider the boundary layer effects and other losses in flow. The flow losses contributes to reduction of Cu-Rin and boundary layer effects contributes to increase in Cm-Rin. Hence, the difference in velocity triangles for analytical design and cascade can be accepted as a realistic phenomenon. Furthermore, the cascade has been designed for the prototype discharge conditions, but due to practical limitations, the tests have been conducted at the 80% of the design discharge. The periodic boundary walls may not be able to generate the same

Table 4. Difference in velocity components at runner inlet with respect to analytical values

Parameter at Rin	Symbol	Diff. (%)
Tangential velocity	Cu-Rin	13.3
Meridional velocity	Cm-Rin	17.5
Absolute velocity	C-Rin	11.5
Relative velocity	W-Rin	40.9
Inlet angle	βin	14.8

velocity components for the lower discharge. However, the velocity triangles for the different periodic positions inside the cascade are close to each other and also proportionate to the ideal velocity triangle. Hence, it is considered that this cascade setup can be used to evaluate the relative change in flow conditions at the runner inlet due to change in upstream flow parameters.

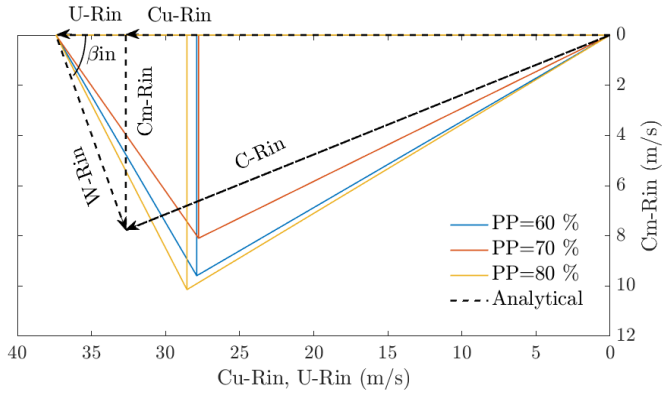

Figure 29. Velocity triangles at runner inlet

5. Summary and Conclusions

A test setup has been developed to investigate the flow conditions around the stator of a low specific speed Francis turbine. The setup includes flow passage with one TGV between the periodic boundary walls, covering $1/12^{th}$ of a reference prototype turbine in circumferential direction. Some simplifications in the design have been introduced, and optimization of periodic walls has been done, to produce the velocity distribution at the position of runner inlet close to that of the reference prototype turbine. NACA 0012 airfoil has been taken as a reference profile to shape TGV for this study. Pressure and velocity measurements are done inside the cascade at 80% of prototype discharge.

A 2D PIV measurement technique has been used to capture velocity field inside the flow channel. A tailor made *'in-situ'* calibration method has been developed for this study. Unique velocity vectors with spatial resolution of 4.7 mm and temporal resolution of 4 HZ has been computed for a flow area of 0.026 m^2. It has been estimated that minimum 100 pairs of images are needed for the statistical convergence of the velocity field. The uncertainty of the conversed velocity measurements is estimated to be ± 2.5%. The PIV measurements are done inside the flow cascade from the TGV wall up to the TGV mid-span in 25 different parallel planes along the TGV chord.

It is observed that simplifications introduced by replacing spiral casing with flat plates changes the tangential velocity at the position of TGV inlet of cascade by 16%. However, as the flow develops and approaches to the runner inlet position, the average tangential

velocity is close to that of the prototype turbine, with the difference falling below 4%. The boundary layer flow is found to be present within 5% of GV span. Despite of absence of runner, the cascade flow is able to produce most of the flow phenomenon as in a turbine, expect the rotor-stator-interaction. The strong influence of periodic walls of cascade on the velocity distribution is observed. It is identified that flow inside the cascade between periodic positions of 50% to 80%, which represents one third of the total flow area, in meridional direction, give the most uniform velocity components. The velocity triangles, within these periodic positions, at runner inlet for the cascade, are comparable to that for the reference prototype turbine.

It is concluded that the cascade test setup, as developed for this study, is able to produce flow conditions comparable to prototype Francis turbine. However, one GV cascade setup incurs strong effects of periodic walls on velocity distribution. Furthermore, the investigations with the one GV cascade setup are limited only at the single position of GV. In order to have a complete flow field between adjacent GV and with different GV opening angles, a cascade with minimum two GV is necessary. It is also concluded that the NACA 0012 profile used to shape the GV surfaces induces very high pressure difference between its surfaces. Such high pressure difference causes, secondary flow with vortices and also leakage flow in case of presence of clearance gap between GV and its walls. Optimization of shape of GV profile to minimize pressure difference between GV surfaces should be conducted as the further study.

References:

[1] Thapa B. Sand erosion in hydraulic machinery: PhD thesis, Norwegian University of Science and Technology, Faculty of Engineering Science and Technology, 2004.

[2] 2016 Key trends in hydropower. International Hydropower Association, (https://www.hydropower.org/2016-key-trends-in-hydropower).

[3] Twidell J, Weir T. Renewable energy resources: Routledge, 2015.

[4] Darmawi, Sipahutar R, Bernas SM, Imanuddin MS. Renewable energy and hydropower utilization tendency worldwide. Renewable and Sustainable Energy Reviews. 2013;17(0):213-5.

[5] Brekke H. Design, Performance and Maintenance of Francis Turbines. Global Journal of Researches In Engineering. 2013;13(5).

[6] Brekke H. Hydraulic design strategy for Francis turbines. International Journal on Hydropower and Dams. 1996;3(3):38-42.

[7] Negru R, Muntean S, Marsavina L, Susan-Resiga R, Pasca N. Computation of stress distribution in a Francis turbine runner induced by fluid flow. Computational Materials Science. 2012;64:253-9.

[8] Magnoli MV, Schilling R. Numerical Simulation of Pressure Pulsations in Francis Turbines. In: Gourbesville P, Cunge J, Caignaert G, editors. Advances in Hydroinformatics: Springer Singapore; 2014. p. 389-403.

[9] Thapa BS, Dahlhaug OG, Thapa B. Sediment erosion in hydro turbines and its effect on the flow around guide vanes of Francis turbine. Renewable and Sustainable Energy Reviews. 2015;49(0):1100-13.

[10] Wu J, Shimmei K, Tani K, Niikura K, Sato J. CFD-based design optimization for hydro turbines. Journal of Fluids Engineering, Transactions of the ASME. 2007;129(2):159-68.

[11] Flores E, Bornard L, Tomas L, Liu J, Couston M. Design of large Francis turbine using optimal methods. Conference Design of large Francis turbine using optimal methods, Beijing vol. 15.

[12] Enomoto Y, Kurosawa S, Kawajiri H. Design optimization of a high specific speed Francis turbine runner. Conference Design optimization of a high specific speed Francis turbine runner, Beijing vol. 15.

[13] Padhy MK, Saini RP. A review on silt erosion in hydro turbines. Renewable and Sustainable Energy Reviews. 2008;12(7):1974-87.

[14] Thapa BS, Thapa B, Dahlhaug OG. Current research in hydraulic turbines for handling sediments. Energy. 2012;47(1):62-9.

[15] IEC. Hydraulic turbines, storage pumps and pump-turbines – Model acceptance tests 2nd edn 1999-11. IEC 60193: The International Electro technical Commission; 1999.

[16] Thapa BS, Thapa B, Eltvik M, Gjosater K, Dahlhaug OG. Optimizing runner blade profile of Francis turbine to minimize sediment erosion. IOP Conference Series: Earth and Environmental Science: IOP Publishing; 2012. p. 032052.

[17] Rajkarnikar B, Neopane HP, Thapa BS. Development of rotating disc apparatus for test of sediment-induced erosion in francis runner blades. Wear. 2013;306(1-2):119-25.

[18] Zobeiri A, Ausoni P, Avellan F, Farhat M. How oblique trailing edge of a hydrofoil reduces the vortex-induced vibration. J Fluids Struct. 2012;32:78-89.

[19] Schabowski Z, Hodson H. The Reduction of over tip leakage loss in unshrouded axial turbines using winglets and squealers. Journal of Turbomachinery. 2014;136(4).

[20] Wei Z, Finstad PH, Olimstad G, Walseth E, Eltvik M. High Pressure Hydraulic Machinery. In: Publication N, editor. Compendium 2009.

[21] Thapa BS, Trivedi C, Dahlhaug OG. Design and development of guide vane cascade for a low speed number Francis turbine. Journal of Hydrodynamics, Ser B. 2016;28(4):676-89.

[22] Westerweel J, Elsinga GE, Adrian RJ. Particle image velocimetry for complex and turbulent flows. Ann Rev Fluid Mech2013. p. 409-36.

[23] Ciocan GD, Iliescu MS. PIV Measurements Applied to Hydraulic Machinery: Cavitating and Cavitation-Free Flows. The Particle Image Velocimetry – Characteristics, Limits and Possible Applications2012.

[24] Aeschlimann V, Beaulieu S, Houde S, Ciocan GD, Deschênes C. Inter-blade flow analysis of a propeller turbine runner using stereoscopic PIV. European Journal of Mechanics - B/Fluids. 2013;42(0):121-8.

[25] Adrian RJ, Westerweel J. Particle image velocimetry: Cambridge University Press, 2011.

[26] Boutelier D. TecPIV—A MATLAB-based application for PIV-analysis of experimental tectonics. Computers & Geosciences. 2016;89:186-99.

[27] Cavazzini G, Dazin A, Pavesi G, Dupont P, Bois G. Post-Processing Methods of PIV Instantaneous Flow Fields for Unsteady Flows in Turbomachines. The Particle Image Velocimetry – Characteristics, Limits and Possible Applications: InTech; 2012.

[28] Raffel M, Kompenhans Jr, Wereley S, Willert C. Particle Image Velocimetry: A Practical Guide. Berlin, Heidelberg: Springer-Verlag Berlin Heidelberg; 2007.

[29] Lazar E, DeBlauw B, Glumac N, Dutton C, Elliott G. A practical approach to PIV uncertainty analysis. Conference A practical approach to PIV uncertainty analysis, vol. 28.

[30] Pu J, Yu J, Wang J-h, Yang W-s, Zhang Z-q, Wang L. An experimental investigation of secondary flow characteristics in a linear turbine cascade with upstream converging slot-holes using TR-PIV. Exp Therm Fluid Sci. 2014;59:56-71.

[31] Antonsen Ø. Unsteady flow in wicket gate and runner with focus on static and dynamic load on runner: PhD thesis, Norwegian University of Science and Technology, Faculty of Engineering Science and Technology, 2007.

[32] Pradhan PMS, Dahlhaug OG, Joshi PN, Støle H. Sediment and Efficiency Measurements at Jhimruk Hydropower Plant – Monsoon 2003. Report from HydroLab, Nepal; 2004.

[33] Trivedi C, Cervantes MJ, Gandhi BK, Dahlhaug OG. Experimental and numerical studies for a high head francis turbine at several operating points. Journal of Fluids Engineering, Transactions of the ASME. 2013;135(11).

Paper-D

Sediment erosion induced leakage flow from guide vane clearance gap in a Francis turbine

Biraj Singh Thapa, Ole Gunnar Dahlhaug and Bhola Thapa

Submitted to Journal, Renewable Energy, 2016

Sediment erosion induced leakage flow from guide vane clearance gap in a low specific speed Francis turbine

Biraj Singh Thapa [1]; Ole Gunnar Dahlhaug [1]; Bhola Thapa[2]

[1]Department of Energy and Process Engineering, Norwegian University of Science and Technology, Norway

[2]Department of Mechanical Engineering, Kathmandu University, Nepal

Abstract

Opportunities of future hydropower developments comes with challenges of handling sediments in rivers. Hard minerals in flow causes turbine parts to erode with several undesirable effects. In Francis turbines, sediment erosion causes an increase of clearance gap between guide vane walls and cover plates. Due to inherit pressure difference between guide vane surfaces, a leakage flow arises from the clearance gap. A guide vane cascade is developed to study the characteristics of the leakage flow in a low specific speed Francis turbine. Velocity and pressure measurements are done at 80% of BEP flow as that in a reference prototype turbine. Cases with five different sizes of clearance gaps are investigated. Strong cross-wise jet-like leakage flow is observed from the clearance gap. A vortex filament developed due to mixing of leakage flow with the main flow is found to hit the hub at runner inlet. The existence of a critical clearance gap size for which the leakage velocity and its effects are maximum is revealed. Interpretations of the experimental results show a close match with the observations of eroded turbine parts from a power plant.

***Keywords*:** Francis turbine; Guide vane; Sediment erosion; Cascade; PIV; Leakage flow.

1. Introduction

The total global sediment flux from rivers to the oceans has been estimated as 20E+12 kg per year, of which 6.3E+12 kg is contributed by Asian rivers, particularly those draining the Himalaya–Tibetan Plateau region [1]. Thus, hydropower in Asian region suffers the problems of sediment handling, which

includes filling up of dams in reservoir projects and damaging mechanical components in run-off-the-river projects [2]. More than 55% of global undeveloped hydropower potential lies in Asia alone [3]. Hence, in recent future, hydropower developments will be focused on these regions, where sediment handling has been a major issue. It has been reported that

conventional designs of hydro turbines are facing numerous operational challenges in sediment-laden projects, despite of several preventive methods [4]. Studies have shown the need and possibilities of design optimization of turbine components to minimize consequences of sediment erosion in such projects [5].

Nomenclature	
C	total flow velocity, m/s
CG	clearance gap, mm
H_n	net/effective head to turbine, m
N_{QE}	specific speed,-
Q	discharge through turbine, m^3/s
Re	Reynold's number
v	kinematic viscosity of water, m^2/s
Subscripts	
in, o	inlet and outlet of respective parts
Abbreviation	
BEP	best efficiency point
GV	guide vane
IEC	international electrotechnical commission
MS	mid-span
PP	periodic position
PIV	particle image velocimetry
TGV	test guide vane
VC	crosswise velocity from CG

Francis type of turbines are widely used in hydroelectric projects, due to its flexibility and high efficiency. These are reaction machines, which utilizes both pressure energy and kinetic energy in water and convert them to mechanical energy inside rotating runner. Guide vanes (GV) are the most important unit inside the distributor, which facilitates the conversion of pressure energy to velocity energy. It also directs water at the desired amount and at the required angle into the runner. A dry clearance gap (CG) between GV and facing plates usually exists from the design to allow GV to be positioned at a particular opening angle. Typical design value of such dry clearance ranges from 0.1 mm to 0.3 mm, depending upon the designs and operating conditions. Due to deflection of cover plates under high pressure, the CG further increase. Leakage flow induces from the CG due to inherit pressure difference between its adjacent GV surfaces. Flow with spin, together with leakage flow from CG, horseshoe vortex, and wakes from the GV trailing edge make flow around GV unsteady and non-uniform [6]. This non-uniform flow field further interacts with rotating runner as each blade passes GV, which is also called as rotor-stator interaction. Thus, the flow conditions at runner inlet in a reaction machines can become very complex.

The presence of hard minerals in flow, with a high turbulence, and with high velocities, causes rapid erosion of turbine material [8]. Brekke [9] has studied several cases and

mechanisms of sediment erosion in GV. Among others, the 'leakage erosion' is identified as the one affecting the flow conditions inside turbine distributor most significantly. It occurs at the CG between GV and facing plate due to local separation and vortex on the suction side. The leakage erosion can cause the formation of a deep groove between the GV and its walls, increasing the CG several times than its design value. **Figure 1** shows a typical case of the leakage erosion of GV operating under the Himalayan basins and its effects on increase of the CG. The design dry clearance for GV is reported to be 0.3 mm. **Figure 1a** shows the leakage erosion at GV walls towards the trailing edge. The increase in CG between GV walls and facing plates can be seen in **Figure 1b**. Measurements of such CG is done at the positions shown in **Figure 1c**. It can be observed (in **Figure 1d** & **Figure 1e**) that the CG has increased considerably from its design value to 1.45 mm at the leading edge and 1.41 mm at the trailing edge respectively, within the operational time of 8500 hours. It further increases to 2.5 mm at the leading edge and 4.7 mm at the trailing edge respectively, within the operational time of 16500 hours. This shows rapid erosion towards the trailing edge compared to that in the leading edge. It matches with the findings that, a strong crossflow occurs towards the trailing edge, than that at the leading edge, due increased CG [10]. This crossflow, together with other secondary flows disturbs the

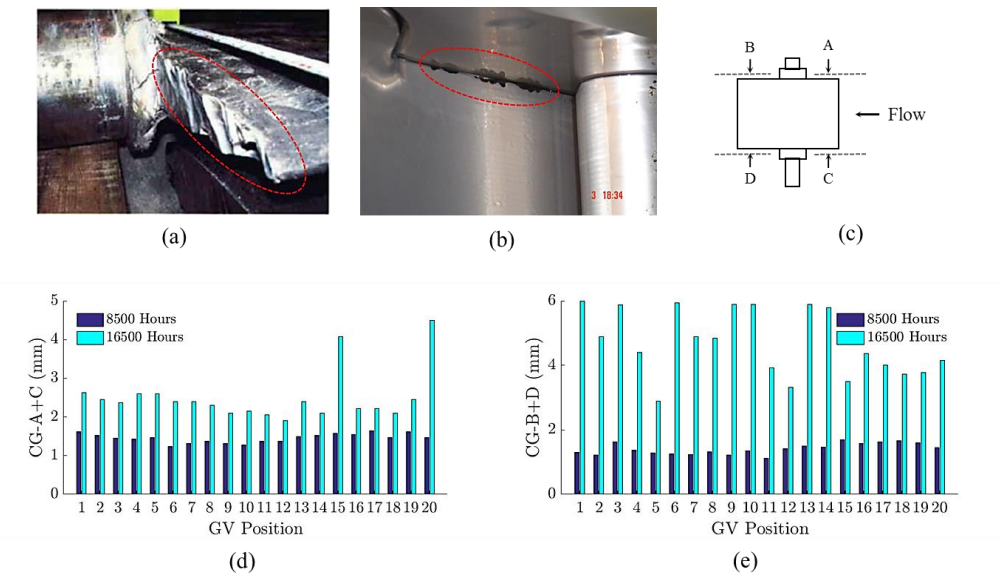

Figure 1. Sediment erosion in GV of Francis turbine in Himalaya [7]

(a) Erosion of GV end wall surface. **(b)** Formation of GV clearance gap. **(c)** Measurement location of GV clearance gap. **(d)** GV clearance gap towards leading edge. **(e)** GV clearance gap towards trailing edge

velocity profile at the runner inlet. Change in velocity profile at the inlet can causes additional erosion damage of turbine components and also induces pressure pulsations. Numerical studies have verified the negative effects of leakage flow from the CG [11]. Measurements in power plants have shown direct loss in turbine efficiency due to increased CG [12]. However, the experimental investigations of the characteristics of the leakage flow from the CG in a Francis turbine has not been found to be reported so far.

The presented work is a part of a study to identify the effects of sediment erosion of GV on the performance of Francis turbine. The overall goal of the study is to optimize the design methods of the guide vanes in Francis turbines for sediment-laden projects. A guide vane cascade has been developed to reproduce the flow inside Francis turbine with the prototype operating conditions, and with the flexibility for Particle Image Velocimetry (PIV) measurements. Pressure and velocity measurements have been conducted to study flow characteristics inside the distributor system. The details of methods used for PIV measurement technique, and the results for the reference case (without CG) has been presented in earlier works by the same authors [13]. This work presents the results of measurements inside the cascade with different sizes of CG.

2. Test Setup

2.1 Cascade and flow conditions

An experimental setup with GV cascade representing flow inside the distributor of a Francis turbine has been developed for this study. A reference prototype turbine with the low specific speed (N_{QE} = 0.086), calculated as per IEC guidelines [14], is considered for the design of the cascade. Flow in-between three adjacent GV, out of total 24 GV in the prototype turbine, is developed inside the cascade. The two outer GV forms part of cascade walls and middle GV directs flow into the channel. Angular position covered by the periodic walls of cascade is 30 degrees from the turbine center, which is $1/12^{th}$ size of turbine in angular direction. Simplifications are introduced for ease of manufacturing and for optical excess to PIV instrumentation. Optimization of cascade's walls profile has been done to compensate the limitations of the simplifications. The main criteria to satisfy the optimization goal is to have similar distribution of both tangential and meridional velocity components, at the runner inlet position in the cascade, as that observed in case of the reference prototype turbine. Details of design procedures, optimization methods and validation of flow inside the cascade is discussed in earlier work by the same authors [15].

Figure 2 shows the sectional view of the test setup along the plane of measurement. The test section contains the test guide vane (TGV) inside a plexi-glass flow channel. The flow channel is made by plexi-glass and is packed inside steel cover plates to hold the pressure up to 10 bars. Cover plates are designed to give optical excess for laser and camera for PIV recording. **Figure 3** shows the sectional view of the test section along the TGV chord.

Position of clearance gap and taps for pressure measurements in the gap can be observed. The TGV has been designed as an assembly of multiple parts to get a desired clearance gap with respect to the flow channel wall. Separate TGV are designed for velocity and pressure measurements to meet the specific requirements. Both the pressure and the velocity measurements are done for the cases with CG of 0 mm, 0.5 mm, 1.5 mm, 2 mm and 3 mm respectively. The test setup is installed at the facilities of the Waterpower Laboratory at NTNU. The setup is mounted in a closed loop system consisting of pump, flow meter, and a pressure tank. The flowmeter is calibrated with volumetric methods as per IEC guidelines [14] with total uncertainty to be below ± 0.15%.

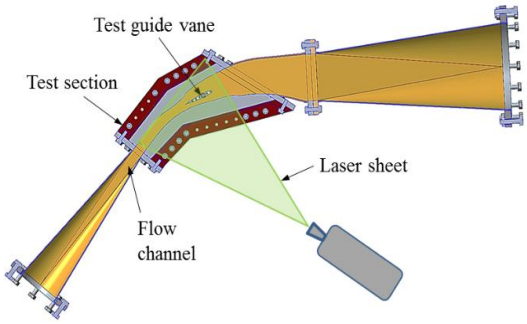

Figure 2. Sectional view of test setup along measurement plane

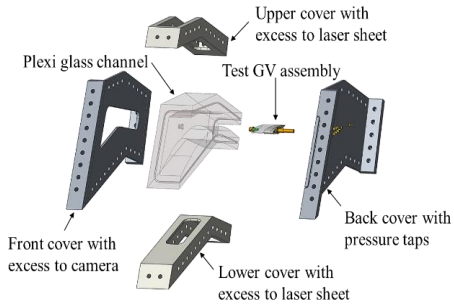

Figure 3. Sectional view of test section along TGV chord

Table 1 shows the comparison of flow conditions inside cascade with the prototype turbine at BEP. Equivalent turbine head for cascade is calculated for the same reduced velocity, as for the prototype, defined by Brekke [16]. Reynold's number for runner and GV is calculated as defined by IEC guidelines [14]. All the measurements for this study are conducted with flow rate of 0.155 m^3/s. This flow is close to 80% of design flow for the equivalent area in the prototype turbine at BEP. With this flow, the average velocity obtained at the runner inlet position, is 33.29 m/s. For obtaining the prototype operating conditions inside the cascade, the maximum pressure inside test loop exceeded above ten bars. Due practical limitations, all the measurements for this study are conducted with the conditions listed in **Table 1**.

2.2 Pressure Measurements

Pressure measurements are done along the TGV surface, close to the test section wall, with and without CG. Fourteen pressure taps are inserted in the test section cover plate to measure pressure around the TGV surface (**Figure 3**). One each pressure tap is located at the TGV leading edge and trailing edge respectively. Remaining twelve taps are located at six different symmetric positions along the TGV chord at pressure side and suction side respectively. The desired CG for the pressure measurements is created towards the wall

with pressure taps. Thus, velocity and pressure measurements at CG are done with different sets of TGV. Pressure measurements are also done along the TGV chord with 2 mm CG. Five pressure taps are located at the same position along TGV chord as for the respective position of surface pressure measurements. Reference pressure measurements are done at two points to insure the repeatability of the follow conditions for different sets of measurements. These measurement points are located at the inlet of test setup as a high pressure reference point, and at runner inlet position in test section as a low pressure reference point. Each pressure tap is connected to piezo-resistive pressure transducer through a plastic hosepipe of 1.6 mm inner diameter. Pressure measurements from all the taps are conducted simultaneously with the same flow conditions as that for the PIV measurements. This insures direct comparison of pressure and velocity fields inside the test section for all the cases of measurements. All pressure sensors are pre-calibrated against a dead weight calibrator. Measurement uncertainly was maintained to be below ±0.05% at all the measuring points. An average of 2000 samples, for each pressure point, measured at 5 HZ, is considered for the pressure analysis.

Table 1. Operating conditions for prototype and cascade

Parameters	**Symbol**	**Unit**	**Prototype**	**Cascade**
Flow rate per channel	Q	m^3/s	0.195	0.155
Total velocity at runner inlet	C-Rin	m/s	41.86	33.29
Equivalent turbine head	H_n	m	201.5	129.8
Shape of GV profile	-	-	NACA 0012	NACA 0012
Reynold's no for runner	Re-R	-	1.52E+07	1.15E+07
Reynold's no for guide vane	Re-GV	-	1.05E+06	8.58E+05

2.3 Velocity Measurements

PIV method is applied for the velocity measurements. A pulsed light sheet with a thickness of 2 mm is generated by two double-cavity Nd-YAG lasers providing 120 mJ by pulse. The lighted field is visualized by a HiSense 2M CCD PIV cameras, with a series of paired images acquired at 150 μs and 4 Hz. Fluorescent seeding particles, with a density of 1.016 kg/m^3, refractive index of 1.52 and mean diameter of 55 μm are used during the measurements. The camera resolution is 1280x1024 pixels for a 350x400 mm spatial domain. A tailor made *'in-situ'* calibration method for the PIV setup has been developed for this study. The image processing is carried out with 32-pixel resolution cross-correlation technique with 50% overlap. **Figure 4** shows the region of interest from PIV image along the plane of CG. Circumferential position of respective turbine components, from stay vane outlet to runner inlet, inside the flow channel can be observed. Periodic position (PP)

between the cascade walls represents 30˚ angular position in circumferential direction with respect to turbine center. It can be observed that the PP from 0% to 50% represents the pressure side of flow, and PP from 50% to 100% represents the suction side of flow respectively. Total 1103 grid points are equally spaced under the measurement area of 0.026 m^2 inside the flow channel. Unique velocity vectors are obtained by PIV for each grid point, which are separated by 4.7 mm in physical space. It has been estimated that minimum 100 images pairs are needed for the statistical convergence of the velocity field. The uncertainty of the statistically conversed velocity measurements is estimated to be below ±2.5% [13]. **Figure 5** shows the measurement planes with respect to position of runner blade in axial view. It can be observed that plane of measurement along GV mid-span corresponds to position of mid-height at runner inlet. Similarly, plane of measurement along clearance gap corresponds to position of hub at runner inlet. In this study, results of measurements at these two planes are presented.

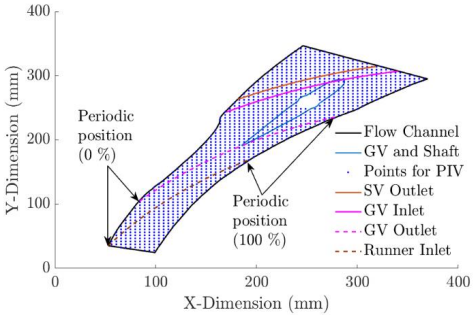

Figure 4. PIV measurement section and positons

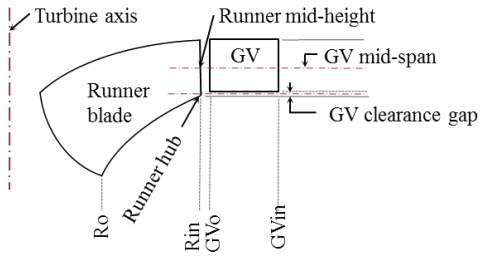

Figure 5. Measurement span relative to runner blade

3. Results and Discussions

This article presents the results of pressure and velocity measurements with the flow conditions inside the cascade as described in **Table 1**. The details of procedures followed for data analysis, and the results for reference case without CG is presented in earlier work by the same authors [13]. In this work, the efforts are made to analyze the effects of CG on leakage flow inside Francis turbine distributor.

Figure 6 shows the pressure distribution along the TGV surface for the reference case. Highest pressure at the leading edge shows the stagnation point. A clear pattern of pressure and suction side can be observed as the flow progresses towards the trailing edge. Equal distribution of pressure up to 10% of the TGV chord from the leading edge shows angle of attack close to zero. Due to high swirl in flow towards trailing edge, a gradual development of pressure difference between GV surfaces is observed, with the maximum difference occurring at around 75% of the chord length. It is estimated that the maximum pressure

difference between GV surfaces is equivalent to 20% net hydraulic pressure head acting on the turbine. Such a high pressure difference predicts development of cross-flow in case of presence of a clearance gap. **Figure 7** shows velocity distribution inside the flow cascade obtained from PIV measurements along the plane of GV mid-span for reference case. The basic flow phenomenon as stagnation point at the leading edge of GV, development of flow around pressure and suction sides and formation of wake at the trailing edge can be observed in the velocity contour. Lower velocities along the pressure side of GV and higher for the suction side matches the results from pressure measurements. The highest velocities inside the cascade, reaching close to 35 m/s at runner inlet position of a Francis turbine, is not found to be reported earlier, from any PIV measurements.

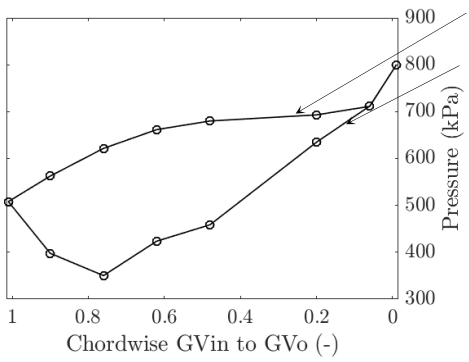

Figure 6. Pressure measurements along GV surfaces

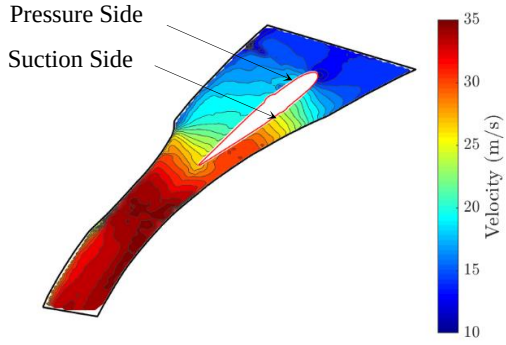

Figure 7. Velocity measurement inside flow channel MS

Flow through middle of 2 mm CG is shown in **Figure 8**. Compared to the flow along mid-span (**Figure 7**), flow along CG is highly distorted. A very strong cross-flow is observed at the trailing edge, which corresponds to the high pressure difference at 75% of chord (**Figure 6**). The cross-flow occupies the flow area close to runner inlet position and causes the blockage of flow passage at the suction side. The cross-flow is mixed with main flow, at increasing incidence angle, as the flow passes towards the GV trailing edge. Close to the trailing edge on suction side, a sudden drop of local velocity indicates the formation of a vortex core. Mixing of two different flows at high incidence angle, producing local spin, appears to be sufficient to form this vortex core.

Figure 9 shows the pressure distribution around the TGV surface with different cases of CG. A very clear pattern of shift in pressure distribution due to increasing CG size can be seen. A systematic drop of pressure, from leading edge to trailing edge on pressure side of the TGV can be observed with the increasing CG. There is also drop in stagnation pressure

at the leading edge for increasing CG. On the suction side, two different effects of CG on pressure distribution can be observed. From the leading edge up to 70% of chord, pressure increases with increasing CG. After 70% of chord up to the trailing edge, pressure drops with increasing CG. These observations suggest that pressure gradient between the GV surfaces drives cross-flow through the CG. The cross-flow is drawn into CG from pressure side uniformly between leading edge and trailing edge. The cross-flow exits out of CG from the trailing edge of suction side, between 70-90% of chord length, causing drop in pressure at this region. The increase in pressure from the leading edge up to 70% of chord, in the suction side, for the flows with CG, is due to blockage of flow passage for main flow by the cross-flow through CG.

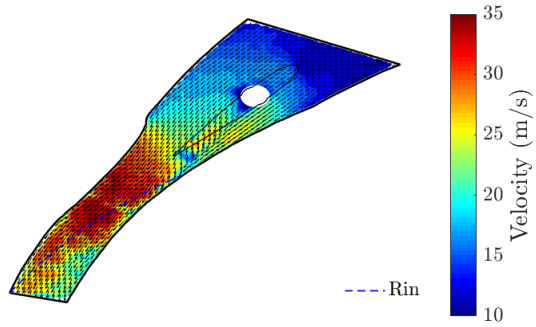

Figure 8. PIV measurements of flow velocity along CG

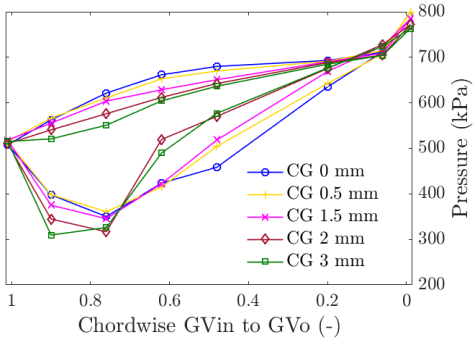

Figure 9. Pressure measurements along GV surface

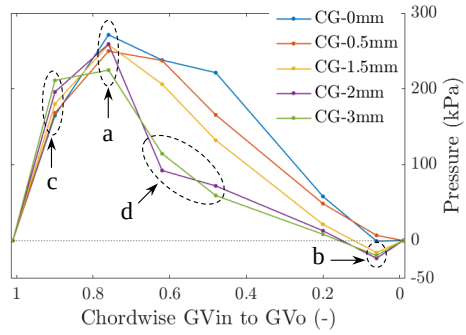

Figure 10. Pressure difference between GV surfaces

Figure 10 shows the pressure difference between the pressure side and the suction side of the TGV, along the chord, for different sizes of CG. The maximum pressure difference, for all cases of CG, is observed to be around 75% of the chord (region 'a'). This indicates the center of cross-flow lies at around this position of chord. Drop in pressure difference, towards leading edge, for increasing CG, indicates local acceleration of flow inside the CG. It can be observed that close to the leading edge (region 'b') there is negative pressure gradient between the TGV surfaces for the cases with CG more than 0.5 mm. Interaction between non-stagnation flow through CG and stagnation flow close to CG can cause this

effect in flow distribution at the leading edge. The negative pressure gradient at the leading edge indicates, a small but opposite, cross-flow originating from the suction side towards the pressure side. It can be noticed that close to the trailing edge (region 'c'), the pressure difference between GV surfaces increases with the size of CG. It can be expected that local effects of cross-flow prevent the main flow reach in this area. Hence, a sudden drop of local velocity in this area (seen in **Figure 8**), causes rise in local pressure. It can be observed that the flow with 2 mm CG shows a peculiar drop in pressure difference at position between 50-70% of chord (region 'd'). It indicates a presence of higher flow velocity inside the CG for case of 2 mm than that for 3 mm. These phenomenon are further analyzed in following sections, together with the results from velocity measurements. It can be observed in **Figure 10** that the maximum pressure difference between adjacent GV is for the case with no CG, which is 271.3 kPa. Analysis shows that this pressure difference is more than 20% of net head acting on the turbine. Such a huge differential pressure is responsible for a high leakage flow with CG. Based on this study it is noticed that the symmetric NACA profiles may not be a good choice for the high head Francis turbines, particularly for the sediment-laden projects.

Pressure difference between GV surfaces causes torsional forces to develop in GV shaft. Position of the GV shaft axis is often selected to minimize the torque on the GV shaft, and to stabilize GV at fully open position in case of failure of GV control mechanism. Correct estimation of the torque on the GV shaft is important to design the control mechanism to regulate flow inside turbine, as a part of governing system. For this study the position of the TGV shaft axis is located at one third of chord from the leading edge, as recommended by literatures [17]. It is evident from **Figure 10** that CG has significant effect on GV shaft torque due to redistribution of pressure difference between the GV surfaces. A conservative estimation of the GV shaft torque has been made for different cases of CG. The differential pressure between the GV surfaces, as presented in **Figure 10**, is considered to be uniform along the GV span for respective CG. The torque generated by piece wise segment of the TGV, due to differential pressure in each segment, about the GV shaft axis, is summed to estimate the total torque on the TGV shaft. **Figure 11** shows the estimated torque on the TGV shaft for different cases of CG. An exponential increment on the TGV shaft torque is observed due to increase in size of CG. There is an addition of 28% torque on the TGV shaft for 3 mm CG compared to that for 0 mm CG. Increase of negative differential pressure at leading edge (region 'b' in **Figure 10**) and increase in positive differential pressure at trailing edge (region 'c', **Figure 10**), for increasing CG, both contributes to clockwise moment at the TGV shaft axis. This causes such increase in the TGV shaft torque for increasing CG size. High initial value of the TGV shaft torque for case of no CG is due higher pressure difference towards the trailing edge, as discussed in earlier paragraph. Position of the TGV shaft axis being at one third of chord from leading edge seems not be a good choice for such a pressure distribution. Repositioning the shaft further downstream

of chord can reduce initial torque on the TGV shaft. For precise study of increment in the TGV shaft torque due to CG, a direct measurement of torque on the TGV shaft is necessary.

Figure 12 shows results of pressure measurements along the chord for 2 mm CG with respect to wall pressure measurement at CG for the same case. A significant reduction in pressure inside the CG, with respect to surface pressure can be observed. Pressure along the chord, towards the leading edge at the CG, is falling lower than the pressure at the suction side. However, towards the trailing edge, the pressure along the chord at CG is close to the average of pressure between the adjacent surfaces. It is possible that due to larger GV thickness towards leading edge, and the lower pressure difference, the flow along chord, inside CG, is not affected by the flow over the GV surfaces. Thus, flow in this region can follow the meridional flow. However, at the trailing edge, the pressure difference is significantly high and GV thickness is quite low. Considerable effects of the flow from GV surfaces can be expected on the flow along chord at this region. This can cause the flow driven by pressure difference between adjacent GV surfaces, along the chord inside CG, at the trailing edge. Hence, the pressure at chord, in this region, is close to the average pressure between the adjacent GV surfaces.

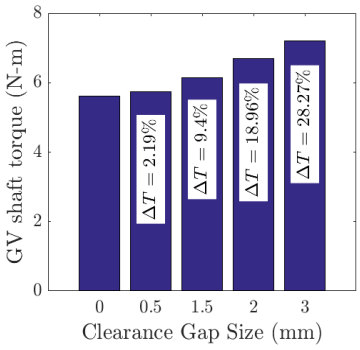

Figure 11. Torque on GV shaft

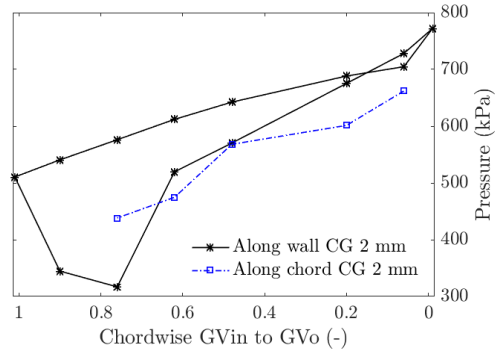

Figure 12. Pressure inside CG along GV chord

A systematic study of amount of cross-flow developed through different sizes of CG has been done with this study. Velocity vectors are obtained from PIV measurements along middle of CG, for the different sizes of CG. The velocity vectors, along the chord in the CG, are resolved to estimate the velocity component normal to the chord. This velocity normal to the chord, named as crosswise velocity (VC), is considered as the basis to estimate the crosswise leakage flow through the sectional area at the CG. **Figure 13** shows VC for the case of 2 mm CG. It can be observed that the maximum VC is at around 80% of chord. A small negative VC is also seen towards the leading edge. Both of these observations corresponds to the results of pressure measurements as discussed with **Figure 10**. The VC, along the chord, for different size of CG is presented in **Figure 14**. For comparison, an average of velocity inside the flow channel along circumferential direction,

at the mid span of GV (C-MS), for respective position of the GV chord, is also presented. As indicated by pressure measurements (region 'b', **Figure 10**), a small negative VC, increasing with increasing CG can be observed towards the leading edge. Region of zero VC corresponds to location of GV shaft. Towards the trailing edge, a peculiar relation of VC with CG has been observed. It is found that VC, at the trailing edge, increases with the size of CG, reaches maximum with 2 mm CG and falls down for 3 mm CG. This observation corresponds to the results from the pressure measurements. It can be observed in region 'a' of **Figure 10** that pressure difference between adjacent GV surfaces, for case of 2 mm CG is the highest among the different cases of the CG. The higher pressure difference forces flow with the higher velocity (**Figure 14**). Higher VC for 2 mm CG creates more blockage to flow passage for the main flow than that for other CG. The drop in differential pressure for 2 mm CG (in region 'd', **Figure 10**) is due to increase in pressure at the same region in suction side (**Figure 9**), caused by the blockage of flow passage. These observations show that CG of 2 mm is the critical size, which produces the highest VC. The highest VC, for critical CG, can reach close to 50% of velocity of main flow (C-MS), as seen in **Figure 14**. Size of CG reaching the critical due the turbine erosion should be avoided as far as possible. Dreyer [18] has also conducted similar studies with different size of CG and have concluded the presence of critical CG, which have highest effects on main flow.

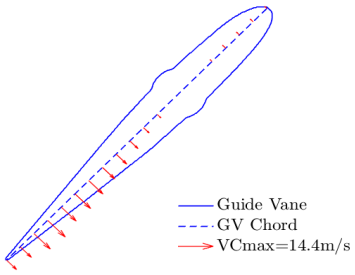

Figure 13. Crosswise velocity from CG 2 mm

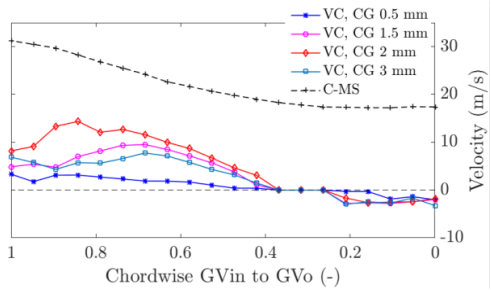

Figure 14. Intensities of crosswise velocity from CG

A crosswise leakage flow from CG has been estimated by summing up the individual leakage flow from each segment of GV chord length, with corresponding VC at the each segment as shown in **Figure 14**. Reynold's number ($Re=VC \cdot CG/\nu$, where ν is kinematic viscosity of water) for the leakage flow is estimated with the VC presented in **Figure 14**. Both maximum Re with the maximum VC and average Re from different chord position along trailing edge is estimated. **Figure 15** shows total crosswise leakage flow from each CG as the percentage of main flow. It can be observed that due to the highest VC, the highest leakage flow occurs from 2 mm CG, which is more than 1% of the main flow. Due to the lower VC, the leakage flow for CG 3 mm is lower than that for CG 2 mm. The

leakage flow for 0.5 mm CG is very low compared to the other cases. **Figure 16** shows Re for the crosswise leakage flow through different size of CG. It can be observed that Re for all the CG except for 0.5 mm falls into turbulent regime. As also indicated by the higher VC for 2 mm CG, the Re for this case is the highest among others. Studies made by Eide [19] also concludes the turbulent flow inside CG between GV and its walls. These observations indicate that CG between GV and its walls can be accepted up to 0.5 mm. This amount of CG can accommodate the dry clearance gap for positioning GV, and additional CG due to head cover deflection under high head operation. Larger CG than 0.5 mm can cause turbulent leakage flow with flow vortices, which disturbs the flow at the runner inlet.

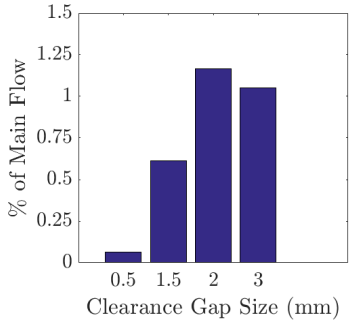

Figure 15. Crosswise leakage flow from CG

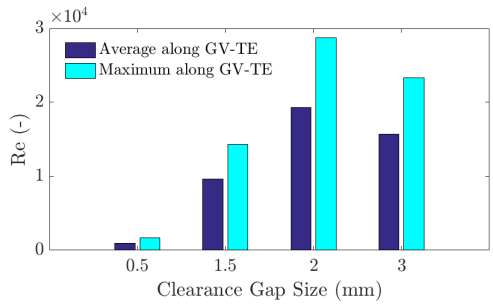

Figure 16. Reynold's number for flow through CG

Figure 17 shows the observation of the flow inside test setup for the critical case of 2 mm clearance gap. As indicated by **Figure 9** the vortex filament is induced towards the trailing edge of GV, as the crossflow mixes with the main flow. The filament starts from clearance gap at the 75% of chord, from the suction side, and is carried downstream towards the position of runner inlet. As the flow moves downstream of GV, location of the filament is shifted towards the suction side due to pressure gradients. As shown in **Figure 5**, this vortex filament hits the runner hub, which is at the position close to the plane of CG. Several cases of severe erosion at the runner hub in Francis turbines have been reported [20, 21]. **Figure 18** shows a case of sediment erosion at the runner hub for turbine in the same power plant, which is shown in **Figure 1**. Symmetric NACA profile has been used to shape the GV and are found to be heavily eroded towards the trailing edge (**Figure 1**). It can be explained from this study that the higher pressure difference towards trailing edge of GV causes higher secondary flows with vortex at the corner of the suction surface. This causes an increase in CG due to higher erosion towards the GV trailing edge. The increase in the GV-CG induces strong cross-flow, which can produce the vortex filament hitting the runner hub. Cavitation due to vortex core and sediment erosion due to high velocities can cause significant material removal at the runner hub, as shown in **Figure 18**. Alternative designs

of GV profiles to minimize the pressure difference between its surfaces could be helpful to reduce such erosion of hub at the runner inlet of Francis turbine. The crosswise leakage flow and the vortex filament have significant effects on turbine performance and sediment erosion, by disturbing the ideal velocity triangle at runner inlet. Such effects need further investigations to relate GV design with runner efficiency.

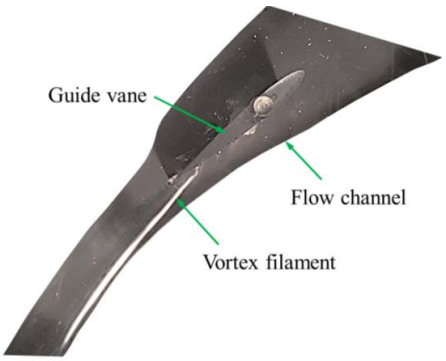

Figure 17. Observation of vortex filament from CG

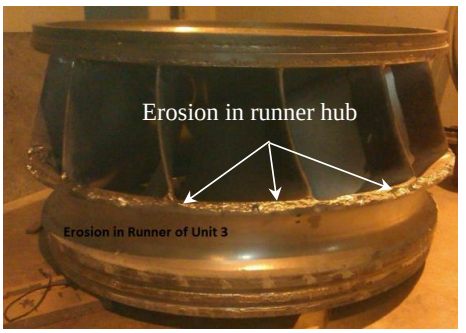

Figure 18. Erosion of Francis runner hub [20]

4. Conclusions

Sediment erosion of turbine components has been a technical challenge under Himalayan basins. Erosion of guide vanes, with increase in CG is one of consequences of operating Francis turbines in sediment-laden flows. An experimental setup is developed to study flow around distributor of Francis turbine with the flow conditions close to a prototype low specific speed Francis turbines at BEP. Pressure and velocity measurements are conducted to estimate the amount and effects of leakage flow from different sizes of GV clearance gaps. The results show that, GV of Francis turbine with a symmetric NACA profiles induces the pressure difference between its adjacent surfaces. The highest pressure difference between the GV surfaces, which is equivalent to 20% of net hydraulic head acting on the turbine, occurs at around 75% of GV chord. Such a high differential pressure is sufficient to force leakage flow through the CG between GV and cover plates.

It is found that CG size up to 0.5 mm can be accepted without much effects of the leakage flow on the main flow, inside the distributor of Francis turbines. All sizes of CG larger than 1 mm induces turbulent cross-flow, like a jet, which mixes with main flow and disturbs the runner inlet flow conditions. A critical size of CG for which the leakage flow velocity and its effect is maximum is identified to be 2 mm. Such critical CG has to be avoided as far as possible. Differences in effects of CG on the leakage flow at the leading edge and at the trailing edge GV has been observed. At the leading edge, CG induces a negative pressure gradient between GV surfaces, which causes a small leakage flow from suction side to

pressure side. At the trailing edge, a very strong cross-flow is induced from pressure side to suction side, with the maximum leakage velocity approaching 50% of mainstream velocity, for the critical CG. Such a high velocity cross-flow blocks the flow passage at the suction side and hence changes the pressure distribution, pushing maximum pressure difference towards the GV edges. Such change in pressure distribution increases the torque on GV shaft significantly and can affect the control system to regulate the GV openings. For the critical CG, the total cross-wise leakage flow is estimated to be more than 1% of total flow. Such a high flow rate through a narrow gap falls into turbulent regime with the Reynold's number close to 3E+4. A vortex filament is found to be developed due to mixing of leakage flow from the critical CG with the main flow. The vortex filament hits the hub at the runner inlet causing severe erosion damage.

It is concluded that symmetric NACA profiles are not suitable choice for shaping GV in high head Francis turbines for the sediment-laden projects. It is also concluded that position of GV shaft axis, which is empirically considered to be at one third of chord from the leading edge is not a good choice for the symmetric NACA profiles. Further study on quantification of flow disturbances at the runner inlet, due to CG, and their effects on turbine performance is necessary. Study on alternative designs of GV to minimize pressure gradients between the GV surfaces is also very important.

References

[1] Milliman JD, Meade RH. World-wide delivery of river sediments to the oceans. Journal of Geology. 1983;91:1.

[2] Higgitt DL, Lu XX. Sediment delivery to the three gorges: 1. Catchment controls. Geomorphology. 2001;41(2):143-56.

[3] Edenhofer O, Pichs Madruga R, Sokona Y, United Nations Environment P, World Meteorological O, Intergovernmental Panel on Climate C, et al. Renewable energy sources and climate change mitigation : special report of the Intergovernmental Panel on Climate Change. New York: Cambridge University Press, 2012.

[4] Thapa B. Sand erosion in hydraulic machinery: PhD thesis, Norwegian University of Science and Technology, Faculty of Engineering Science and Technology, 2004.

[5] Thapa BS, Thapa B, Dahlhaug OG. Current research in hydraulic turbines for handling sediments. Energy. 2012;47(1):62-9.

[6] Chitrakar S, Neopane HP, Dahlhaug OG. Study of the simultaneous effects of secondary flow and sediment erosion in Francis turbines. Renewable Energy. 2016.

[7] Koirala R, Thapa B, Neopane HP, Zhu B, Chhetry B. Sediment erosion in guide vanes of Francis turbine: A case study of Kaligandaki Hydropower Plant, Nepal. Wear. 2016;362–363:53-60.

[8] Chhetry B, Rana K. Effect of Sand Erosion on Turbine Components: A Case Study of Kali Gandaki "A" Hydroelectric Project (144 MW), Nepal. Hydro Nepal: Journal of Water, Energy and Environment. 2015;17:24-33.

[9] Brekke H. Design of hydraulic machinery working in sand laden water. In: Duan CG, Karelin VY, editors. Abrasive erosion and corrosion of hydraulic machinery. London: Imperial college press; 2002. p. 155-81.

[10] Thapa BS, Dahlhaug OG, Thapa B. Velocity and pressure measurements in guide vane clearance gap of a low specific speed Francis turbine. 28th IAHR Symposium on Hydraulic Machinery and Systems. Grenoble, France, 2016.

[11] Koirala R, Zhu B, Neopane HP. Effect of guide vane clearance gap on Francis turbine performance. Energies. 2016;9(4).

[12] Thapa BS, Dahlhaug OG, Thapa B. Sediment erosion in hydro turbines and its effect on the flow around guide vanes of Francis turbine. Renewable and Sustainable Energy Reviews. 2015;49(0):1100-13.

[13] Thapa BS, Dahlhaug OG, Thapa B. Flow measurements in guide vane cascade of a Francis turbine: A PIV approach. Renewable Energy. Submitted, July 2016.

[14] IEC. Hydraulic turbines, storage pumps and pump-turbines – Model acceptance tests 2nd edn 1999-11. IEC 60193: The International Electro technical Commission; 1999.

[15] Thapa BS, Trivedi C, Dahlhaug OG. Design and development of guide vane cascade for a low speed number Francis turbine. Journal of Hydrodynamics, Ser B. 2016;28(4):676-89.

[16] Brekke H. Hydraulic design strategy for Francis turbines. International Journal on Hydropower and Dams. 1996;3(3):38-42.

[17] Wei Z, Finstad PH, Olimstad G, Walseth E, Eltvik M. High Pressure Hydraulic Machinery. In: Publication N, editor. Compendium 2009.

[18] Dreyer M, Decaix J, Münch-Alligné C, Farhat M. Mind the gap: a new insight into the tip leakage vortex using stereo-PIV. Exp Fluids. 2014;55(11):1-13.

[19] Eide S. Numerical analysis of the head covers deflection and the leakage flow in the guide vanes of high head Francis turbines. 2004.

[20] Dahlhaug OG, Skåre PE, Mossing V, Gutierrez A. Erosion resistant coatings for Francis runners and guidevanes. International Journal on Hydropower and Dams. 2010;17(2):109-12.

[21] Sharma HK. Power generation in sediment laden rivers: The case of Nathpa Jhakri. International Journal on Hydropower and Dams. 2010;17(6):112-6.

Paper-E

Effects of sediment erosion in guide vanes of Francis turbine

Biraj Singh Thapa, Ole Gunnar Dahlhaug and Bhola Thapa

Submitted to Journal, Renewable Energy, 2016

Effects of sediment erosion in guide vanes of Francis turbine

Biraj Singh Thapa [1]; Ole Gunnar Dahlhaug [1]; Bhola Thapa[2]

[1]Department of Energy and Process Engineering, Norwegian University of Science and Technology, Norway

[2]Department of Mechanical Engineering, Kathmandu University, Nepal

Abstract

Guide vanes (GV) in Francis turbines are often reported to have a severe material erosion in case of sediments laden projects. A small clearance gap (CG) between GV wall and facing plate is allowed from the design to pivot GV as a part of flow regulating mechanism. Erosion in GV causes to increases the CG, which induces a leakage flow through the CG due to the inherent pressure difference between GV surfaces. Limited scientific studies on understanding the effects of the leakage flow from the eroded GV on turbine performance have been documented. Presented work aims to characterize the velocity conditions at the runner inlet of Francis turbine due to increase in the CG. Pressure and velocity measurements are done inside a GV cascade producing the similar velocity distribution as that in a reference prototype turbine. With a 2 mm CG, the relative velocity close to hub of runner inlet is found to increase up to three times of its nominal value. A vortex filament is found to be developed due to the mixing of the leakage flow with the main flow, and is observed to pass into the runner with the flow.

***Keywords**:* Francis turbine; Guide vane; Cascade; PIV; Clearance gap; Leakage flow

1. Introduction

Asian region contributes to the highest growth in energy demand, accounting for 70% of the growth in global energy consumption since 2000 [1]. This region also holds the highest capacities of the both, developed and also undeveloped hydropower potential worldwide [2]. It is projected that China and India will lead the hydropower energy production by adding 50000 MW and 30000 MW of new hydroelectric generating capacity, respectively, by 2020 [3, 4]. However, both of these regions suffer from soil erosion due to weak geological formation and heavy precipitation in short time interval causing floods. In the central Himalaya and Ganges plain, more than 80% of annual rainfall occurs during the

Indian summer monsoon season (May–October) [5]. This causes drastic increase of sediment concentration in rivers every year. Hence, the hydropower plants in these regions are reported to be worst hit by erosion of turbine components due hard sediments and cavitation [6]. Several methods including, prevention of sedimentation in the catchment areas, tapping sediments at intakes, and applying preventative coatings on the turbine components, have been practiced to minimize material erosion of turbines components [7]. However, such conventional methods to prevent turbine erosion have not shown acceptable results [8]. This has created a need and also the possibilities of design optimization of turbine components, in addition to the existing solutions, for better performance of hydro turbines in sediment-laden projects [9].

Nomenclature	
C	total flow velocity, m/s
Cm	radial component of C, m/s
Cu	tangential component of C, m/s
CG	clearance gap, mm
H	height of runner, m
n	rotational speed of runner, s^{-1}
N_{QE}	specific speed,-
S	span, m
U	runner peripheral velocity, m/s
W	relative velocity, m/s
β	runner inlet angle, deg
$\overline{\omega}$	total vorticity, s^{-1}
ω_z	vorticity for 2D flow
Subscripts	
fr	factor with respect to no CG
in, o	inlet and outlet of respective parts
Abbreviation	
BEP	best efficiency point
GV	guide vane
IEC	international electrotechnical commission
R	runner
PIV	particle image velocimetry
PP	periodic position
SV	stay vane
TGV	test guide vane

Francis type hydraulic turbines are widely used for low to medium head operation, as it can meet the real time demand with its ability to maintain high efficiency even in fluctuating load. Single unit of these turbines are capable to generate power up to 1000 MW [10]. During the operation of Francis turbines, the GV controls the discharge into the runner according to power requirement. In a conventional Francis turbine, about 50% of pressure head is converted to kinetic head as the flow accelerates through the GV [11]. For a high head Francis turbines, this accelerated flow causes unstable flow conditions contributing to vortex shedding, high amplitude pressure pulsation, flow separation and sometimes cavitation [12]. Operating conditions with sediment-laden flows add additional

challenges and escalates the problems with the eroded surfaces due material removal [13]. Several cases of severe material removal in GV of Francis turbines operating in sediment-laden projects are reported by different authors [14-16]. High velocity and acceleration, with the unstable flow conditions around GV, makes the hard sediments more vulnerable for material removal. Studies show that erosion of GV significantly effects the flow conditions inside the turbine, which further escalates the erosion rates, and hence exponential increase in material removal with time can be expected [17]. **Figure 1** shows a case of sediment erosion in GV and facing plates in Francis turbine. Removal of material on the both components can be observed. GV is mostly eroded towards the wall of trailing edge. Facing plate is eroded mainly towards the corner at the suction side of GV. Such material removal changes the geometry of the components, which imparts adverse effects of flow distribution inside turbine.

Brekke [19] has studied several cases and mechanisms of sediment erosion in GV. Among others, the 'leakage erosion' is identified as the one affecting the flow conditions inside turbine distributor most significantly. It occurs at the clearance gap (CG) between GV and facing plate due to local separation and horseshoe vortex in the suction side. The leakage erosion can cause the formation of a deep groove between the GV and its walls, increasing the CG several times than its design value (**Figure 1**). Typical design value of such dry clearance ranges from 0.1 mm to 0.3 mm, depending upon the designs and operating conditions. Chhetri [20] has measured an increase CG in the largest hydropower plant in Nepal, from its design value of 0.3 mm, to an average value of 2.5 mm at the leading edge and 4.7 mm at the trailing edge respectively, within the operational time of 16500 hours under high sediment load. The maximum CG up to 10 mm has been reported in the same power plant, which has GV span of 500 mm [21]. Similar cases of rapid increase of CG towards the trailing edge of GV due to sediment erosion have been reported in other power plants as well [14-16]. There has been a very limited study on the effects of CG on performance of Francis turbines. Brekke [22] has studied the influence of the guide vane clearance gap on efficiency for different specific speeds Francis turbines. A loss of 0.5% efficiency at best efficiency point (BEP) was measured in prototype with 0.5 mm clearance gap compared to the original runner with 0.3 mm clearance gap. Similarly, for 1 mm clearance gap the decrease in turbine efficiency was measured to be 0.8%. Chen [23] and Koirala [21] has observed the flow inside Francis turbine distributor with different size of CG. It was observed that the crosswise leakage flow develops from CG due to pressure gradient between GV surfaces. This leakage flow was found to be dominant on suction side of GV trailing edge and disturbs the main flow at the runner inlet by formation of vortex filament. Studies made by Thapa [24] shows a close connection between the leakage flow from the CG and erosion of the turbine runner.

Figure 1. Erosion of GV and facing plate in Francis turbine [18]

The presented work is a part of a study to identify the effects of sediment erosion of guide vanes on the flow conditions in Francis turbine distributor. The overall goal of the study is to optimize the design methods of the guide vanes for sediment-laden projects. A guide vane cascade has been developed to reproduce the flow inside Francis turbine with the prototype operating conditions, and with the flexibility for Particle Image Velocimetry (PIV) measurements. Pressure and velocity measurements have been conducted to study flow characteristics inside the distributor system. A part of results from the measurements have been presented separately by the same authors [25]. Those results show that, GV of Francis turbine with a symmetric NACA profiles bears the pressure difference between its adjacent surfaces, which more than 20% of net pressure head on turbine. Such a high differential pressure forces leakage flow through the CG and creates a blockage to the main flow. A critical CG size of 2 mm is found to have the highest crosswise leakage velocity, maximum of which is close to 50% of mainstream velocity at GV outlet. Such a high flow velocity through a narrow CG falls into turbulent region. All sizes of CG larger than 1 mm are found to induce turbulent crossflow like a jet, which mixes with main flow and disturbs the runner inlet flow conditions. This work presents the results of the measurements with further analysis of the effects of GV-CG on flow conditions at runner inlet of Francis turbines. Efforts have been made to quantify the relative distortion on each flow parameter representing the velocity triangle at the runner inlet. Formation of vortex filament due to leakage flow and its trajectory into the runner is also investigated.

2. Test Setup

2.1 Cascade and flow conditions

An experimental setup with one GV cascade representing flow inside the distributor of a Francis turbine has been developed for this study. A reference prototype turbine with the specific speed 0.086, as defined in **Eq. 1**, by IEC guidelines [26], is considered for the design of the cascade. Flow in-between three adjacent GV, out of total 24 GV in the prototype turbine, is developed inside the cascade. The two outer GV forms part of cascade walls and middle GV directs flow into the channel. Angular position covered by the

periodic walls of cascade's is 30 degrees from the turbine center, which is 1/12th size of turbine in angular direction. Simplifications are introduced for ease of manufacturing and for optical excess to PIV instrumentation. CFD based optimization of cascade's walls profile has been done to compensate the limitations of the simplifications. The main criteria to satisfy the optimization goal is to have similar distribution of both tangential and meridional velocity components, at the runner inlet position in the cascade, as that observed in case of the reference prototype turbine. Details of design procedures, optimization methods and validation of flow inside the cascade is discussed in earlier work by the same authors [27].

$$N_{QE} = \frac{n \cdot Q^{0.5}}{E^{0.75}} \qquad (-) \qquad \textbf{Eq. 1}$$

Where, N_{QE} is specific speed, n is speed of runner (s^{-1}), Q is discharge through turbine (m^3/s) and E is specific hydraulic energy of turbine (Jkg^{-1}).

Figure 2 shows the sectional view of the test setup along the plane of measurement. The test section contains the test guide vane (TGV) inside a plexi-glass flow channel. The flow channel is made by plexi-glass and is packed inside steel cover plates to hold the pressure up to 10 bars. Cover plates are designed to give optical excess for laser and camera for PIV recording. **Figure 3** shows the sectional view of the test section along TGV chord. Position of CG and taps for velocity measurements with different CG size can be observed. The TGV has been designed as an assembly of multiple parts to get a desired clearance gap with respect to the flow channel wall. The measurements are done for the cases with CG of 0 mm, 0.5 mm, 1.5 mm, 2 mm and 3 mm respectively. The test setup is installed at the facilities in the Waterpower Laboratory at NTNU. The setup is mounted in a closed loop system consisting of pump, flow meter, and a pressure tank. The flowmeter is calibrated with volumetric methods as per IEC guidelines [26] and total uncertainty is found to be below $\pm$ 0.15%.

Table 1 shows the comparison of flow conditions inside cascade with the prototype turbine at BEP. Equivalent turbine head for cascade is calculated for the same reduced velocity, as for the prototype, defined by Brekke [11]. Reynold's number for runner and GV is calculated as defined by IEC guidelines [26]. All the measurements for this study are conducted with flow rate of 0.155 m^3/s. This flow is close to 80% of design flow for the equivalent area in the prototype at BEP. At this flow rate, the average velocity obtained at the runner inlet position, is 33.29 m/s. For obtaining the prototype operating conditions inside the cascade, the maximum pressure inside test loop exceeded ten bars. Due practical limitations, all the measurements for this study are conducted with the conditions listed in **Table 1**.

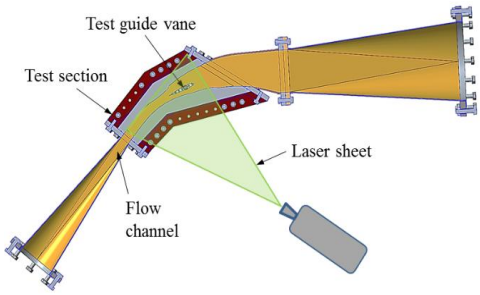

Figure 2. Sectional view of test setup along measurement plane

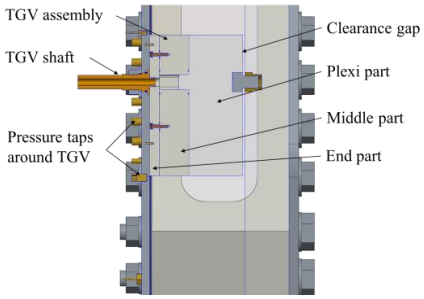

Figure 3. Sectional view of test section along TGV chord

Table 1. Operating conditions for prototype and cascade

Parameters	**Symbol**	**Unit**	**Prototype**	**Cascade**
Flow rate per channel	Q	m^3/s	0.195	0.155
Total velocity at runner inlet	C-Rin	m/s	41.86	33.29
Equivalent turbine head	H_{eq}	m	201.5	129.8
Shape of GV profile	-	-	NACA 0012	NACA 0012
Reynold's no for runner	ReR	-	1.52E+07	1.15E+07
Reynold's no for guide vane	ReGV	-	1.05E+06	8.58E+05

2.2 Velocity measurements

PIV method is applied for the velocity measurements. A pulsed light sheet with a thickness of 2 mm is generated by two double-cavity Nd-YAG lasers providing 120 mJ by pulse. The lighted field is visualized by a HiSense 2M CCD PIV cameras, with a series of paired images acquired at 150 µs and 4 Hz. Fluorescent seeding particles, with a density of 1.016 kg/m^3, refractive index of 1.52 and mean diameter of 55 µm are used during the measurements. The camera resolution is 1280x1024 pixels for a 350x400 mm spatial domain. A tailor made *'in-situ'* calibration method for the PIV setup has been developed for this study. The image processing is carried out with 32-pixel resolution cross-correlation technique with 50% overlap. **Figure 4** shows the region of interest from PIV image along the plane of CG. Circumferential position of respective turbine components, from stay vane outlet to runner inlet, inside the flow channel can be observed. Periodic position (PP) between the cascade walls represents 30˚ angular position in circumferential direction with

respect to turbine center. It can be observed that the PP from 0% to 50% represents the pressure side of flow, and PP from 50% to 100% represents the suction side of flow respectively. Total 1103 grid points are equally spaced under the measurement area of 0.026 m^2 inside the flow channel. Unique velocity vectors are obtained by PIV for each grid point, which are separated by 4.7 mm in physical space. It has been estimated that minimum 100 images pairs are needed for the statistical convergence of the velocity field. The uncertainty of the statistically conversed velocity measurements is estimated to be below ±2.5% [28].

The test section is designed to conduct PIV measurements from the TGV wall up-to the TGV mid-span. **Figure 5** shows the measurement span inside test section with respect to position of runner blade in axial view. At runner inlet position, the measurement span covers the position between the runner hub to the runner mid height. The plane of measurement along the TGV mid-span and the plane of measurement along the CG corresponds to position of the runner mid-height and the runner hub respectively. The PIV measurement is started from the plane of test rig's wall towards the CG and is preceded towards the TGV mid span. Total 25 different measurement planes are distributed inside the measurement span with higher spatial resolution towards the CG. These measurement planes are separated by 0.25 mm for first 4 planes, and by 0.5 mm for next 8 planes. Similarly next 5 measurement planes are separated by 2 mm and last 6 measurement planes are separated by 5 mm respectively. It is expected that this spatial distribution of measurement planes is sufficient to capture the steady state flow field within the volume of measurement span.

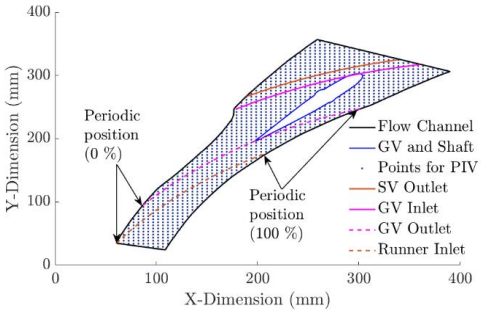

Figure 4. PIV measurement section and positons

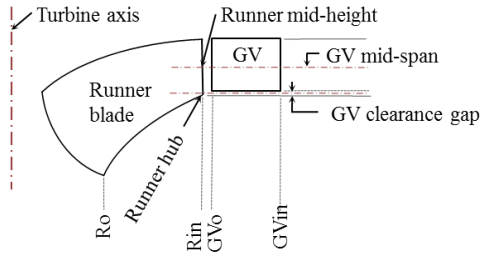

Figure 5. Measurement span relative to runner blade in axial view

3. Results and Discussions

This article presents the results of velocity measurements with the flow conditions inside the cascade as described in **Table 1**. The details of procedures followed for data analysis, and the results for reference case without CG is presented in earlier work by the same

authors [28]. Results of pressure measurements and analysis of quality and effects of leakage flow from CG with different sizes is presented in earlier article by the same authors [25]. In this work, the efforts are made to analyze the effects of the leakage flow from different sizes of CG on the velocity conditions at the runner inlet.

Figure 6 shows the velocity distribution inside the cascade obtained from PIV measurements along the plane of TGV mid-span. The basic flow phenomenon as stagnation point at the leading edge of GV, development of flow around the pressure and the suction sides, and the formation of wake at the trailing edge can be observed in the velocity contour. The highest velocities inside the cascade, reaching close to 35 m/s at runner inlet position of a Francis turbine, is not found to be reported earlier, from any PIV measurements. Flow through middle of 2 mm CG is shown in **Figure 7**. Compared to the flow along mid-span (**Figure 6**), flow through the CG is highly distorted. A very strong cross-flow is observed close to the trailing edge, which occupies more than 50% of flow area close to runner inlet position. This causes the blockage of flow passage at suction side. The cross-flow is mixed with main flow, at increasing incidence angle, as the flow passes towards the trailing edge. Close to the trailing edge, on the suction side a sudden drop of local velocity indicates the formation of a vortex core. Mixing of two different flows at high incidence angle, producing local spin, appears to be sufficient to form this vortex core.

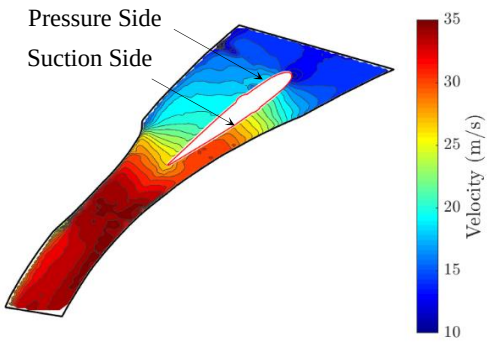

Figure 6. Velocity measurement inside flow channel MS

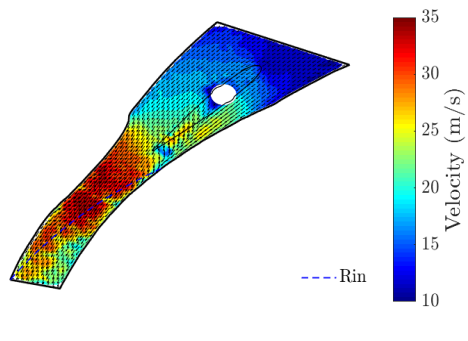

Figure 7. Velocity measurement inside flow channel CG

Figure 8 shows the observation of the flow inside test setup for the case of 2 mm clearance gap. As indicated in **Figure 7**, vortex filament originates from the trailing edge of the TGV, as the crossflow mixes with the main flow. The filament starts from clearance gap at the 75% of chord length, from the suction side, and is carried downstream towards the position of runner inlet. As the flow moves downstream of GV, location of the filament is shifted

towards the suction side due to pressure gradients. The filament diffuses with main flow as it approaches outlet of test section, where flow becomes more uniform. This vortex filament is able to change the velocity distribution at the runner inlet quite significantly. Further analysis of effects of cross-flow from different CG sizes, on velocity components at runner inlet, is presented in the following section.

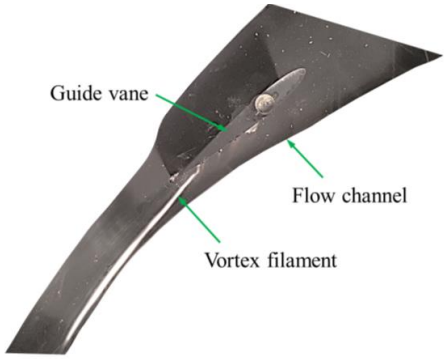

Figure 8. Observation of vortex filament from CG

Figure 9 shows the velocity triangle at the inlet of a Francis turbine runner. The total velocity at runner inlet (C-Rin) is resolved as two components. The tangential component (Cu-Rin) is associated with turbine efficiency based on Euler's turbine equation, and the meridional component (Cm-Rin) is responsible for the flow inside the runner. The runner inlet angle (β) governs the blade loading and plays an important role for the design of blade geometry at inlet. Relative velocity (W-Rin) does not have direct influence on turbine performance, but it plays a major role in sediment erosion of turbine components. Studies have shown that erosion of turbine components is proportional to third power of relative velocity [13, 29]. This makes relative velocity the most important indicator to investigate sediment erosion of turbine components.

A term named as '*factor*', with subscript '*fr*' is defined, as **Eq. 2**. It indicates the proportionate change in respective flow parameter due to CG, with respect to the same flow parameter without CG. Thus, with no CG, respective factor is 1 for all velocity components, along all measuring locations. Change in respective factor for the cases with different CG, indicates effects of leakage flow on respective velocity components. This method of analysis gives the relative values only; hence, the local effects due to flow channel walls on the flow conditions are minimized.

$$\boldsymbol{factor\ (fr) = \frac{flow\ parameter\ \ with\ CG}{flow\ parameter\ without\ CG}} \qquad \textbf{(-)} \qquad \textbf{Eq. 2}$$

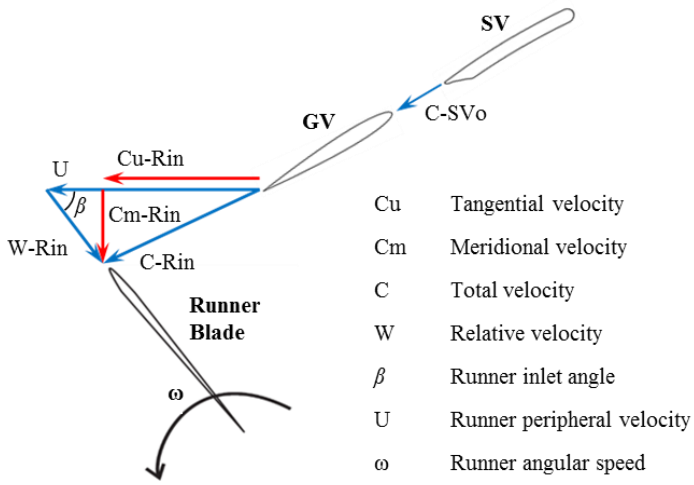

Figure 9. Velocity components at runner inlet of a Francis turbine

Figure 10 shows tangential velocity factor at runner inlet (Cu_{fr}-Rin) for different sizes of CG between the TGV and test rig wall. The plots show the measurements along circumferential direction at runner inlet, between the test section periodic positions (**Figure 4**), from the test rig's wall up to 50% of runner inlet height (Rin-Height) (**Figure 5**). It can be observed that the leakage flow through CG causes a significant drop of Cu_{fr}, locally at the suction side, for all the cases. The location of drop in Cu_{fr} corresponds to the position of the leakage flow hitting at runner inlet, as seen in **Figure 7**. A clear pattern of increase of effected area, both in circumferential wise and span wise direction, due to increase in CG size can be observed. The largest effected area is for the case with CG 2 mm. Approximately 25% of flow area experiences drop in Cu component by 50% of its nominal value. Such a drop in Cu directly contributes to loss in hydraulic efficiency of turbine. It also creates dynamic loading in runner, affecting its life. This observation matches to the earlier studies made by same authors, concluding that CG 2 mm is the critical size to have the highest effects on flow conditions [25].

Figure 11 shows the effects of different sizes of CG on meridional velocity factor (Cm_{fr}-Rin) at the runner inlet. A similar pattern of effected area, for Cm_{fr}-Rin, as that for Cu_{fr}-Rin, can be observed. Effect of CG 0.5 mm is negligible compared with that for CG 2 mm, which is also the CG producing the highest local effects. It can observed that Cm_{fr}-Rin increases by three times, locally between 80-100% PP and 5-20% of Rin-Height, for the case with CG 2 mm. High Cm_{fr} indicates the local acceleration of the flow in this region.

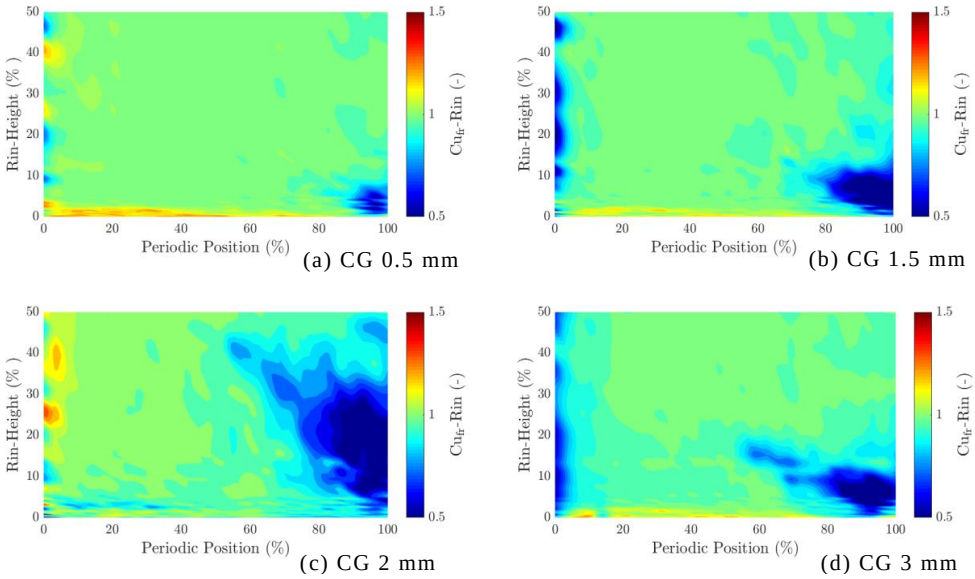

Figure 10. Tangential velocity factor at runner inlet for different size of clearance gap

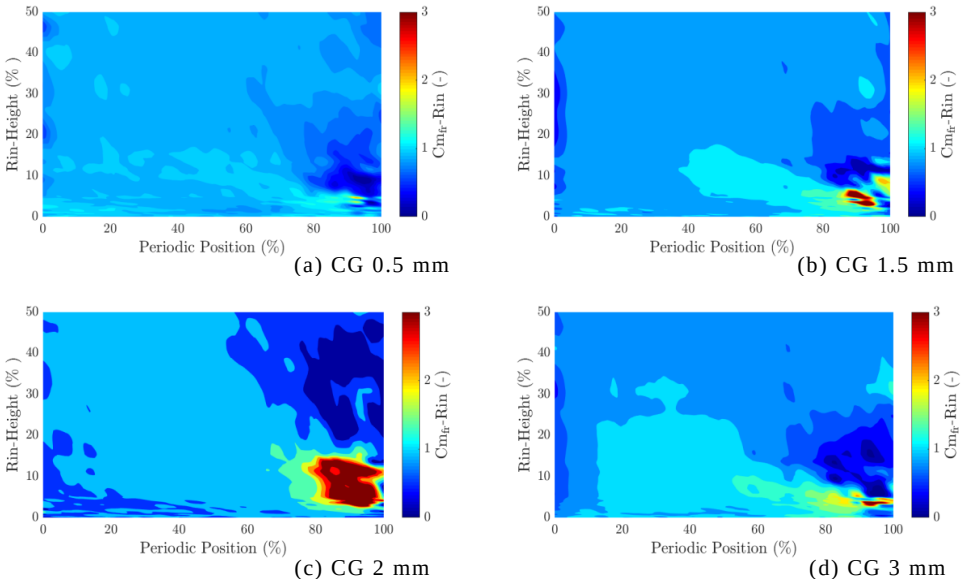

Figure 11. Meridional velocity factor at runner inlet for different size of clearance gap

This local acceleration is compensated by local deceleration of flow towards the mid-span. Such an adverse flow velocity, along different sections of the runner inlet height, affects the relative velocity (W) and inlet angle (β), at the runner inlet as discussed in following sections.

Figure 12 shows the effects of different sizes of CG on relative velocity factor (W_{fr}-Rin) at the runner inlet. As in earlier cases the highest effects is observed for CG 2 mm and the lowest effects with at for CG 0.5 mm. A cumulative effect of changes in Cu_{fr}-Rin and Cm_{fr}-Rin, as per velocity triangle shown in **Figure 9**, causes the W_{fr}-Rin to redistribute inside the flow area. Parts of flow area bears an increment of the W_{re}-Rin, more than three times than that of the nominal value, for case of CG 2 mm. This indicates a very high chance of erosion of runner blades, in those areas, in case of sediment-laden flows. The case with CG 1.5 mm bears higher effects on W_{re}-Rin than that of CG 3 mm. This indicates that erosion rates at runner inlet will reduce after crossing the critical CG size, which for this study is found to be 2 mm.

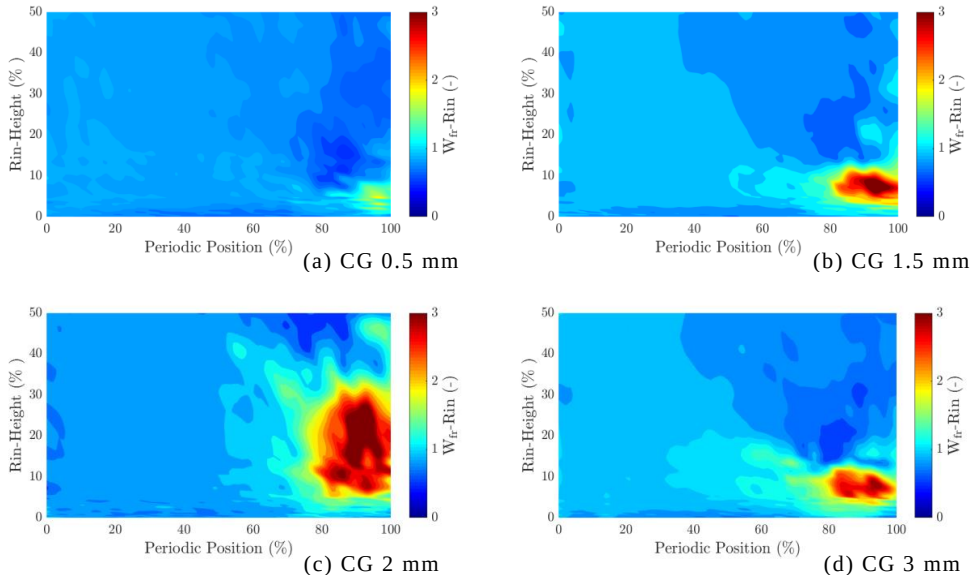

Figure 12. Relative velocity factor at runner inlet for different size of clearance gap

Figure 13 shows the effects of different sizes of CG on the runner inlet angle factor (β_{fr}-Rin). For all cases of CG, β_{fr}-Rin suffers the significant deviations along the runner height. A very nonlinear dependency of β_{fr}-Rin on size of CG has been observed. It can be seen in **Figure 9** that, β is highly dependent on Cm. The case of CG 2 mm shows a drop in Cm_{fr}-Rin between 20-45% of Rin-Height (**Figure 11**). This causes the drop in β_{fr}-Rin in this area as well. Distribution of β_{fr}-Rin for all cases of CG size shows correspondence to the distribution of Cm_{fr}-Rin. Runner inlet angle is often standardized to load runner blades uniformly and also to minimize cavitation effects due to flow separation at adverse flow angles. Incoming of flow with such a fluctuation in inlet angle, can clause flow separation at runner inlet causing cavitation and pressure pulsation at runner inlet, reducing both life and efficiency of runner.

These observations suggest that leakage flow from the CG has adverse effects on flow conditions at the runner inlet. Velocity triangle at the runner inlet faces significant changes, both in circumferential and span-wise direction, as the runner rotates in flow field with the leakage flow from the GV clearance gap. It is also evident that clearance gap of 2 mm is the critical size, which has highest effects of all the flow parameters at the runner inlet.

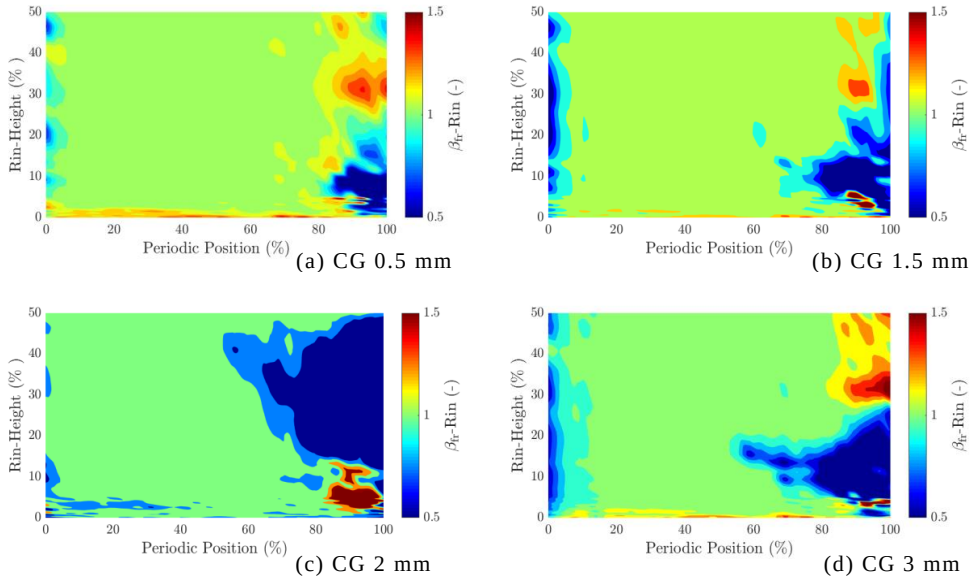

Figure 13. Runner inlet angle factor for different size of clearance gap

Mixing of the leakage flow from CG with the main flow, at a high incidence, causes to form a vortex filament, as observed in **Figure 8**. Further investigations of the vortex flow downstream of GV has been investigated with this study. Total vorticity ($\overline{\omega}$) is defined by **Eq. 3**, which represents measure of the local rotation, or spin, of a fluid element at a particular point in the flow field. For a 2-D flow, the vorticity component can be estimated along the axis perpendicular to the flow plane. For this study vorticity component perpendicular to the respective measurement plane, is computed as ω_z, defined by **Eq. 4**.

$$\overline{\boldsymbol{\omega}} = \boldsymbol{\nabla} \times \overline{\boldsymbol{V}} = \left(\frac{\partial W}{\partial y} - \frac{\partial V}{\partial z}\right)\overline{\boldsymbol{i}} + \left(\frac{\partial U}{\partial z} - \frac{\partial W}{\partial w}\right)\overline{\boldsymbol{j}} + \left(\frac{\partial V}{\partial x} - \frac{\partial U}{\partial y}\right)\overline{\boldsymbol{k}} \qquad (\mathbf{s^{-1}}) \qquad \textbf{Eq. 3}$$

$$\boldsymbol{\omega_z} = \frac{\partial V}{\partial x} - \frac{\partial U}{\partial y} \qquad (\mathbf{s^{-1}}) \qquad \textbf{Eq. 4}$$

Where $\boldsymbol{\nabla} \times \overline{\boldsymbol{V}}$ represents the curl of velocity vector ($\overline{\boldsymbol{V}}$). $\boldsymbol{U}, \boldsymbol{V}, W$ are respective velocity components in $\boldsymbol{x}, \boldsymbol{y}, \boldsymbol{z}$ directions with the unit vectors $\overline{\boldsymbol{i}}, \overline{\boldsymbol{j}}, \overline{\boldsymbol{k}}$ respectively. ω_z is the vorticity component in the direction of unit vector $\overline{\boldsymbol{k}}$, which is perpendicular to $\boldsymbol{x}, \boldsymbol{y}$ plane.

Study of the vorticity ($\boldsymbol{\omega_z}$), are done at the different planes of measurements, from the test rig wall up to the plane of GV mid-span. Thus, qualitative analysis of formation and propagation of vortex can compared for different cases of CG. This work presents the results for the cases with CG 0 mm as the reference case and for the case of CG 2 mm as the critical case. **Figure 14** shows plots of $\boldsymbol{\omega_z}$ for case of CG 0 mm. At the plane of GV mid-span, vorticity is observed only at the flow channel periodic walls, due to boundary effects. At the measurement planes 1% and 2% of GV-Span from wall, a clear pattern of vorticity can be observed at the trailing edge of GV towards suction side. This indicates the formation of corner vortex between GV and walls, even in absence of any CG. Positive magnitude of vorticity indicates that the vorticity propagates towards the mid-span along with the flow downstream of the TGV. This phenomenon can be observed with shift of the position of vortex core to the downstream of GV, for the measurement plane towards the mid-span from the wall. Brekke [19] has described the corner vortex as the main cause of secondary flows in the Francis turbine distributor. He has also identified the corner vortex being responsible to cause increased local sediment erosion at the suction side of GV at the trailing edge. This causes an increase in size of CG causing leakage flow, which further intensifies the vorticity and its effects on flow conditions. At the measurement plane 4% of GV-Span from the wall, the corner vortex appears to hit the runner inlet. This affects the local flow condition at the runner inlet and also higher erosion of runner hub. Due to viscos mixing with the main flow, the corner vortex dissipates after the measurement plane 20% of GV-Span from the wall.

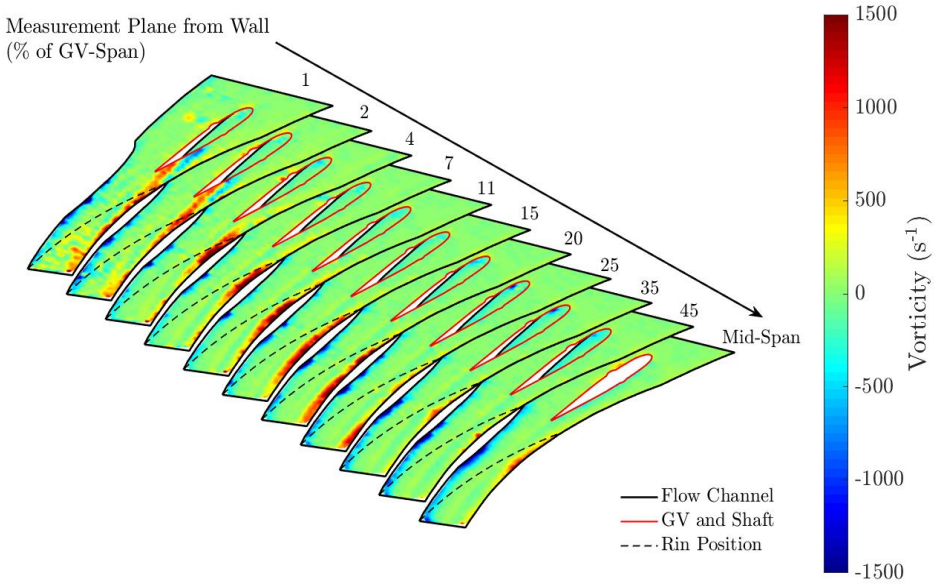

Figure 14. Vorticity along GV span with CG of 0 mm

Figure 15 shows plots of ω_z for case of CG 2 mm. A similar pattern of formation and propagation of the vortex core as in case of CG 0 mm can be seen. However, it can be observed that the vortex core does not appear at close to the test section wall, as it is observed for the corner vortex. The flow appears to pass through the plane of the CG without any vorticity. The vorticity appears only after crossing the plane of CG (2% of GV-Span), and gets more dominant at the measurement plane of 4% of GV-Span from the wall. This suggests that the vortex rope is formed due to mixing of leakage flow from CG with the main flow as discussed with **Figure 7** and **Figure 8**. The high velocity leakage flow can roll up with the main flow causing to form the vortex core. Thus the vortex formed with case of CG is called as the 'leakage vortex', which by its nature different from the corner vortex. It is also observed that the intensity of the leakage vortex for CG 2 mm is almost twice of the corner vortex. It appears that the leakage vortex enters inside the runner blade with the flow in between 11-15% of GV-Span from the test section wall. Further investigations of interaction of the leakage vortex with rotating turbine runner are necessary for better understating its effects on turbines performance.

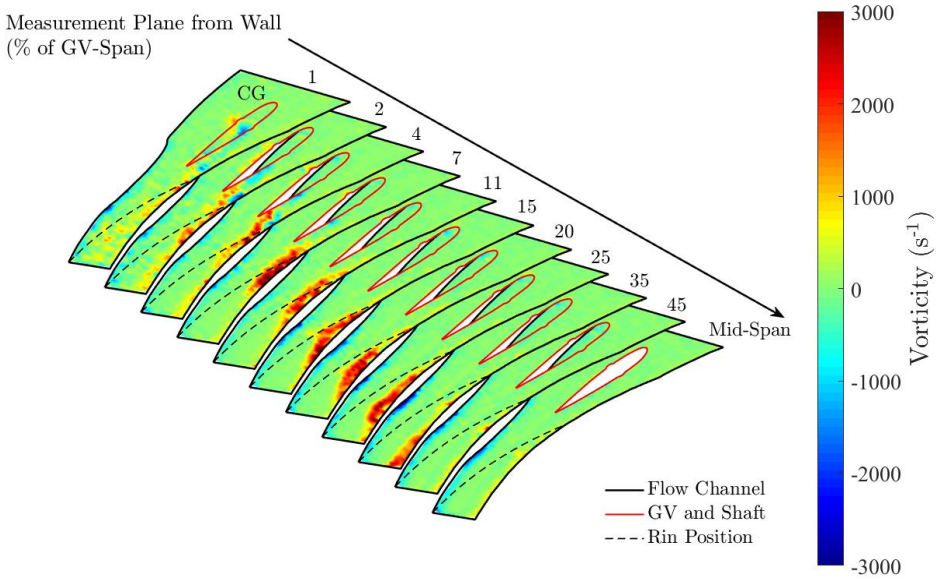

Figure 15. Vorticity along GV span with CG of 2 mm

4. Conclusions

Sediment erosion in Francis turbine causes the clearance gap between the guide vane and cover plates to increase significantly from its design value. This study is focused to identify causes and consequences of such increased clearance gap on the flow conditions at the runner inlet Francis turbines. An experimental setup is developed to study flow around

distributor of Francis turbine with the flow conditions close to a prototype low specific speed Francis turbines at the best efficiency point. PIV measurements are conducted to estimate the effects of leakage flow from different sizes of guide vane clearance gaps on the each parameter contributing to the velocity triangle at runner inlet. Study of formation and propagation of flow vortex with and without clearance gap is also done.

It is observed from this study that the leakage flow from the guide vane clearance gap mixes with the main flow and effects all the velocity components that contributes to design and performance of the runner. It is observed that clearance gap up to 0.5 mm does not have significant effects on the flow parameters. The leakage flow, with clearance gap more than 1 mm, is found to change the velocity components and also blade loading, in both the circumferential direction and in the span wise direction, at the runner inlet. The case with clearance gap 2 mm is found to have the highest effects on the flow velocities and is considered as the critical size, which has to be avoided as far as possible. For the critical size of clearance gap, the relative velocity at the runner inlet is found to increase up to three times locally. The local increase of the relative velocity is identified as the cause of high erosion at the inlet to the runner at the hub. Formation of corner vortex between guide vane and walls, even in absence of any clearance gap has been observed from this study. A leakage vortex, with the higher strength than that of the corner vortex, has been observed with the case of flow with clearance gap. Both the corner vortex and the leakage vortex originates from the suction side of guide vane at about 75% of chord, close to the wall. The leakage vortex is drawn towards the mid-span as flow progresses down stream of guide vane. The leakage vortex is observed to pass into the runner with the flow. Further investigation of interaction of corner vortex and the leakage vortex with the runner is necessary.

References

[1] Matsuo Y, Yanagisawa A, Yamashita Y. A global energy outlook to 2035 with strategic considerations for Asia and Middle East energy supply and demand interdependencies. Energy Strategy Reviews. 2013;2(1):79-91.

[2] Darmawi, Sipahutar R, Bernas SM, Imanuddin MS. Renewable energy and hydropower utilization tendency worldwide. Renewable and Sustainable Energy Reviews. 2013;17(0):213-5.

[3] Huang H, Yan Z. Present situation and future prospect of hydropower in China. Renewable and Sustainable Energy Reviews. 2009;13(6–7):1652-6.

[4] Sharma NK, Tiwari PK, Sood YR. A comprehensive analysis of strategies, policies and development of hydropower in India: Special emphasis on small hydro power. Renewable and Sustainable Energy Reviews. 2013;18(0):460-70.

[5] Bookhagen B. Appearance of extreme monsoonal rainfall events and their impact on erosion in the Himalaya. Geomatics Nat Hazards Risk. 2010;1(1):37-50.

[6] Gohil PP, Saini RP. Coalesced effect of cavitation and silt erosion in hydro turbines - A review. Renewable and Sustainable Energy Reviews. 2014;33(0):280-9.

[7] Padhy MK, Saini RP. A review on silt erosion in hydro turbines. Renewable and Sustainable Energy Reviews. 2008;12(7):1974-87.

[8] Singh M, Banerjee J, Patel PL, Tiwari H. Effect of silt erosion on francis turbine: A case study of Maneri Bhali stage-II, Uttarakhand, India. Journal of Hydraulic Engineering. 2013;19(1):1-10.

[9] Thapa BS, Thapa B, Dahlhaug OG. Current research in hydraulic turbines for handling sediments. Energy. 2012;47(1):62-9.

[10] Flores E, Bornard L, Tomas L, Liu J, Couston M. Design of large Francis turbine using optimal methods. Conference Design of large Francis turbine using optimal methods, vol. 15. IOP Publishing, p. 022023.

[11] Brekke H. Hydraulic design strategy for Francis turbines. International Journal on Hydropower and Dams. 1996;3(3):38-42.

[12] Yexiang X, Zhengwei W, Zongguo Y, Jin Z. Experimental and numerical analysis of pressure pulses characteristics in a Francis turbine with partial load. Conference Experimental and numerical analysis of pressure pulses characteristics in a Francis turbine with partial load, vol. 12. IOP Publishing, p. 012023.

[13] Thapa BS, Dahlhaug OG, Thapa B. Sediment erosion in hydro turbines and its effect on the flow around guide vanes of Francis turbine. Renewable and Sustainable Energy Reviews. 2015;49(0):1100-13.

[14] Sharma HK. Power generation in sediment laden rivers: The case of Nathpa Jhakri. International Journal on Hydropower and Dams. 2010;17(6):112-6.

[15] Koirala R, Thapa B, Neopane HP, Zhu B, Chhetry B. Sediment erosion in guide vanes of Francis turbine: A case study of Kaligandaki Hydropower Plant, Nepal. Wear. 2016;362–363:53-60.

[16] Xue-Zhong L. Guidevane erosion at Mao Tiao He. Int Water Power & Dam Constr. 1982;34(2 , Feb. 1982):23-6.

[17] Chitrakar S, Neopane HP, Dahlhaug OG. Study of the simultaneous effects of secondary flow and sediment erosion in Francis turbines. Renewable Energy. 2016.

[18] Thapa B. Sand erosion in hydraulic machinery: PhD thesis, Norwegian University of Science and Technology, Faculty of Engineering Science and Technology, 2004.

[19] Brekke H. Design of hydraulic machinery working in sand laden water. In: Duan CG, Karelin VY, editors. Abrasive erosion and corrosion of hydraulic machinery. London: Imperial college press; 2002. p. 155-81.

[20] Chhetry B, Rana K. Effect of Sand Erosion on Turbine Components: A Case Study of Kali Gandaki "A" Hydroelectric Project (144 MW), Nepal. Hydro Nepal: Journal of Water, Energy and Environment. 2015;17:24-33.

[21] Koirala R, Zhu B, Neopane HP. Effect of guide vane clearance gap on Francis turbine performance. Energies. 2016;9(4).

[22] Brekke H. The influence from the guide vane clearance gap on efficiency and scale effect for Francis turbines. Conference The influence from the guide vane clearance gap on efficiency and scale effect for Francis turbines. p. 825-37.

[23] Chen X. Theoretical and experimental study of flow through the double cascade of a Francis turbine: PhD thesis, Norwegian University of Science and Technology, Faculty of Engineering Science and Technology, 1992.

[24] Thapa BS, Dahlhaug OG, Thapa B. Velocity and pressure measurements in guide vane clearance gap of a low specific speed Francis turbine. 28th IAHR Symposium on Hydraulic Machinery and Systems. Grenoble, France, 2016.

[25] Thapa BS, Dahlhaug OG, Thapa B. Sediment erosion induced leakage flow from guide vane clearance gap in a low specific speed Francis turbine. Renewable Energy. Submitted, July 2016.

[26] IEC. Hydraulic turbines, storage pumps and pump-turbines – Model acceptance tests 2nd edn 1999-11. IEC 60193: The International Electro technical Commission; 1999.

[27] Thapa BS, Trivedi C, Dahlhaug OG. Design and development of guide vane cascade for a low speed number Francis turbine. Journal of Hydrodynamics, Ser B. 2016;28(4):676-89.

[28] Thapa BS, Dahlhaug OG, Thapa B. Flow measurements in guide vane cascade of a Francis turbine: A PIV approach. Renewable Energy. Submitted, July 2016.

[29] Thapa BS, Thapa B, Dahlhaug OG. Empirical modelling of sediment erosion in Francis turbines. Energy. 2012;41(1):386-91.

Additional Papers F-G

Paper-F

Flow field measurement in guide vane cascade of a high head Francis turbine

Biraj Singh Thapa, Ole Gunnar Dahlhaug and Bhola Thapa

In Proceedings of 6th International Conference on Water Resources and Hydropower Development in Asia, 1-3 March 2016, Vientiane, Lao PDR

Flow field measurement in guide vane cascade of a high head Francis turbine

Biraj Singh Thapa [1]; Ole Gunnar Dahlhaug [1]; Bhola Thapa[2]

[1]Department of Energy and Process Engineering, Norwegian University of Science and Technology, Norway

[2]Department of Mechanical Engineering, Kathmandu University, Nepal

Abstract

Francis turbine is a reaction machine, which converts both pressure energy and kinetic energy in fluid to the mechanical energy at the runner. A part of conversion of the pressure energy into the kinetic energy is done by guide vanes. Guide vanes also direct the flow into the runner at an angle appropriate to the design, imparting a tangential velocity and hence an angular momentum to the flow. Several unsteady flow phenomenon including cross flow from the clearance gaps, secondary flows due to pressure gradients, wakes, and rotor stator interaction are associated with guide vane flow fields. Operational challenges as sediment erosion and part load operations further complicates the flow characteristics. There is still a need of further research to understand the flow phenomenon around guide vanes of Francis turbines to improve the design methods to address these issues in better ways.

A guide vane cascade of a high head Francis turbine has been developed for the experimental investigations. The test setup is able to produce similar velocity distributions at the runner inlet as that of a reference prototype turbine. Standard analytical methods are used to design the reference turbine and CFD based optimization methods are used to define the final layout of the test setup. The cascade consists one guide vane between two flow channels from the position of stay vane outlet to runner inlet. This paper discuss about the methods used to design and optimize the test setup. Results of pressure and velocity measurements in the cascade with 30% of design flow of prototype is presented. Formation and transportation of wake downstream of guide vane to the runner inlet is discussed concisely. Development of vortex filament due to crossflow from clearance gap in guide vane is also presented.

1. Introduction

Hydraulic turbine is an important component of a hydropower plant. The turbine converts available hydraulic energy into mechanical energy, which is then converted to electrical

energy by the generators. Francis type of hydraulic turbines are widely used for this energy conversion, as it can meet the real time demand with its ability to maintain high efficiency even in fluctuating load. Single unit of these turbines are capable to generate power up to 1000 MW [1]. During the operation of Francis turbines, the guide vanes (GV) control the discharge to the runner according to power requirement. Water usually accelerates when it passes through the guide vanes and is directed to the runner at an appropriate inlet angle. In a conventional Francis turbine, about 50% of pressure head is converted to kinetic head as the flow accelerates through the guide vanes [2]. For the high head Francis turbines, this accelerated flow causes unstable flow conditions contributing to vortex shedding, high amplitude pressure pulsation, flow separation and sometimes cavitation [3]. Non-uniform pressure and velocity distribution significantly affects the turbine operation and induce dynamic load on runner affecting life of the turbine [4]. Operating conditions with sediment-laden flows add additional challenges and escalates the problems with the eroded surfaces due material removal [5].

Guide vanes direct flow at an appropriate angle to the runner imparting the flow an angular momentum. This makes GV positioned such that at two points, along the same chord length, are located at different radii. Thus, despite of uniform airfoil structure GV will have a pressure difference between each side along the chord. The pressure difference between the GV causes wakes and effects velocity distribution at the trailing edge**.** These wakes further interacts with pressure field between runner blades and creates non uniform flow field. **Figure 1** shows such non-uniform flow at the inlet of Francis runner due to flow distortion. Velocity field between adjacent runner blades is non-uniform both in magnitude and in direction. The pressure difference across the GV surfaces will also induce leakage flow from the GV clearance gap, which generates vortices from the GV trailing edge. This makes the flow conditions at runner inlet to become further disturbed. As the runner rotates, each blade interacts with such flow field while passing every GV. This is also called as rotor-stator interaction. It causes vibrations and pressure pulsations in runner, and affects the performance of the turbine.

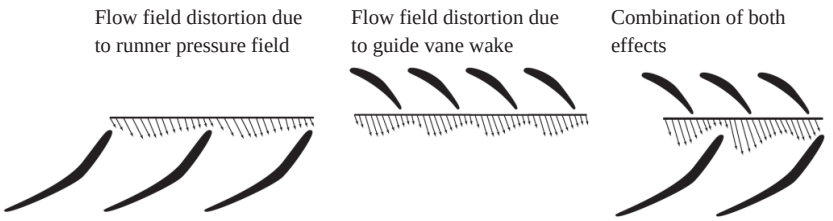

Figure 1. Flow field at inlet of Francis runner displaying runner and guide vane effects on flow velocity and angles. Adapted from Ruchonnet [6].

Minimizing the unsteady flow in vaneless space and achieving uniform velocity distribution at the runner inlet is one of the challenging tasks for a turbine designer. Larsson [7] has conducted experimental and theoretical analysis of inlet flow of a Francis turbine runner. He has used LDA methods to measure the characteristics of velocity distribution in vane less space. It was found that the velocity fluctuations in a guide vane passage can be up to 15% of theoretical value due to the rotor stator interaction. Qian [8] has used PIV methods to measure the pressure and velocity distribution around the pressure side and suction side of the two neighboring guide vanes in a model Francis turbine. It was found that both radial and tangential components of velocity between the guide vanes fluctuate significantly. Kobro [9] has measured the effects of such velocity fluctuations on the dynamic load in runner blades in a model Francis turbines. It was found that fluctuations of stresses inside the runner blades were highest for 50-70% of nominal discharge. However, pressure and velocity measurements around guide vanes of high head Francis turbines, with the prototype flow conditions, has not been reported so far.

A test setup is developed, at NTNU, for the investigations of inlet flow of Francis runner at the prototype conditions [10]. The test setup is able to produce steady state flow conditions from the position of stay vane outlet to the runner inlet of a low speed number Francis turbine at the best efficiency point (BEP). The design goal is to acquire similar flow conditions as that observed in a prototype high head Francis turbine. The purpose of this setup is to examine the effects of leakage flow around GV on the velocity distribution at the runner inlet. The setup isolates the effects of runner on the flow field and hence allows precise study of flow characteristics in the distributor part of Francis turbines. This paper discusses design procedure followed to develop the test setup. Results of pressure and velocity measurements at the guide vane mid span and in the clearance gap are presented in this study.

2. Development of Test Setup

2.1 Reference turbine

Jhimruk Hydroelectric Center (JHC) in Nepal is considered as the reference case for this study. The power plant has three units of Francis turbine and each produces 4.2 MW at the BEP. These are low speed number (**Eq. 1**) splitter bladed Francis turbines.

$$\Omega = \boldsymbol{\omega} \cdot \sqrt{\boldsymbol{Q}} / (\boldsymbol{2g} \cdot \boldsymbol{H})^{\boldsymbol{3/4}} \qquad \textbf{(-)} \qquad \textbf{Eq. 1}$$

With head above 200 m and speed number 0.32 these turbine can be considered as a case of high head Francis units. This power plant represents a typical case of projects operating under large sediment load in Himalayan basin [11]. Several academic studies [12-14] have been conducted to improve hydraulic design of this turbine to handle large sediment load. Design and drawings of the installed prototypes are not available therefore an in-house tool

named as "*Khoj*", was developed to design a reference turbine with the aim to replace with the existing one [13]. Extensive investigations were carried out on this reference turbine for optimizing hydraulic design to minimize sediment erosion without compromise in efficiency [15-17]. Understanding the consequences of erosion on guide vanes and investigating its effects on velocity distribution at runner inlet was identified as the further works.

Table 1 presents the relevant analytical values for the reference turbine at BEP. These parameters with the original design values are used to develop the test setup for this study. Thus, the test setup is able to re-create the prototype flow conditions. Velocity component at different sections of the reference turbine has been used to design the cascade. These sections include center of spiral casing, inlet and outlet of stay vanes, inlet and outlet of guide vanes and inlet of runner. The design goal is to dimension the cascade to deliver the same velocity components at these sections as for the prototype turbine.

2.2 Design and optimization of flow cascade

A symmetric section of reference turbine forms the flow cascade. Some of the researchers have considered a straight channel with single guide vane, while others have considered a section of prototype or model turbine to investigate the passage flow conditions. Choice of channel profile depends upon objectives and requirements of the measurements. For the present study, three guide vane (GV) with two flow passages out of 24 passages of the GV is considered as a reference case. This configuration has a single GV inside the flow channel. Two outer GV remains as walls of cascade and middle GV guides flow in the channel. Thus, this layout of the test setup is named as 1 GV test setup.

Table 1. Reference turbine analytical design values

Parameters	**Symbol**	**Unit**	**Value**
Net head	H	m	201.5
Flow rate per unit turbine	Q	m^3/s	2.35
Rotational speed	n	rpm	1000
Speed number	Ω	-	0.32
Number of blades in runner	Z_Blades	-	17
Inlet diameter of runner	D_1	m	0.89
Number of Guide vanes	Z_gv	-	24
Chord length of GV	L_gv	m	0.14

Figure 2 shows the layout of 1 GV cascade. GV located at the end section of spiral casing (SC) are considered for this design. The choice of GV at the end section of SC will minimize the overall size of test setup. Walls defined by the symmetric boundary between each flow passage is considered as a reference profile for the boundary of cascade. These sections include from the center of spiral casing to the inlet of guide vane, from the outlet of guide vane to the inlet of runner and from the inlet of runner to the middle of runner blade. Profile of wall above the center of spiral casing up to the inlet of cascade is designed to give same distribution of tangential and radial component of velocity at the center of spiral casing from the completely axial flow at the inlet of cascade. Stay vanes are not included as the part of cascade, as they are mainly for strengthening spiral casing and do not play significant role for hydraulic design [18]. Circular portion of spiral casing is replaced with flat plates with the same height as that of the span of guide vane. Thus, section from inlet to outlet of cascade is embedded between two flat plates. This makes the design relatively simple and easy for manufacturing. However, such simplification would affect the flow conditions and hence the optimization of walls' profile is necessary.

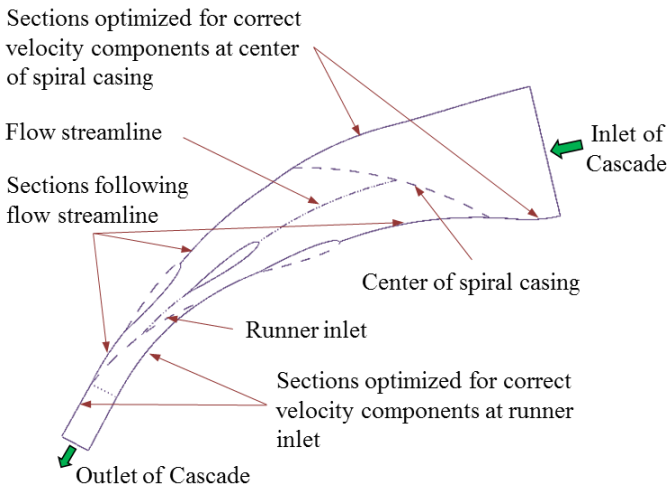

Figure 2. Test setup layout and sections for optimization

Optimization techniques are applied to redesign the profile from the inlet of cascade to the center of spiral casing, and from the inlet of runner to the outlet of cascade until the satisfactory flow conditions are obtained. The main criteria to satisfy the optimization goal is to have similar profile of both tangential and radial velocity at the position of runner inlet, as that observed in the case of reference prototype turbine. Several optimized designs are obtained and CFD evaluations of each alternative are done to verify its performance. Thus, the optimum geometrical layout of the test setup is identified to satisfy the need of

this investigation. Details of design optimization and CFD analysis is discussed in earlier work by the same authors [10].

3. Experimental Methods

3.1 Test Setup

Development of the experimental test setup is based on the layout of optimum design of one GV cascade. This configuration re-creates the flow around one GV, inside equivalent two periodic flow channels of a compete Francis turbine. Angular position covered by the flow passage is 30 degrees from the turbine center. This flow passage is 1/12th size of turbine in angular direction. For the convenience of manufacturing, assembly and testing, the setup is divided into several parts as shown in **Figure 3a**. The test section contains the test guide vane inside a plexi-glass flow channel. The cover plates of test section have openings for excess to the laser sheet and camera exposure for PIV images parallel to GV chord. **Figure 3b** shows the cross section view of the test section along the chord of GV. Position of clearance gap and taps for pressure measurements in the gap can be observed. The test guide vane (TGV) has been designed as an assembly of multiple parts. Plexi part of TGV imparts transmission of the laser sheet, allowing excess to entire plane inside plexi glass channel. Intermediate part of TGV has been 3D printed with the inner holes giving excess to pipes for pressure tapping. The end part of TGV can replaced with the parts of different thickness to get the desired clearance gap inside the flow channel.

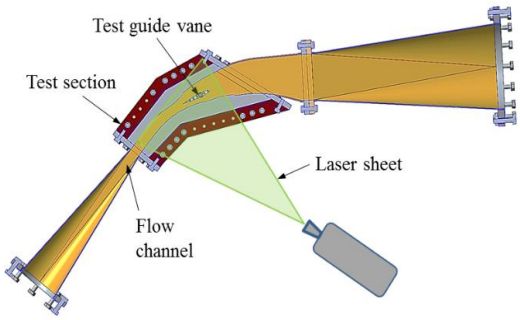

Figure 3a. Cross section view of test setup

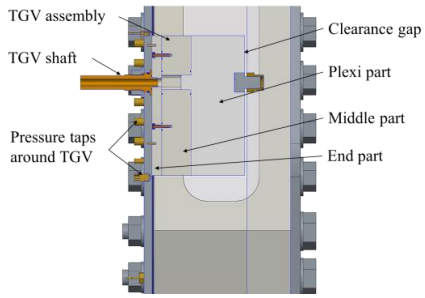

Figure 3b. Sectional view of test section

The test setup is installed at the facilities of the Waterpower laboratory in NTNU. The setup is mounted in a closed loop system consisting of pump, flow meter, and a pressure tank. All the measurements for this study is conducted with flow rate of 58.2 liter per second. This is 30% of design flow for the same flow area in the prototype at BEP. This is a maximum flow through the setup for the normal operating conditions and avoiding the cavitation at the outlet of test section. With this flow, the average velocity obtained at the runner inlet position, is 12.45 m/s. For higher velocities, the test setup should be pressurized

to the corresponding velocity to avoid the cavitation. In order to achieve the prototype flow conditions, maximum pressure inside the test loop could reach up to 10 bars. The main aim of presented experiment is to investigate velocity distribution from GV outlet to runner inlet inside the flow passage and relate it with the pressure measurements around GV.

3.2 Pressure Measurements

Pressure measurements are done at along the GV surface at the end span. 14 pressure taps (2 mm dia) are inserted in the test section wall to measure pressure from both pressure and suction side of GV. The measurements are done at eight different sections along the chord length. Symmetric positions at pressure and suction side of GV are taken for the measurements at the respective section. Each pressure tap is connected to piezo-resistive pressure transducer through a plastic pipe. All the sensors are pre-calibrated against the dead weight calibrator. Measurements from all the taps are conducted simultaneously with the same flow conditions as for the velocity measurements. This insures direct comparison of pressure and velocity fields in the test setup for respective flow conditions. An average of 2000 samples, for each pressure point, measured at 5 HZ, is considered for the pressure analysis.

3.3 Velocity measurements

Particle Image Velocimetry (PIV) methods is applied for capturing velocity field, from the position of stay vane outlet to the position of runner inlet with a Dantec system. The pulsed light sheet with a thickness of 2 mm is generated by two double-cavity Nd-YAG lasers providing 120 mJ by pulse. The lighted field is visualized by a HiSense 2M CCD PIV cameras, with a series of paired images acquired at 150 μs and 4 Hz. Alignment of laser and camera with respect to the measurement plane is achieved with separate laser pointers. Fluorescent seeding particles, with a density of 1.016 kg/m^3, refractive index of 1.52 and mean diameter of 55 μm are used during the measurements. The camera resolution is 1280x1024 pixels for a 350x400 mm spatial domain. The PIV system is calibrated using a 2D calibration target. The calibration was performed *in-situ* with a specially designed calibration system. The camera exposition and its synchronization with laser and the image processing is done with a Dantec DynamicStudio 3.40 PIV specific processor. The image processing is carried out with 32-pixel resolution cross-correlation technique with 50% overlap. Velocity vectors along the mid span and along the mid of 2 mm clearance gap is obtained from the PIV measurements with the time-averaged value for 100 images.

4. Results and Discussions

This paper presents the results of pressure and velocity measurements at the flow conditions described in section 3.1. Pressure measurement is done along the GV surface (pressure and suction side) and velocity measurement is done along the mid span section of GV.

Figure 4 shows the pressure distribution along the GV surface. All the pressure values are normalized by the pressure at the leading edge of GV. Highest pressure at the leading edge shows the stagnation point. A clear pattern of pressure and suction side can be observed as the flow progresses towards the trailing edge. Equal distribution of pressure up to 10% of GV chord from the leading edge shows angle of attack close to zero. Gradual development of pressure difference towards trailing edge is observed with maximum pressure difference occurring at 60% of the chord length. Unequal swirl component on pressure and suction side, due to chord of GV being positioned at different radii with respect to turbine center, causes this pressure difference. Fixed walls above and below GV can also effect the flow properties. Lowest pressure in the suction side of GV is at the section 60-80% of chord length. At the trailing edge, flow from the pressure side has a negative pressure gradient and flow from suction side has a positive pressure gradient. This causes an 'unbalanced' mixing of flow with different pressure gradients at the trailing edge of GV. Thus, the pressure distribution along the angular position of GV outlet in Francis turbine becomes non-uniform. Hence, turbine runner pass through different gradients of pressure as it moves from one GV to other.

Figure 5 shows velocity distribution inside the flow cascade obtained from PIV measurements. Lower velocities along the suction side of GV and higher for the pressure side matches the results from pressure measurements. Contours of velocity field, showing the stagnation point and flow development around GV, also matches the pressure field. The

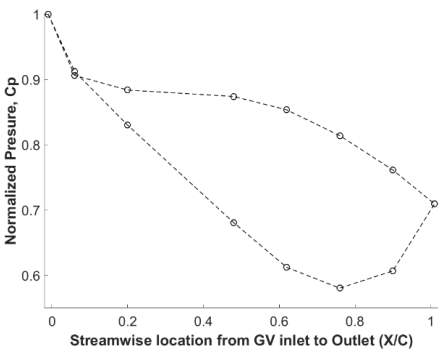

Figure 4. Pressure measurements along GV surface

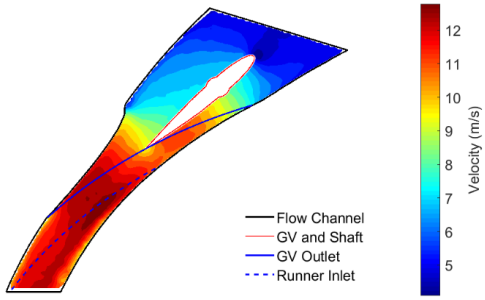

Figure 5. Velocity felid inside flow channel (PIV)

'unbalanced' mixing of flow at the GV training edge, as suggested by the pressure measurement can also be observed. Formation of wake, at downstream of GV, and its dissipation as flow approaches to runner inlet can also be seen.

Figure 6 shows the velocity distribution from GV outlet to runner inlet position in the cascade. Geometrical positions GV outlet and runner inlet in the measurement area can be seen in **Figure 5**. All the positions downstream of GV are respective concentric arc between

arc of GV out let and runner inlet. Profiles of velocity, downstream of GV suggest how flow pattern changes from GV outlet to runner inlet progressively. Significant effects of wake can observed that at the GV trailing edge. At GV outlet position, the wake is close to the center of flow channel walls. Two lobes on either side of wake suggests non-uniform velocity distribution between adjacent GV in angular direction. Velocity profile towards suction side from GV outlet is having smaller peak than that towards the pressure side. This can be caused by the opposite pressure gradient between the pressure and suction side, towards trailing edge, as discussed in previous paragraph. As the flow progresses downstream of GV, wake appears to be dampened out gradually due to viscous effects. It can be clearly noticed that wake is slipping towards suction side, as flow proceeds downstream of GV. At the runner inlet, effect of wake is negligible and its position is shifted by approximately 10 degrees towards suction side. This observation suggests that the transport of wake from GV to runner does not follow the direction of flow. The wake slips towards the suction side of flow from GV to runner on the suction side. It is believed that pressure felid around GV can cause this slipping of the wake form higher pressure zone to lower pressure zone. Larsson [7] has also found the wake at the runner inlet position being shifted towards the suction side in his LDV measurements in a cascade test setup with five GV.

Antonsen [19] has also noticed that the wake position downstream of GV being not along the same angular position. For current measurements, the slip of wake peak appears to be more than anticipated by earlier studies. The measurement being done with about 30% of design flow, could cause the velocity distribution inside the cascade appear differently than for BEP. The test setup having only one GV can also experience effects of walls on the flow causing the flow not being developed as that for the real case. Future measurements with the prototype flow conditions will provide better understanding of flow phenomenon in the distributor of low speed number Francis turbines.

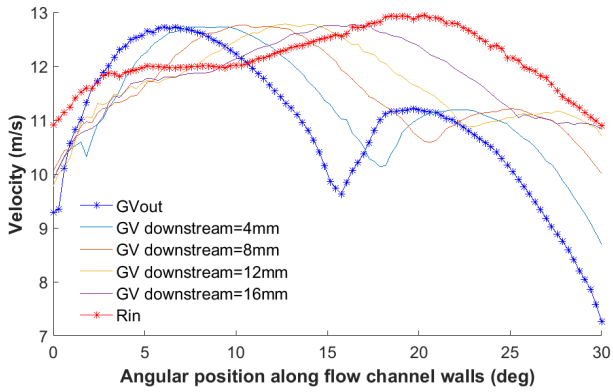

Figure 6. Velocity Profile from GV outlet to Runner inlet

Figure 7 shows the observation of the flow inside test setup for the case of 2 mm clearance gap. As indicated by the pressure measurements, crossflow occurs towards the trailing edge of GV. It can be seen that vortex rope is developed as the cross flow mixes with the main flow. The vortex starts from clearance gap at the 75% of chord length, at the suction side, and is carried downstream towards the position of runner inlet. As the flow moves downstream of GV, location of vortex appears to be shifted towards the suction side due to pressure gradients. The vortex rope mixes with the main flow as it approaches the outlet of test section, where flow becomes more uniform.

Figure 8 shows the results of PIV measurements at the plane middle of 2 mm clearance gap. Contours of total velocity together with the velocity vectors can be observed. Close to the leading edge, the velocity vectors are close to that of main stream flow both in magnitude and direction. Stagnation of flow by the GV shaft can be seen. Behind the GV shaft, gradual development of crossflow and its mixing with main stream flow can be observed. As also indicated by the pressure measurements, the highest amount of crossflow, both in magnitude and direction, occurs at 70-75% of chord length. Mixing of cross flow with main flow seen in **Figure 8** justifies the formation and development of vortex rope as observed in **Figure 7**.

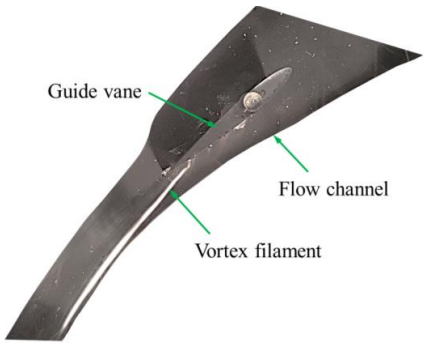

Figure 7 Observation of vortex in clearance gap

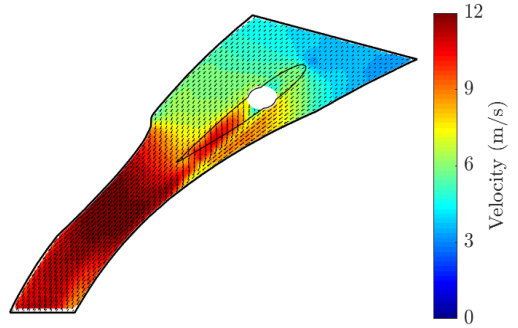

Figure 8 Velocity felid inside flow channel (PIV)

Erosion of guide vanes has been reported as a severe problem in many hydropower projects [20, 21]. Losses in turbine efficiency and the erosion at runner hub has also been observed in such cases. This study shows that leakage flow from eroded guide vanes have considerable effects on flow conditions at runner inlet. Vortex developed by the crossflow can be contribute to efficiency loss and heavy erosion in runner hub. Further investigation on formation of this vortex rope and its effects on turbine performance has to be conducted.

5. Conclusions

A test setup has been developed to investigate flow conditions around guide vane of low speed number Francis turbine. The setup includes flow passage with one guide vane, which is able to create similar velocity conditions as in a prototype turbine. Presented measurements are conducted at 30% of BEP flow. Pressure measurements are done along eight different symmetric sections of the guide vane chord length. Velocity measurements are done by PIV methods to capture the flow field from the stay vane outlet to the runner inlet for 30 degrees angular position. It is concluded from this study that both the velocity and pressure distributions around the guide vane in a Francis turbine is non-uniform along the circumferential direction. Flow with negative pressure gradient from the pressure side, and that with positive pressure gradient from suction side, meet at the trailing edge of guide vane. This effects the formation and transport of wake downstream of guide vane. Transport of wake does not follow the normal flow direction but is slipped towards lower pressure zone as the flow progresses towards the runner. Higher pressure difference at the trailing edge induces a strong crossflow from the clearance gap. This crossflow mixes with the main flow and develops a vortex rope, which is transported downstream into the runner. This makes flow at the in Francis turbines runner inlet further non-uniform and complex for the cases with clearance gap around guide vanes.

References:

[1] E. Flores, L. Bornard, L. Tomas, J. Liu, and M. Couston, "Design of large Francis turbine using optimal methods," in IOP Conference Series: Earth and Environmental Science, 2012.

[2] H. Brekke, "Hydraulic design strategy for Francis turbines," International Journal on Hydropower and Dams, vol. 3, pp. 38-42, 1996.

[3] X. Yexiang, W. Zhengwei, Y. Zongguo, and Z. Jin, "Experimental and numerical analysis of pressure pulses characteristics in a Francis turbine with partial load," in IOP Conference Series: Earth and Environmental Science, 2010, p. 012023.

[4] M. V. Magnoli and R. Schilling, "Numerical Simulation of Pressure Pulsations in Francis Turbines," in Advances in Hydroinformatics, P. Gourbesville, J. Cunge, and G. Caignaert, Eds., ed: Springer Singapore, 2014, pp. 389-403.

[5] B. S. Thapa, O. G. Dahlhaug, and B. Thapa, "Sediment erosion in hydro turbines and its effect on the flow around guide vanes of Francis turbine," Renewable and Sustainable Energy Reviews, vol. 49, pp. 1100-1113, 2015.

[6] N. Ruchonnet, C. Nicolet, and F. Avellan, "One-dimensional modeling of rotor stator interaction in Francis pump-turbine," in Proceedings of the 23rd IAHR Symposium on Hydraulic Machinery and Systems, 2006.

[7] C. Larsson, Experimental and theoretical analysis of inlet flow of a Francis turbine runner: PhD thesis, Norwegian University of Science and Technology, Faculty of Engineering Science and Technology, 2003.

[8] R. Qian, "Flow field measurements in a stator of a hydraulic turbine," PhD thesis, Laval University, Faculty of Science and Engineering, 2008.

[9] E. Kobro, A. Gamboa, R. Bloch, and T. Nielsen, "Onboard pressure measurement in high head Francis prototype runners," in 3rd IAHR International Meeting of the WorkGroup on Cavitation and Dynamic Problems in Hydraulic Machinery and Systems, Czech Republic, 2009, pp. 14-16.

[10] B. S. Thapa, C. Trivedi, and O. G. Dahlhaug, "Design and development of guide vane cascade for a low speed number Francis turbine," Journal of Hydrodynamics, Ser. B, Accepted on 22 November, 2015.

[11] P. M. S. Pradhan, O. G. Dahlhaug, P. N. Joshi, and H. Støle, "Sediment and Efficiency Measurements at Jhimruk Hydropower Plant – Monsoon 2003," Report from HydroLab, Nepal2004.

[12] K. Gjosater, "Hydraulic Design of Francis Turbine Exposed to Sediment Erosion," Masters Thesis, Norwegian University of Science and Technology, 2011.

[13] B. S. Thapa, "Hydraulic design of Francis turbine to minimize sediment erosion," Masters Thesis, Kathmandu University, 2012.

[14] M. Eltvik, "Sediment erosion in Francis turbines," PhD thesis, Norwegian University of Science and Technology, Faculty of Engineering Science and Technology, 2013.

[15] B. S. Thapa, M. Eltvik, K. Gjøsæter, O. G. Dahlhaug, and B. Thapa, "Design Optimization of Francis Runners for Sediment Handling," in Fourth International Conference on Water Resources and Renewable Energy Development in Asia, Thailand, 2012.

[16] B. S. Thapa, B. Thapa, M. Eltvik, K. Gjosater, and O. G. Dahlhaug, "Optimizing runner blade profile of Francis turbine to minimize sediment erosion," in IOP Conference Series: Earth and Environmental Science, 2012, p. 032052.

[17] B. Rajkarnikar, H. P. Neopane, and B. S. Thapa, "Development of rotating disc apparatus for test of sediment-induced erosion in francis runner blades," Wear, vol. 306, pp. 119-125, 2013.

[18] Z. Wei, P. H. Finstad, G. Olimstad, E. Walseth, and M. Eltvik, "High Pressure Hydraulic Machinery," in Compendium, N. Publication, Ed., ed, 2009.

[19] Ø. Antonsen, "Unsteady flow in wicket gate and runner with focus on static and dynamic load on runner," Doctoral Thesis, PhD thesis, Norwegian University of Science and Technology, Faculty of Engineering Science and Technology, 2007.

[20] O. G. Dahlhaug, P. E. Skåre, V. Mossing, and A. Gutierrez, "Erosion resistant coatings for Francis runners and guidevanes," International Journal on Hydropower and Dams, vol. 17, pp. 109-112, 2010.

[21] H. K. Sharma, "Power generation in sediment laden rivers: The case of Nathpa Jhakri," International Journal on Hydropower and Dams, vol. 17, pp. 112-116, 2010.

Paper-G

Velocity and pressure measurements in guide vane clearance gap of a low specific speed Francis turbine

Biraj Singh Thapa, Ole Gunnar Dahlhaug and Bhola Thapa

In Proceedings of 28th IAHR symposium on Hydraulic Machinery and Systems, 4-8 July 2016, Grenoble, France

Velocity and pressure measurements in guide vane clearance gap of a low specific speed Francis turbine

Biraj Singh Thapa [1]; Ole Gunnar Dahlhaug [1]; Bhola Thapa[2]

[1]Department of Energy and Process Engineering, Norwegian University of Science and Technology, Norway

[2]Department of Mechanical Engineering, Kathmandu University, Nepal

Abstract

In Francis turbine, a small clearance gap between the guide vanes and the cover plates is usually required to pivot guide vanes as a part of governing system. Deflection of cover plates and erosion of mating surfaces causes this gap to increase from its design value. The clearance gap induces the secondary flow in the distributor system. This effects the main flow at the runner inlet, which causes losses in efficiency and instability. A guide vane cascade of a low specific speed Francis turbine has been developed for experimental investigations. The test setup is able to produce similar velocity distributions at the runner inlet as that of a reference prototype turbine. The setup is designed for particle image velocimetry (PIV) measurements from the position of stay vane outlet to the position of runner inlet. In this study, velocity and pressure measurements are conducted with 2 mm clearance gap on one side of guide vane. Leakage flow is observed and measured together with pressure measurements. It is concluded that the leakage flow behaves as a jet and mixes with the main flow in cross-wise direction and forms a vortex filament. This causes non-uniform inlet flow conditions at runner blades.

1. Introduction

Francis turbine is a reaction machine, which converts both pressure energy and kinetic energy in fluid to the mechanical energy at the runner. Conversion of a part of this pressure energy into the kinetic energy is done by guide vanes (GV). The energy conversion incurs high velocities and high acceleration, which causes unsteady flow phenomenon as wakes and pressure pulsations. GV also direct the fluid into the runner blades at an angle appropriate to the design. GV is pivoted and can be controlled by using a suitable governing mechanism to regulate the flow while the load in the generator changes. Often NACA airfoils are chosen for shaping of GV. However, optimization of profiles are often done to maximize the overall turbine efficiency and minimize the operational constraints. Design of GV is usually combined together with the design of stay vanes, and both components as a single unit in a reaction turbine is often called as the distributor system.

GV imparts a tangential velocity and hence an angular momentum or spin to the water before it enters to the runner. This makes GV positioned such that at two points, along the same chord length, are located at different radii. Thus, despite of uniform airfoil structure GV will have a pressure side and a suction side. A dry clearance between GV and cover plates usually exists from the design to allow GV to be positioned, so as to maintain the desire flow. Typical design value of such dry clearance ranges from 0.1 mm to 0.3 mm, depending upon the designs and operating conditions. Due to deflection of cover plates under high pressure the clearance further increase. Leakage flow starts from the clearance gap due to inherit pressure difference between adjacent GV surfaces. Flow with spin, together with leakage flow from the GV clearance gap, and wakes and vortices from the GV trailing edge make the flow non-uniform. This non-uniform flow field further interacts with rotating runner as each blade passes GV, which is also called as rotor-stator interaction. Thus, the flow conditions at runner inlet in a reaction machines becomes very complex.

Chen [1] has done a study on flow field in distributor of a high head Francis turbine and concluded that the exit flow from the guide vane cascade is neither uniform in circumferential direction, nor in span wise direction. Eide [2] has investigated the effects of head cover deflection on flow field and found that clearance gap induces leakage flow and vortices from trailing edge of GV. Brekke [3] has investigated the influence of the guide vane clearance gap on turbine efficiency. He measured a decrease of 0.5% efficiency at BEP in a prototype with 0.5 mm clearance gap compared to the original runner with 0.3 mm clearance gap. These studies suggest that secondary flow occurs from the GV clearance gap and has significant impact on turbine performance.

Increasing number of hydropower plants are being built in the regions where rivers are heavily loaded with sediments. High concentration of sediments in flow induces material erosion in turbines. This leads to change in flow pattern, losses in efficiency, vibrations and even final breakdown of components. Due to secondary flows and corner vortex, higher erosion occurs between GV and its wall. Erosion in this region causes further increase of clearance gap. **Figure 1** shows typical damages of distributor system of a Francis turbine, operating under heavy sediment load. Deep groves on the mating surfaces gives an indication of level of crossflow occurring from this region. Such high crossflow can completely change the velocity profile at the runner inlet. Change in velocity profile at the inlet causes additional erosion damage and other undesired effects in the turbine runner. It has been reported that more than 25% of runner blade area has been eroded by sediments within 3 years of operation in Nepal's largest power plant [5]. Such scale of erosion in turbine component causes significant loss in hydraulic efficiency and incurs heavy maintenance costs. There has been very limited studies regarding the effects of leakage flow from GV clearance gap on velocity profile at runner inlet of a Francis turbine.

A test setup is developed, at NTNU, for the experimental investigations of flow around guide vanes of Francis turbines [6]. The test setup is able to produce steady flow conditions from the position of stay vane outlet to the runner inlet of a low specific speed Francis turbine. The design goal is to acquire similar flow conditions as that observed in a prototype Francis turbine. The objective of this setup is to examine the effects of leakage flow around guide vanes on flow conditions at runner inlet. The setup isolates effects of runner on the flow field and hence allows study of effects of leakage flow alone on the flow conditions at the position of runner inlet. This paper briefly discusses design procedure followed to develop the test setup. The main is to investigate nature of flow from GV clearance gap, and analyze its effects on velocity distribution at the runner inlet.

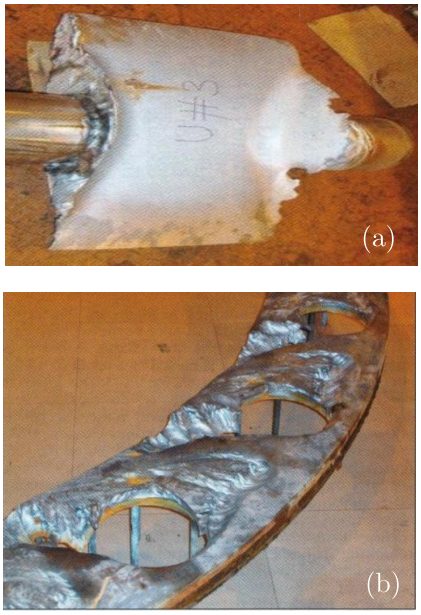

Figure 1. Sediment erosion damage: (a) in GV, (b) in facing plates [4]

2. Development of Test Setup

2.1 Reference turbine

Jhimruk Hydroelectric Centre (JHC) in Nepal is considered as the reference case for this study. The power plant has three units of Francis turbine, each producing 4.2 MW at best efficiency point (BEP). These are splitter bladed Francis turbines as with specific speed 0.086, as defined by **Eq. 1** [7].

$$N_{QE} = \frac{n \cdot Q^{0.5}}{E^{0.75}} \qquad \textbf{(-)} \qquad \textbf{Eq. 1}$$

Where, N_{QE} is specific speed, n is speed of runner (s^{-1}), Q is flow in turbine (m^3/s) and E is specific hydraulic energy of turbine (Jkg^{-1}).

This power plant also represents a typical case of projects operating under large sediment load in Himalayan basin [8]. Design and drawings of the prototypes are not available. An in-house tool named as "*Khoj*", was developed to design a reference turbine with the aim to replace with the existing one [9]. Extensive investigations has been carried out on this reference turbine for optimizing hydraulic design to minimize sediment erosion without compromise in efficiency [10-13].

Table 1 presents the relevant analytical values for the reference turbine at BEP. These parameters are used to develop the test setup for this study.

Table 1. Reference turbine analytical design values

Parameters	**Symbol**	**Unit**	**Value**
Net head	H	m	201.5
Flow rate per unit turbine	Q	m^3/s	2.35
Rotational speed	N	rpm	1000
Specific speed	N_{QE}	-	0.086
Number of blades in runner	Z_Blades	-	17
Inlet diameter of runner	D_1	m	0.89
Number of Guide vanes	Z_gv	-	24
Chord length of GV	L_gv	m	0.14

2.2 Design and optimization of flow cascade

A symmetric section of reference turbine forms the flow cascade. Some of the researchers have considered a straight channel with single guide vane [14, 15], while others have considered a section of model turbine to investigate the passage flow conditions [1, 16]. Choice of channel profile depends upon objectives and requirements of the measurements. For the present study, three GV with two flow passages out of 24 passages of the GV is considered as a reference case. This configuration has a single GV inside the flow channel. Two outer GV forms as part of walls of cascade and middle GV guides flow in the channel. Thus, this layout of the test setup is named as one GV test setup.

Figure 2 shows the layout of cascade considered as the reference design. Walls defined by the profile of free vortex flow with **Eq. 2** is considered from center of spiral casing to inlet of guide vane, from outlet of guide vane to inlet of runner and from the inlet of runner to outlet of cascade. Stay vanes are not included as part of cascade, as they are mainly for strengthening spiral casing and do not play significant role for hydraulic design [17]. Circular portion of spiral casing is replaced with flat plates with the same height as that of the span of guide vane. Thus, section from inlet to outlet of cascade is embedded between two flat plates. This makes the design relatively simple and easy for manufacturing. However, such simplification would affect the flow conditions and hence the optimization of walls' profile is necessary. CFD based optimization techniques are applied to redesign the profile from the inlet of cascade to the center of spiral casing, and from the inlet of runner to the outlet of cascade until the satisfactory flow conditions are obtained.

$$C_u \cdot R = Constant \qquad \text{Eq. 2}$$

Where Cu is tangential velocity of flow at the radius R from center of turbine.

Profile of wall upstream of the center of spiral casing up to the inlet of cascade is re-designed to develop the necessary flow conditions at the center of spiral casing from completely axial flow at the inlet of cascade. The main criteria to satisfy the optimization goal is to have similar profile of both tangential and radial velocity components, at the position of runner inlet of cascade, as that observed in case of the reference prototype turbine. Details of design optimization and CFD analysis is discussed in earlier work by the same authors [6].

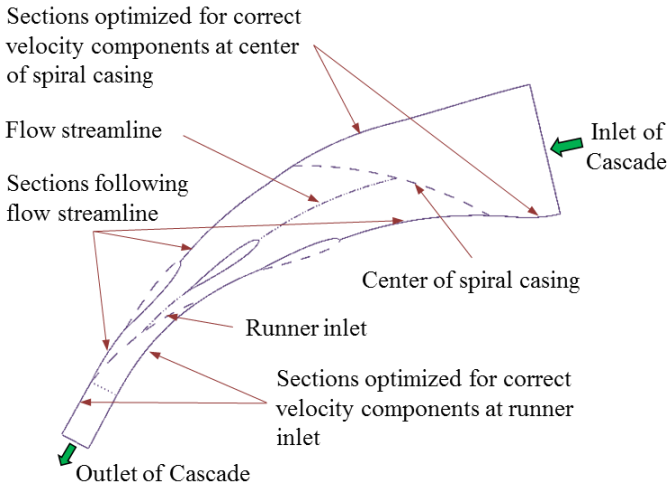

Figure 2. Reference design and sections for optimization

3. Experimental Methods

3.1 Test Setup

Development of the experimental test setup is based on the layout of optimum design of one GV cascade. This configuration re-creates the flow around one GV, inside equivalent two periodic flow channels of a Francis turbine. Angular position covered by the flow passage, inside the cascade, is 30 degrees from the turbine center. This flow passage is $1/12^{th}$ size of turbine in angular direction. **Figure 3** shows the cross section view of the test setup along the plane of measurement. For the convenience of manufacturing, assembly and testing, the setup is divided into parts shown. The test section contains the test guide vane (TGV) inside a plexi-glass flow channel for optical excess to PIV system. **Figure 4** shows the cross section view of the test section along GV chord. Position of clearance gap and taps for pressure measurements in the gap can be observed. TGV has been designed as

an assembly of multiple parts. Plexi part of TGV imparts transmission of the laser sheet, allowing excess to entire plane inside the flow channel. Other two parts are made of aluminum. The middle part of TGV is attached to the plexi part, and the end part of TGV is screwed with the middle part. The end part of TGV can be replaced with the similar parts of different thickness to get desired clearance gap with respect to the flow channel wall.

The test setup is installed at the facilities of the Waterpower laboratory in NTNU. The setup is mounted in a closed loop system consisting of pump, flow meter, and a pressure tank. Air pressure inside the pressure tank is maintained to atmospheric pressure. All the measurements for this study is conducted with flow rate of 0.058 m^3/s. This is 30% of design flow for the same flow area in the prototype at BEP. This is also the maximum flow through the setup for avoiding the cavitation at the outlet of test section. With this flow, the average velocity obtained at the runner inlet position, is 12.45 m/s. For higher velocities, the test setup should be pressurized by applying external pressure in the pressure tank. The external pressure is corresponds to the desired maximum velocity inside test setup while avoiding the cavitation. In order to achieve the prototype flow conditions, the pressure inside the test loop could reach up to 10 bars.

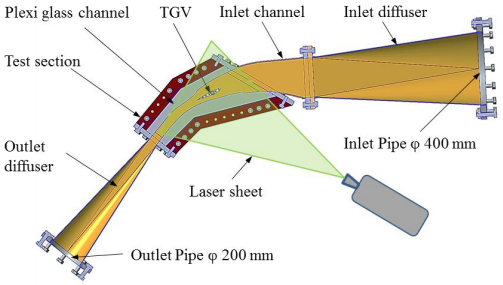

Figure 3. Sectional view of test setup along plane of measurement

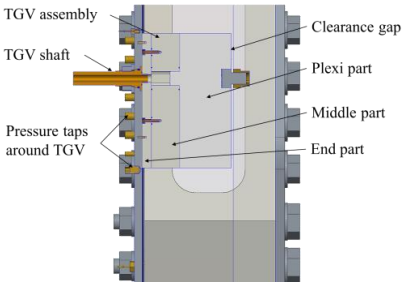

Figure 4. Sectional view of test section along GV chord

3.2 Pressure Measurements

Pressure measurements are done along the TGV surface, close to the test section wall without clearance gap. 14 pressure taps with 2 mm diameter are inserted in the test section cover plate to measure pressure from both pressure and suction side of TGV (**Figure 5**). These measurements are done at eight different sections along the chord length. Symmetric positions at pressure and suction side of TGV are taken for the measurements at the respective section. Each pressure tap is connected to piezo-resistive pressure transducer through a plastic hosepipe. All the sensors are pre-calibrated against the dead weight calibrator. Measurement uncertainly was maintained to be below ±0.05% at all the

measuring points. An average of 2000 samples, for each pressure point, measured at 5 HZ, is considered for the pressure analysis.

3.3 Velocity measurements

Particle Image Velocimetry (PIV) method is applied for the velocity measurements. Flow field from the position of stay vane outlet to the position of runner inlet is captured and analyzed. A pulsed light sheet with a thickness of 2 mm is generated by two double-cavity Nd-YAG lasers providing 120 mJ by pulse. The lighted field is visualized by a HiSense 2M CCD PIV cameras, with a series of paired images acquired at 150 μs and 4 Hz. Alignment of laser and camera with respect to the measurement plane is achieved with separate laser pointers. Fluorescent seeding particles, with a density of 1.016 kg/m^3, refractive index of 1.52 and mean diameter of 55 μm are used during the measurements. The camera resolution is 1280x1024 pixels for a 350x400 mm spatial domain. The PIV system is calibrated using a 2D calibration target. The calibration was performed *'in-situ'* with a specially designed system. The camera exposition, its synchronization with laser and image processing are done with a Dantec DynamicStudio 3.40 PIV specific processor. The image processing is carried out with 32-pixel resolution cross-correlation technique with 50% overlap.

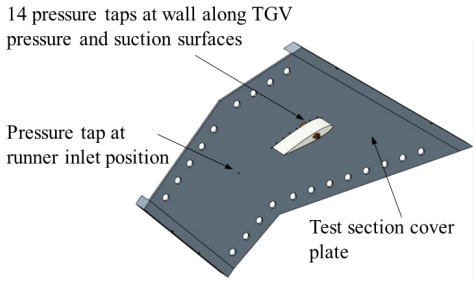

Figure 5. Positions for pressure taps along GV walls

Figure 6 shows the region of interest from PIV image along the clearance gap. Circumferential position respective turbine components from SV outlet to runner inlet, inside the flow channel, can be observed. Periodic position (PP) between the cascade walls represents 30˚ angular position in circumferential direction with respect to turbine center. It can be observed that the PP from 0% to 50% represents the pressure side of flow, and PP from 50% to 100% represents the suction side of flow respectively.

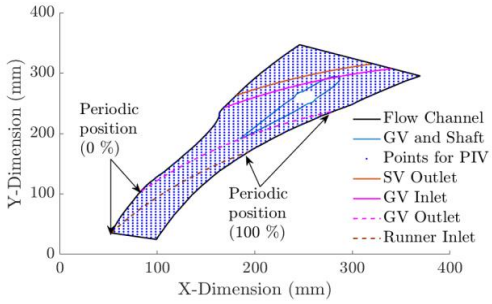

Figure 6. Flow section and positions for velocity study

Grid points for each interrogation area for PIV processing can also be seen. Unique velocity vector is obtained for each grid point with the time-averaged value for 100 image pairs. Running mean convergence test and bad vector position analysis has confirmed that 100

number of image pairs are sufficient to keep the standard deviation of time averaged velocity of good vectors below 0.1% of mean velocity.

Figure 7 shows the measurement planes with respect to position of runner blade in axial view. It can be observed that plane of measurement along GV mid-span corresponds to position of mid-height at runner inlet. Similarly, plane of measurement along clearance gap corresponds to position of hub at runner inlet.

For this study, the measurements are conducted and analyzed at these two planes. Effects of clearance gap on the main flow is studied by comparing the flow conditions at the runner hub with respect to the flow conditions at runner mid-height.

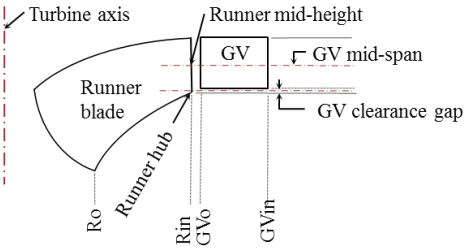

Figure 7 Measurement planes relative to runner blade

4. Results and Discussions

This paper presents the results of pressure and velocity measurements at the flow conditions described in section 3.1. Pressure measurements are done along the pressure and suction side of GV. Velocity measurements are done along plane of GV mid-span and along plane of middle of clearance gap.

Figure 8 shows the pressure distribution along the GV surface. All the pressure values are normalized by the pressure at the leading edge of GV. Highest pressure at the leading edge shows the stagnation point. A clear pattern of pressure and suction side can be observed as the flow progresses towards the trailing edge. Equal distribution of pressure up to 10% of GV chord from the leading edge shows angle of attack close to zero. Gradual development of pressure difference towards trailing edge is observed with maximum pressure difference occurring at 60-70% of the chord length. This pressure difference predicts development of cross flow in case of presence of clearance gap.

Figure 9 shows velocity distribution inside the flow cascade obtained from PIV measurements along the plane of GV mid-span. The basic flow phenomenon as stagnation point at the leading edge of GV, development of flow around pressure and suction sides and formation of wake at the trailing edge can be observed in the velocity contour. Lower velocities along the pressure side of GV and higher for the suction side matches the results from pressure measurements. At the trailing edge, flow from the pressure side has a negative pressure gradient and flow from suction side has a positive pressure gradient (**Figure 8**). This causes an unbalanced mixing of fluids with different pressure gradients at

the trailing edge of GV (**Figure 9**). Thus, velocity and pressure distribution along the circumferential direction of GV outlet in Francis turbine becomes non-uniform. Hence, even in the normal operating conditions, turbine runner passes through different gradients of velocity and pressure as it rotates between two GV. It is also observed, in **Figure 9**, that the flow around the GV in the middle of flow channel is not identical with the flow around the GV that forms the part of wall in flow channel. It is partly due to the nature of flow without runner and mainly due to single GV in the cascade.

Figure 10 shows the observation of the flow inside test setup for the case of 2 mm clearance gap. As indicated by the pressure measurements, crossflow occurs towards the trailing edge of GV. It can be seen that a vortex filament is developed as the crossflow mixes with the main flow. The filament starts from clearance gap at the 75% of chord length, from the suction side, and is carried downstream towards the position of runner inlet. As the flow moves downstream of GV, location of the filament appears to be shifted towards the suction side due to pressure gradients. The filament diffuses with main flow as it approaches outlet of test section, where flow becomes more uniform.

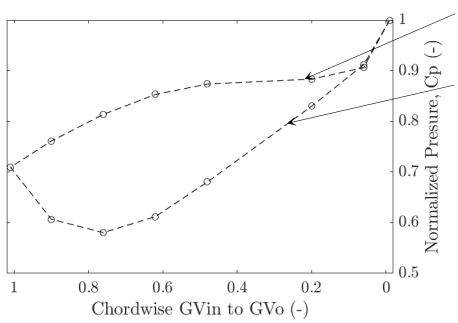

Figure 8. Pressure measurements along GV surface

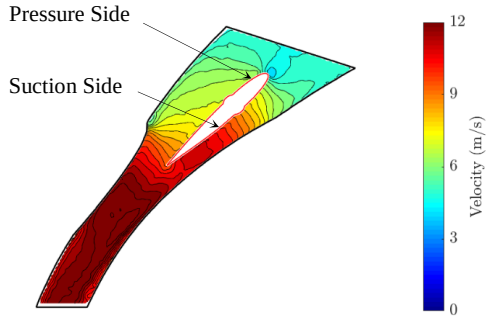

Figure 9. Contour plot of velocity along GV mid-span

Figure 11 shows the results of PIV measurements at the plane middle of 2 mm clearance gap. Contours of total velocity together with the velocity vectors can be observed. Close to the leading edge, velocity vectors are close to that of main stream flow both in magnitude and direction. Stagnation of flow by the GV shaft can also be seen. Behind the GV shaft, gradual development of crossflow and its mixing with main stream flow can be observed. As also indicated by the pressure measurements, the highest amount of crossflow, both in magnitude and direction, occurs at 60-70% of chord length. Mixing of cross flow with main flow seen in **Figure 11** justifies the formation and development of vortex filament as observed in **Figure 8**.

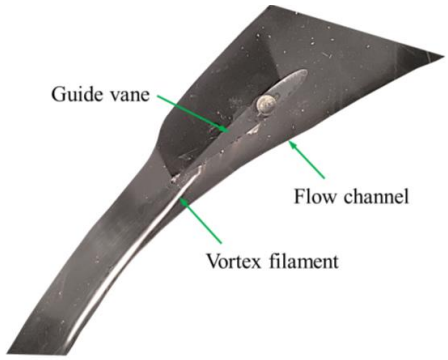

Figure 10. Observation of vortex filament from clearance gap

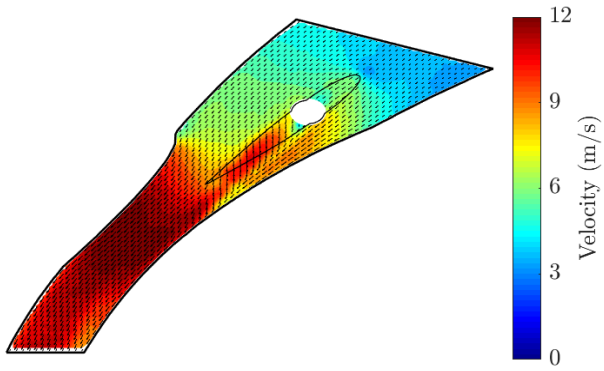

Figure 11. PIV measurements of flow field along clearance gap

A term 'Velocity Ratio (VR)' is defined, as **Eq. 3**. VR measure the change in respective velocity components along any GV span with respect to velocity components along GV-mid span. Thus, along the GV mid-span VR is 1 for all velocity components, at all locations and all periodic positions. Change in VR for other GV spans, at each location, e.g. runner inlet, indicates disturbance of clearance flow on respective velocity components at that location.

$$\boldsymbol{Velocity\ Ratio\ (VR)} = \frac{\boldsymbol{Velocity\ component\ along\ any\ GV\ span}}{\boldsymbol{Velocity\ component\ along\ GV\ mid-span\ at\ the\ same\ location}} \quad \textbf{(-)}$$

Eq. 3

Figure 12 shows VR at the runner inlet position along the plane of clearance gap. Thus, this figure demonstrates the relative distortion of each velocity components at the runner inlet due clearance gap. Velocity components along the circumferential direction is presented. It can be seen that at the clearance gap, the radial component of velocity has increased by more than 3.5 times than that at the mid-span. The other two velocity

components have reduced proportionality. Since magnitude of radial component is very small with respect to the tangential component, vector law of velocity components is still valid with such seemingly unproportioned change in VR for individual velocity components. Deviations in velocity components occurring towards the suction side (50-100% PP), matches with the location of crossflow and vortex filament being at the same location (**Figure 11**). This indicates that velocity components, at the runner inlet, are non-uniform, in both angular direction and span wise direction, due to disturbance of crossflow originating from the clearance gap.

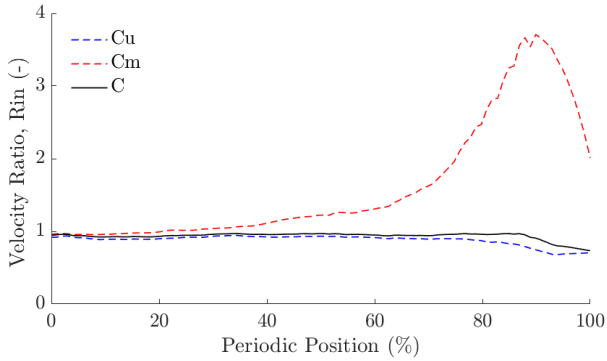

Figure 12. Velocity components at runner inlet along clearance gap

Figure 13 shows effects of clearance flow on the velocity conditions at the runner inlet. Based on PIV results, proportionate velocity triangles are drawn at position of mid-height and hub at runner inlet (**Figure 7**). It is seen that the distorted velocity component at runner hub has significant effects on inlet flow conditions. Close to the hub, the tangential velocity is reduced by 26% and the radial velocity is increased more than 3.5 times. This causes the relative velocity at the hub to be increased by 3.8 times than that at the middle of inlet height. Such changes on tangential and relative velocity at runner inlet have considerable consequences on turbine performance.

Euler turbine equation defines the turbine efficiency in terms of tangential velocities at runner inlet and outlet respectively as **Eq. 4.**

$$\eta_h = \frac{Cu1 \cdot U1 - Cu2 \cdot U2}{gH} \qquad (-) \qquad \textbf{Eq. 4}$$

Where η_h is hydraulic efficiency of turbine, Cu is the tangential velocity, U is runner peripheral velocity, g is acceleration due to gravity and H is pressure head at runner.

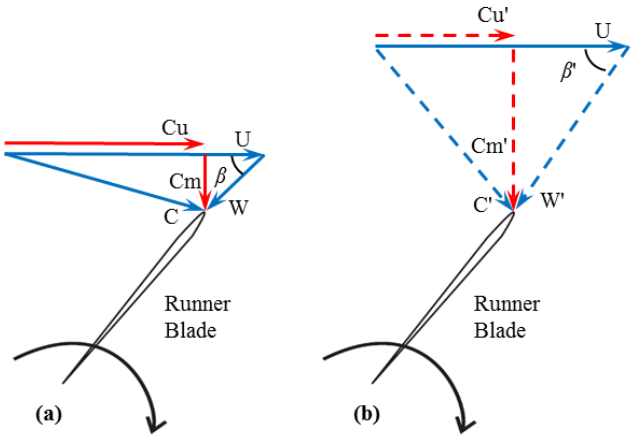

Parameter	Symbol	Unit	Mid	Hub	VR
Tangential velocity	Cu	m/s	11.68	8.69	0.74
Radial velocity	Cm	m/s	1.67	6.21	3.72
Total velocity	C	m/s	11.78	10.69	0.91
Relative velocity	W	m/s	1.93	7.35	3.81
Runner inlet angle	β	deg	60.01	57.68	0.96
Runner peripheral velocity	U	m/s	12.63	12.63	1

Figure 13. Velocity conditions at runner inlet: (a) at mid-height, (b) at hub with 2 mm clearance gap

1 & *2* are symbols for inlet and outlet respectively. Equation (4) shows that reduction of tangential velocity towards hub due to clearance flow causes on direct loss in turbine efficiency. However, this analysis does not include the runner, which will have an effect on the velocity distribution.

Studies have shown that sediment erosion on turbine components is proportional to third power of relative velocity [18]. Thus, such a high increase in relative velocity at around hub of runner at the inlet would causes severe erosion this location. Furthermore, non-uniform relative velocity long runner height and also between adjacent blades would cause secondary flows and turbulence. These effects may further accelerate erosion of blade surfaces and cause further loss in efficiency.

Several cases of severe erosion at the runner hub have also been reported by past authors [4, 19]. **Figure 14** shows a typical case of sediment erosion at runner hub, together with erosion in GV walls at trailing edge [19]. Significant loss in turbine efficiency, due to erosion, has also been reported. On basis of the presented results, these phenomenon can be explained as follows. Symmetric NACA profile has been used to shape the GV geometry. Thus, higher pressure difference towards trailing edge of GV causes higher secondary flows and corner vortex. This causes higher erosion at walls of the GV trailing edge. Erosion in GV trailing edge induces strong crossflow, which reduces tangential velocity and increases relative velocity at runner hub. Losses in turbine efficiency can be correlated with reduction in tangential component and the erosion at runner hub can be correlated with increase in relative velocity.

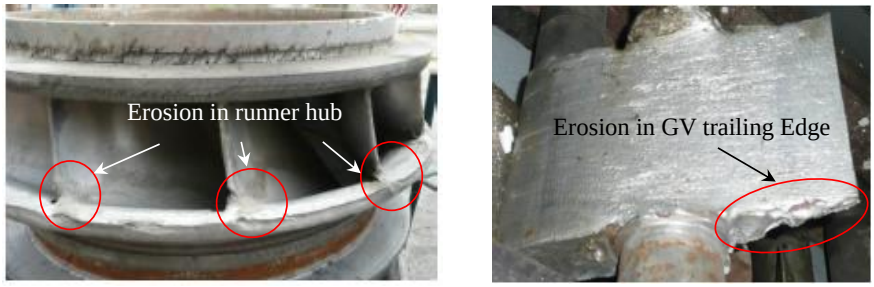

Figure 14. Erosion of Francis Turbine components: (a) Runner hub, (b) Guide vane [19]

5. Conclusions:

A test setup has been developed to investigate flow conditions around guide vane of low specific speed Francis turbine. The setup includes flow passage with one guide (GV), which is able to create similar velocity conditions as in a prototype turbine. NACA 0012 airfoil

has been taken as a reference profile to shape GV. Presented measurements are conducted at 30% flow of prototype at BEP. Pressure and velocity measurements are done to evaluate the effects of GV clearance gap on the flow conditions at runner inlet. It is concluded from this study that a strong crossflow occurs from the GV clearance gap due to high pressure difference between GV surfaces. Relative velocity at runner inlet hub increases more than 3.5 times that that at mid height. This has been related as a cause of high sediment erosion, often observed around inlet hub of Francis runner, operating in sediment-laden projects. Crossflow also causes lowering of runner efficiency by reduction in tangential velocity at close to hub. Further investigation on characteristics of vortex filament developed by the crossflow is necessary, to identify its effects on turbine performance and life. Study of alterative profiles for GV can help to identify better designs of GV for sediment-laden projects. A cascade with three GV inside flow channel would be developed for further investigation of problem under consideration.

References:

[1] X. Chen, "Theoretical and experimental study of flow through the double cascade of a Francis turbine," PhD thesis, Norwegian University of Science and Technology, Faculty of Engineering Science and Technology, 1992.

[2] S. Eide, "Numerical analysis of the head covers deflection and the leakage flow in the guide vanes of high head Francis turbines," 2004.

[3] H. Brekke, "The influence from the guide vane clearance gap on efficiency and scale effect for Francis turbines," in Proc. 14th IAHR Symposium on Progress within Large and High-Specific Energy Units, 1988, pp. 825-837.

[4] H. K. Sharma, "Power generation in sediment laden rivers: The case of Nathpa Jhakri," International Journal on Hydropower and Dams, vol. 17, pp. 112-116, 2010.

[5] B. Chhettry, B. Thapa, and B. S. Thapa, "Assembly design to ease turbine maintenance in sediment-laden conditions," International journal on hydropower and dams, pp. 82-88, 2014.

[6] B. S. Thapa, C. Trivedi, and O. G. Dahlhaug, "Design and development of guide vane cascade for a low specific speed Francis turbine," Journal of Hydrodynamics, Ser. B,, Accepted on 22 November, 2015.

[7] IEC, "Hydraulic turbines, storage pumps and pump-turbines – Model acceptance tests 2nd edn 1999-11," in IEC 60193, ed: The International Electro technical Commission, 1999.

[8] P. M. S. Pradhan, O. G. Dahlhaug, P. N. Joshi, and H. Støle, "Sediment and Efficiency Measurements at Jhimruk Hydropower Plant – Monsoon 2003," Report from HydroLab, Nepal2004.

[9] B. S. Thapa, "Hydraulic design of Francis turbine to minimize sediment erosion," Masters Thesis, Kathmandu University, 2012.

[10] B. S. Thapa, M. Eltvik, K. Gjøsæter, O. G. Dahlhaug, and B. Thapa, "Design Optimization of Francis Runners for Sediment Handling," in Fourth International Conference on Water Resources and Renewable Energy Development in Asia, Thailand, 2012.

[11] B. S. Thapa, B. Thapa, M. Eltvik, K. Gjosater, and O. G. Dahlhaug, "Optimizing runner blade profile of Francis turbine to minimize sediment erosion," in IOP Conference Series: Earth and Environmental Science, 2012, p. 032052.

[12] S. Chitrakar, M. Cervantes, and B. S. Thapa, "Fully coupled FSI analysis of Francis turbines exposed to sediment erosion," International Journal of Fluid Machinery and Systems, vol. 7, pp. 101-109, 2014.

[13] B. Rajkarnikar, H. P. Neopane, and B. S. Thapa, "Development of rotating disc apparatus for test of sediment-induced erosion in francis runner blades," Wear, vol. 306, pp. 119-125, 2013.

[14] F. Bario and C. Beral, "Boundary layer measurements on the pressure and suction sides of a turbine inlet guide vane," Experimental Thermal and Fluid Science, vol. 17, pp. 1-9, 1998.

[15] A. Zobeiri, P. Ausoni, F. Avellan, and M. Farhat, "How oblique trailing edge of a hydrofoil reduces the vortex-induced vibration," Journal of Fluids and Structures, vol. 32, pp. 78-89, 2012.

[16] Z. Schabowski and H. Hodson, "The Reduction of over tip leakage loss in unshrouded axial turbines using winglets and squealers," Journal of Turbomachinery, vol. 136, 2014.

[17] Z. Wei, P. H. Finstad, G. Olimstad, E. Walseth, and M. Eltvik, "High Pressure Hydraulic Machinery," in Compendium, N. Publication, Ed., ed, 2009.

[18] B. S. Thapa, O. G. Dahlhaug, and B. Thapa, "Sediment erosion in hydro turbines and its effect on the flow around guide vanes of Francis turbine," Renewable and Sustainable Energy Reviews, vol. 49, pp. 1100-1113, 2015.

[19] O. G. Dahlhaug, P. E. Skåre, V. Mossing, and A. Gutierrez, "Erosion resistant coatings for Francis runners and guidevanes," International Journal on Hydropower and Dams, vol. 17, pp. 109-112, 2010.